Status Report on the Stress Corrosion Cracking Behaviour of OFP Copper in Nitrite and Ammonia Solutions

NWMO TR-2011-06 February 2011

C.D. Litke[1] and B.M. Ikeda[2]

[1] Atomic Energy of Canada Ltd.
[2] University of Ontario Institute of Technology

nwmo
NUCLEAR WASTE MANAGEMENT ORGANIZATION
SOCIÉTÉ DE GESTION DES DÉCHETS NUCLÉAIRES

Nuclear Waste Management Organization
22 St. Clair Avenue East, 6th Floor
Toronto, Ontario
M4T 2S3
Canada

Tel: 416-934-9814
Web: www.nwmo.ca

Status Report on the Stress Corrosion Cracking Behaviour of OFP Copper in Nitrite and Ammonia Solutions

NWMO TR-2011-06

February 2011

C.D. Litke[1] and B.M. Ikeda[2]

[1] Atomic Energy of Canada Ltd.
[2] University of Ontario Institute of Technology

ABSTRACT

Title: **Status Report on the Stress Corrosion Cracking Behaviour of OFP Copper in Nitrite and Ammonia Solutions**
Report No.: **NWMO TR-2011-06**
Author(s): C.D. Litke[1] and B.M. Ikeda[2]
Company: [1] Atomic Energy of Canada Ltd.
[2] University of Ontario Institute of Technology
Date: February 2011

Abstract
This report covers a series of corrosion studies performed in 2009 and 2010, which were undertaken to enhance the understanding of the role of stress corrosion cracking (SCC) agents, particularly nitrite and ammonia, in the stress corrosion cracking (SCC) behaviour of oxygen-free phosphorous-doped (OFP) copper. In a deep geological repository (DGR), these SCC agents could be present as a result of microbial activity, blasting, or radiolysis of moist air. The studies investigated the effects of (i) nitrite and ammonia concentrations, (ii) nitrite/chloride and ammonia/chloride concentrations, (iii) copper concentration, and (iv) applied current on the SCC behaviour of OFP Cu. Constant extension rate tests (CERTs) were performed at room temperature using a compact tension specimen. The findings are summarized as follows:

- SCC was evident in a range of deaerated nitrite concentrations between 0.1 mol·L^{-1} and 1.0 mol·L^{-1}, at an applied current density of 1 $\mu A \cdot cm^{-2}$. Lower concentrations of nitrite (≤0.01 mol·L^{-1}) appeared to be insufficient to induce SCC.
- With nitrite concentration ≥ 0.1 mol·L^{-1}, a 1:1 chloride to nitrite concentration ratio suppressed SCC, as did an overabundance of chloride. High chloride concentrations appeared to increase uniform corrosion, which coincided with a blunting of the crack tip.
- In a deaerated 0.1 mol·L^{-1} nitrite solution, the susceptibility to SCC appeared to decrease with increasing chloride concentration, and increase with increasing applied current density (0.01 $\mu A \cdot cm^{-2}$ to 1 $\mu A \cdot cm^{-2}$).
- Steady-state potential values became more negative with increasing chloride concentration regardless of the nitrite concentration.
- SCC was evident in a range of ammonia concentrations between 0.3 mol·L^{-1} and 1.0 mol·L^{-1}, while a concentration of 0.1 mol·L^{-1} ammonia did not induce SCC. A concentration of 0.3 mol·L^{-1} ammonia appears to approach the threshold concentration required for SCC.
- In a 1.0 mol·L^{-1} ammonia solution, a 1:1 chloride to ammonia concentration ratio suppressed SCC, as did an overabundance of chloride. The addition of chloride in concentrations ≤0.5 mol·L^{-1} had little effect on SCC.
- In a 0.5 mol·L^{-1} ammonia solution, a 1:1 chloride to ammonia concentration ratio appeared to enhance SCC. The addition of 0.7 mol·L^{-1} chloride did not bring about SCC suppression.

In nitrite solutions a 1:1 chloride to nitrite concentration ratio is sufficient to suppress SCC. However in 0.5 mol·L^{-1} ammonia, SCC was not suppressed at that concentration ratio. The body of results from the ammonia work suggest that there may be a threshold concentration of 1.0 mol·L^{-1} chloride required for SCC suppression rather than a concentration ratio.

TABLE OF CONTENTS

LIST OF TABLES

Page

LIST OF FIGURES

Page

1. INTRODUCTION

Oxygen-free phosphorous-doped (OFP) copper is a potential candidate material for the used fuel containers (UFC) that would contain and isolate used fuel in a deep geological repository (DGR) (Maak 1999). Predicting the lifetime performance of a UFC in postulated repository environments is important in assessing the performance of the repository system.

Stress corrosion cracking (SCC) is a well-known phenomenon for copper and copper alloys (Bertocci et al. 1990). Three conjoint factors are required for SCC to occur: a susceptible material, an appropriate environment, and sufficient tensile stress. SCC of pure copper has been observed in nitrite- and ammonia-containing environments (King et al. 2001). In a DGR, SCC agents such as nitrite and ammonia could be present as a result of microbial activity, blasting, or radiolysis of moist air.

In previous Canadian studies, experiments were carried out to investigate the SCC behaviour in nitrite (King et al. 1999a; Ikeda and Litke 2000, 2008) and ammonia environments (King et al. 1999b; Ikeda and Litke 2004, 2008). These studies indicated that SCC susceptibility and crack growth are closely related to the nitrite and ammonia concentrations, corrosion potential values, and mechanical loading conditions (Ikeda and Litke 2000, 2004). In addition, the SCC susceptibility appears to be suppressed by the presence of chloride (Litke and Ikeda 2008). Chloride will be present in the DGR host rock groundwaters found in candidate crystalline or sedimentary rock formations.

The presence of a stable Cu_2O/CuO surface oxide is another essential criterion for SCC to occur on the copper UFCs in a DGR (Maak and King 2006). The formation of the surface oxide film depends on the potential of the system (Cassagne et al. 1990). Combining the electrochemical characteristics of the environment with the potential dependence of the oxide film has led to the development of a model for predicting the occurrence of SCC on copper containers in a DGR (King and Kolar 2005). The model accounts for SCC of copper containers due to the presence of SCC agents and a corrosion potential that promotes the formation of the surface oxide film.

The purpose of the Copper SCC - Experimental Studies project is to develop the required copper SCC experimental data that can be employed in the SCC model. The objectives of the SCC experiments are twofold:

i) to enhance the knowledge and understanding of the environmental conditions that may lead to SCC of copper in a deep geological repository for used fuel; and

ii) to determine the boundaries for the environmental parameters affecting SCC of copper.

The room temperature constant-extension rate tests performed in 2009 and 2010 were designed to study the effect of nitrite and ammonia solution concentrations, nitrite/chloride and ammonia/chloride concentrations, the addition of copper, and applied current. Those test results will be discussed in this report.

2. EXPERIMENTAL

2.1 MATERIALS AND SPECIMENS

Compact tension (CT) coupons were prepared from sections B2, C1 and C2 of the SKB-4 OFP copper plate (Figure 1). The pre-crack was generated using a carefully regulated fatigue crack-growth procedure with an MTS Systems Corp. Universal Testing machine. All specimens tested had the fatigue crack oriented in either the T-S or L-T orientation (Figure 1). The overall dimensions of the specimens were measured using a digital micrometer, and the notch and fatigue crack lengths were measured using a travelling microscope.

The overall shape of the CT specimens follows the specification outlined in ASTM-E 399-90 (ASTM 1994). The ratio of the specimen dimensions conform to this standard, but because of the low yield strength of copper, the overall dimensions do not. The standard requires physically larger specimens to be used to maintain plane-strain fracture conditions for a low strength material such as copper. Such specimens would be unreasonable for laboratory testing. The overall SCC behaviour can be compared for a consistent set of specimens although the estimated (ASTM 1994) stress intensity factor (K_Q) and crack velocity are not strictly valid for the application of plane strain fracture mechanics. The values may be used to qualitatively compare the crack growth for various environmental and loading conditions. Ductile tearing and measurement errors caused by the loss of surface planarity will affect the estimated values for the surface crack velocity and the K_Q for the onset of SCC reported here.

2.2 EQUIPMENT

2.2.1 Constant Extension Rate Tests

The constant extension rate test (CERT) involves a continuous loading of the specimen by increasing the distance between the loading holes at a constant rate. These experiments were performed using a relatively hard, custom designed slow strain rig. Mechanical and electrochemical data were recorded using a computer-based data acquisition system running LabView^{TM} software. The load sustained by the CT specimen as a result of its extension was measured using a load cell attached to both the specimen and the load frame.

A standard 3-electrode cell arrangement was employed. A registered, small-volume pressure vessel with a polytetrafluoroethylene PTFE liner was used as the cell body. CONAX pressure fittings with PTFE inner-sealing ferrules were used to permit electrode connections to penetrate the pressure vessel head yet maintain both the electrical isolation and pressure boundary seal.

All experiments undertaken during 2009 and 2010 were performed in ~0.5 L of solution at room temperature (22°C) and the specimens were pulled at a constant cross-head speed of 8.5×10^{-6} mm·s^{-1}. Copper was added to the ammonia solutions to assist in the reproducibility of the tests (Ikeda and Litke 2004). Summaries of the experimental conditions are presented in Tables 1 to 4.

The experiments, with the exception of CERT127, were carried out under galvanostatic conditions. A constant anodic current was applied to the CT specimen to simulate a supply of oxidant to the container surface. Galvanostatic control was maintained using a Thompson Ministat along with a large-area platinum mesh counter electrode surrounding the CT specimen.

The potentials were measured against a commercially available saturated calomel electrode (SCE) and all potentials are reported against this electrode.

A redox potential was not measured during the galvanostatic experiments, as the platinum counter electrode was used in applying the anodic current. However, at the end of the experiment, but before opening the vessel to the atmosphere, the current was removed from the specimen and the counter electrode was allowed to re-equilibrate with the test solution. The potential of the platinum electrode was measured against the SCE and the value recorded as the final solution redox potential (E_h).

2.3 SOLUTIONS

2.3.1 Nitrite Solutions

The experiments were performed in deaerated solutions containing sodium nitrite, sodium nitrite/sodium chloride mixtures or sodium nitrite/cupric sulphate mixtures. Three nominal nitrite concentrations (0.1, 0.5 and 1.0 mol·L^{-1}) and four nominal chloride concentrations (0.05, 0.5, 1.0 and ~5 mol·L^{-1} (saturated)) were used for the experiments conducted in 2009. A single experiment was also performed using 1.0 mol·L^{-1}nitrite with 0.05 mol·L^{-1}added copper (Table 1). The nitrite, nitrite/chloride and nitrite/copper solutions were prepared by dissolving the appropriate masses of reagent grade sodium nitrite, sodium chloride and cupric sulphate salts in Millipore purified deionized water. In the case of the 1.0 mol·L^{-1} nitrite/saturated chloride solution, the sodium nitrite was first added to the solution and then aliquots of sodium chloride salt were added until the solution reached saturation. Saturation was achieved when solid matter was still present in the bottom of the vessel after a period of 30 minutes. All solutions were adjusted to pH 9.0 using dilute NaOH. The pH was measured using a commercial glass pH electrode. The pH meter was calibrated before each measurement using commercially available pH standards for pH 4, 7 and 10. The solution was deaerated using argon gas for at least 20 minutes before closing the cell.

2.3.2 Ammonia Solutions

The experiments were performed in naturally aerated solutions containing ammonium hydroxide/cupric sulphate or ammonium hydroxide/cupric sulphate/sodium chloride mixtures. Four nominal ammonia concentrations (0.1, 0.3, 0.5 and 1.0 mol·L^{-1}) and four nominal chloride concentrations (0.1, 0.5, 0.7, and 1.0 mol·L^{-1}), were used for the experiments performed in 2010 (Table 3). All experiments contained 4 mmol·L^{-1}copper. The ammonia/copper and ammonia/copper/chloride solutions were prepared by diluting concentrated ammonium hydroxide to the appropriate concentration with Millipore purified deionized water, and then dissolving the appropriate masses of reagent grade cupric sulphate and sodium chloride salts in the ammonia solution. Similar to the nitrite tests, the solution pH was measured using a calibrated pH meter and a commercial glass pH electrode. In order to minimize any displacement of NH_3, the solution was not deaerated.

2.4 POST-TEST ANALYSES

Following the experiment, aliquots of the test solution were submitted for chemical analysis: by inductively coupled plasma atomic absorption spectroscopy to determine the total dissolved copper concentrations; and by ion chromatograph to ascertain the chloride concentration. The specimens were carefully rinsed with distilled, deionized water and then dried.

2.4.1 Image Recording

At the end of each experiment, a visual examination of the specimen was performed and features were noted (Table 2 and Table 4). The surface and the crack views of the specimen were imaged using a Zeiss SR Stereomicroscope equipped with an optical tube for a Sony DXC-93 3CCD colour video camera. A video image was captured using a Pro Series Capture Kit 128 (Media Cybernetics, version 4.03) located in a Pentium-processor-based PC. A digital image was recorded using *Image Pro Plus* (Media Cybernetics, version 4.5.29) software. Images were obtained at three different magnifications: 4X, 10X and 16X. Each image was saved, and then printed and stored for future reference.

The microscope-camera-software system was calibrated at the various magnifications by viewing a ruler with the microscope and recording the image. The ruled-line spacing was measured using *Image Pro Plus* and an internal conversion between pixels and length (in mm) was performed. The calibration was saved as a calibration setting within the program and can be recalled and applied to other images taken at the same magnification using the same camera-microscope arrangement. The calibrated conversion can be saved with the image file.

The microscope images were viewed as “live” images using the *Image Pro Plus* software. Adjustments were made until clear live images were obtained. The quality of the image was generally dependent upon the degree of uniform and diffuse lighting obtained over the entire surface. Reasonable lighting was obtained by using a combination of overhead-ring lighting and directed side lighting and by adjusting the intensity of each light source. Care was taken to ensure trueness of colour on the digital image, but subsequent reproduction may not adequately portray the colour or the observed features reported in Table 2 and Table 4.

2.4.2 Calculation of Cracking Factors

The crack extension and crack-mouth opening values were measured from a 4X magnification overview specimen image (not shown in this report). The longest crack on either surface was measured using the opened end of the specimen as a reference. The crack length was corrected for the length of the notch and initial fatigue crack to give the maximum crack extension. The longest surface crack length was manually measured from an enlarged grey-scale printed copy of the digital image to enhance the appearance of the cracks. The crack growth time was the time from crack initiation to the end of the experiment. For CERT experiments, the crack initiation time was estimated as the time when the load curve intersected a line with a 5% smaller slope than the initial elastic loading line (the 5% secant method). The crack velocity was determined by dividing the maximum crack extension by the crack growth time; this result is the surface-crack extension rate (SCER).

To overcome some of the uncertainty associated with the propagation time, an SCC factor (*SCCF1*) was developed using the ratio of the final corrected notch width to the corrected crack length. The longest crack was measured using a grey-scale paper image as described for the crack velocity measurements. The width of the final notch and the length of the longest crack were determined from the calibrated image using the opened end of the specimen as a reference. The notch width was corrected for the initial machined notch width while the crack length was corrected for the notch length and the initial fatigue-crack length. The SCCF1 factor was then calculated by dividing the corrected notch width by the corrected crack length.

The stress intensity factor (K_Q) at the onset of cracking was estimated using the initial surface fatigue crack length and the 5% secant load (ASTM 1994).

3. RESULTS AND DISCUSSION

In 2009 and 2010, the nitrite work evaluated the effect of three scenarios on the SCC behaviour of OFP Cu: high concentration nitrite solutions, high concentration nitrite/high concentration chloride mixtures, and a high concentration nitrite/low concentration chloride mixture. All nitrite experiments were performed under an applied current density of 1 $\mu A \cdot cm^{-2}$. In the high concentration nitrite only experiments, the results showed crack growth, while in the high concentration nitrite/high concentration chloride mixtures the results showed ductile behaviour. In the high concentration nitrite/low concentration chloride mixture, crack growth behaviour was still evident. A summary of the data for these nitrite-containing experiments is presented in Table 1.

In 2010, the focus of the ammonia work was to both establish a critical ammonia concentration for SCC, and confirm that a 1:1 chloride to ammonia concentration ratio would be sufficient to suppress SCC. All ammonia work was done in solutions containing 4 $mmol \cdot L^{-1}$ added copper and with an applied current density of 1 $\mu A \cdot cm^{-2}$. The results indicated that some degree of crack growth was evident at ammonia concentrations at or above 0.3 $mol \cdot L^{-1}$. In a 1.0 $mol \cdot L^{-1}$ ammonia solution, a 1:1 chloride to ammonia concentration ratio was sufficient to suppress SCC. However, in a 0.5 $mol \cdot L^{-1}$ ammonia solution, neither of the chloride concentrations tested were sufficient to suppress SCC. A summary of the data for these ammonia-containing experiments is presented in Table 3.

The K_Q values calculated for each specimen (Table 1 and Table 3) are > 16 $MPa \cdot m^{1/2}$, which is above the critical value of the threshold stress intensity factor for SCC (K_{ISCC}) reported previously (King et al. 1999a). Thus, each specimen was exposed to sufficient stress for SCC to occur, provided an appropriate environment was present.

The surface crack extension rate and SCCF1 values are indicators of crack growth behaviour. In nitrite environments, low SCER values (< 3 $nm \cdot s^{-1}$) and high SCCF1 values (> 4) are clear indications of ductile behaviour, and high SCER values (> 6 $nm \cdot s^{-1}$) and low values of SCCF1 (< 2) are clear indications of brittle-like SCC. Intermediate values indicate a mixture of brittle-like and ductile cracking behaviour. In ammonia environments, there was generally a degree of ductile behaviour in all of the specimens tested, even for those specimens showing rapid load decrease and other indicators of brittle-like crack growth behaviour. Thus, in ammonia, SCER values were in the low to intermediate range, while SCCF1 values were in the intermediate to high range. An extensive visual examination of the crack is required to determine the degree of brittle-like behaviour (Litke and Ikeda 2006). The visual observations describing the appearance of the specimens following the 2009 and 2010 nitrite and ammonia tests are included in Table 2 and Table 4, respectively.

3.1 NITRITE

The data for Tables 5 through 9 were compiled from our current and previous studies, and represents several series of experiments in the nitrite environment. The effect of nitrite concentration at 1 $\mu A \cdot cm^{-2}$ current density, the effect of a 1:1 chloride to nitrite concentration ratio at 1 $\mu A \cdot cm^{-2}$ current density, the effect of chloride concentration, the effect of current density in 0.1 $mol \cdot L^{-1}$ nitrite, and the effect of added copper will be discussed.

3.1.1 Effect of Nitrite Concentration

The results from tests carried out in 2009 using nitrite concentrations of 0.5 mol·L-1 (CERT122) and 1.0 mol·L-1 (CERT124) were added to our existing body of work in deaerated pH 9 nitrite

solutions under an applied current density of 1 □A·cm-2 (Ikeda and Litke 2000) to produce a test series of nitrite concentrations ranging between 0.001 and 1.0 mol·L-1 (Table 5). The specimen surface and crack images are shown in Figures 2A and 2B, respectively, while the load curve and potential transient plot are shown in Figures 3A and 3B, respectively.

The appearance of the test specimen in the 0.001 $mol \cdot L^{-1}$ nitrite concentration (CERT50) showed a generally rounded region in the zone above the crack, indicating more ductile tearing of the crack than brittle-like SCC (Figure 2i(A)). The view of the specimen looking down the crack (from the notch to the crack tip) is seen in Figure 2i (B). The crack tip is in the centre of the image, and as one moves from the centre of the image to the left or right, one crosses the crack surface, then the fatigue crack, and finally the machined notch. The specimen displayed significant ductility, evident by the dramatic necking in and bulging out of the specimen. The necking in of the centre can be seen in the middle of the image. The bulging out of the end of the specimen can be seen at the top and bottom of the vertical centreline of the crack overview. The region is slightly out of focus. A relatively flat load curve, a high SCCF1 value of 5.49 and a low SCER value of 2.11 $nm \cdot s^{-1}$ were further indications of the ductile nature of the crack extension.

The presence of a reddish-purple film was evident on both the specimen and crack surfaces. This film was similar in appearance to that seen in some of the high-chloride-containing tests (see Section 3.1.2.2). In some areas the film was thin enough to see the underlying specimen surface along with the fine crack arrest markings on the crack surfaces (Figure 2i (B)). Evidence from a previous study of specimens exposed to nitrite-containing solutions (King and Litke 1997) showed that although oxide was present on the crack walls, the crack arrest markings were still evident, and the thickness of the oxide was not sufficient to prevent dissolution of the crack walls and subsequent crack blunting (King et al. 1999a).

As the nitrite concentration increased from 0.1 $mol \cdot L^{-1}$ to 1.0 $mol \cdot L^{-1}$, the film became more adherent, purple-blue coloured and uniform (Figure 2(iii to v)). The gradual change in surface colour from red, to orange, pink, then purple, and eventually to black, is consistent with a change in both the oxide composition and thickness (Litke and Ikeda 2008). Pure, crystalline cuprous oxide (Cu_2O) is a deep, lustrous red, whilst pure crystalline cupric oxide (CuO) is black. The thin, adherent films may be either Cu_2O or CuO grown directly on the bare copper surface (a solid state growth mechanism). The oxidation state of the copper will depend upon the electrochemical potential for the oxidation reaction (King et al. 2001; Ikeda and Litke 2004). As the film grows, the tarnish layer develops by precipitation of copper from solution (Bertocci et al. 1990), but as it thickens it may become less adherent.

As the nitrite concentration increased from 0.1 $mol \cdot L^{-1}$ (CERT43) to 0.5 $mol \cdot L^{-1}$ (CERT122) and finally to 1.0 $mol \cdot L^{-1}$ (CERT124), the load curves (Figure 3 (A)) showed a more rapid decrease after the maximum load, and the steady-state potential values (Figure 3(B)) became less positive, moving from around 0.1 V to approximately 0.05 V. There was evidence for SCC, both in the measured SCCF1 and SCER values (Table 5), and in the appearance of the SCC cracks (Figure 2 (iii to v) (A)). As the concentration of nitrite increased the evidence for SCC was more definite. Although previously tested welded specimens (Ikeda and Litke 2000) had much lower K_Q values they exhibited the same SCC characteristics as the non-welded specimens (Table 5). Long meandering cracks were observed on the surface of the specimens, as illustrated in CERT122 (Figure 2iv (A)). These features are consistent with the coalescence of many small individual cracks to form a larger crack (King et al. 1999a). These larger cracks were produced in shorter times as the nitrite concentration increased.

The test carried out in the 0.01 mol·L^{-1} nitrite concentration (CERT51) was the exception to this trend. The specimen appeared to have little visible film formation and showed purely ductile tearing with little evidence of crack arrest (Figure 2ii (A and B)). The large SCCF1 value of 8.05, and the SCER value of 1.41 nm·s^{-1} were consistent with the visual evidence. The potential transient plot was much more negative than the values seen for the other tests in this series and was unusual in shape (Figure 3(B)), but it corresponded to the visual appearance of specimen and the shape of the load curve (Figure 3(A)). The data acquisition board used to collect the potential data failed early on in the experiment, and an alternate data collection method was used for the duration of the test. This initial problem may have lead to irregularities in the application of the applied current and thus tainted the experiment. Although this experiment did not follow the concentration trend, the correlation between stress corrosion and surface corrosion is consistent with the behaviour observed in this work.

SCC is evident in nitrite concentrations $\geq$ 0.1 mol·L^{-1}. It is difficult to establish if a threshold nitrite concentration for SCC exists, as the result in the 0.01 mol·L^{-1} nitrite test was inconclusive. At the lowest nitrite concentration tested (0.001 mol·L^{-1}) there are signs of crack initiation (see Figure 2i (B)), but the general dissolution of the specimen resulted in crack tip blunting. Traces of chloride found in the post-test solution may have affected this result; see discussion section 3.1.2.2. However, Benjamin et al. (1988) did not see SCC at this nitrite concentration.

3.1.2 Effect of Chloride Concentration

3.1.2.1 Effect of a 1:1 Chloride to Nitrite Concentration Ratio

Two of the tests conducted in 2009 were designed to examine the effect of a 1:1 chloride to nitrite concentration ratio in deaerated pH 9 solutions, under an applied current density of 1 μA·cm^{-2}. The results from CERT123 (0.5 mol·L^{-1} nitrite containing 0.5 mol·L^{-1} chloride) and CERT125 (1.0 mol·L^{-1} nitrite containing 1.0 mol·L^{-1} chloride), were added to our existing body of work (Ikeda and Litke 2000), to produce a series of 1:1 ratio comparisons with a nitrite concentration range between 0.01 and 1.0 mol·L^{-1} (Table 6). The specimen surface and crack images for the chloride-containing tests are shown in Figure 4A and 4B, respectively, while the load curve and potential transient plot are shown Figure 5A and 5B, respectively.

The appearance of all test specimens in the series showed significant ductility with no evidence for SCC, as indicated by the generally rounded region in the zone above the crack (Figure 4 (A)) and the considerable necking in and bulging out of the specimen as seen in the crack overviews (Figure 4 (B)). The crack tips are blunted and appear scooped-out. There is no evidence of the shredding of the crack surface as previously observed in the high concentration nitrite-only solutions. The SCCF1 numbers (Table 6) ranged between 5.2 (0.01 mol·L^{-1}) and 6.2 (1.0 mol·L^{-1}), while the SCER values ranged between 2.23 and 1.85 nm·s^{-1}. Both sets of values are strong indicators of ductile behaviour.

The load curves for all four chloride-containing tests were fairly flat after the maximum load (Figure 5 (A)). The load relaxation observed between 70 and 100 h for experiment CERT123 occurred because the motor stopped and the specimen was not extended during that time. During this period, the load decreased as the specimen relaxed. The motor was restarted at ~ 100 h and the load values recovered. The CERT123 potential values did not appear to be affected by this relaxation of load.

At the higher nitrite concentrations (between 0.1 and 1.0 mol·L^{-1}), the addition of a molar amount of chloride equal to the nitrite concentration was sufficient to move the measured steady-state potential of the given system from the positive values seen in the nitrite only solutions (approx 0.05 to 0.1 V, Figure 3 (B)), to significantly more negative values (-0.1 to -0.3 V, Figure 5 (B)). As the concentrations increased, the measured potential values became more negative, which may be due solely or in part, to the increasing chloride concentration. The specimens were covered with a heavy reddish-purple film (Figure 4 (i to iii)) which appeared more adherent and more uniform with the increasingly more negative potentials. A coarse green-blue deposit, which is consistent with the appearance of basic cupric chloride, was present on the specimens from the intermediate concentration tests.

In the 0.01 mol·L^{-1} nitrite/0.01 mol·L^{-1} chloride mixture (CERT33), the behaviour of the potential transient plot (Figure 5 (B)) was different than that seen for the higher concentration tests. The potential values started around -0.08 V for the first 50 h, then shifted to values between 0.05 and 0.1 V for the remainder of the test. The surface film, although similar in colour to the other specimens from the series, appeared thinner with a more varied colouration. However, the specimen exhibited mainly ductile behaviour. This behaviour is consistent with the process described by Bertocci et al. (1990) where the initial film growth process was a solid state reaction to form a thin adherent layer that was not susceptible to cracking. The SCCF1 and SCER values were also in the ductile behaviour zone (Table 6) consistent with the findings of a minimum nitrite concentration for SCC (Benjamin et al. 1988).

In CERT50 (0.001 mol·L^{-1} nitrite only) the measured chloride concentration in the post-test solution was also 0.001 mol·L^{-1}, which corresponded to an equal ratio of chloride to nitrite at the end of the experiment. This may have contributed to the absence of SCC at this nitrite concentration.

In summary, a 1:1 chloride to nitrite concentration ratio is sufficient to inhibit SCC. This observation is consistent with previous work (Ikeda and Litke 2000, King et al. 1999a).

3.1.2.2 Effect of Chloride Concentration

In 2009, the effect of chloride concentration in deaerated pH 9 nitrite solutions at an applied current density of 1 μA·cm^{-2} was studied to bridge the gaps in our existing experimental series. Two tests, involving the addition of high concentrations of chloride to nitrite-containing solutions (Table 1) were completed: 0.1 mol·L^{-1} nitrite containing 0.5 mol·L^{-1} chloride (CERT126), and 1.0 mol·L^{-1} nitrite containing ~5 mol·L^{-1} (saturated) chloride (CERT128). Data from all chloride-containing nitrite solution tests at an applied current density of 1 μA·cm^{-2}, as well as tests at other current densities, and tests on welded specimens will be included in this discussion.

Our experimental series in deaerated 0.1 mol·L^{-1} nitrite pH 9 solutions with added chloride at an applied current density of 1 μA·cm^{-2} is the most extensive. The specimen surface and crack images are shown in Figure 6A and 6B, respectively, while the load curve and potential transient plot are shown in Figure 7A and 7B, respectively.

As the added-chloride concentration was increased, the steady-state potential values decreased and became more negative (Table 7). A plot of the steady-state potential values versus the log of the measured final chloride concentrations for the added chloride tests shows a linear dependence (Figure 8). A regression analysis for that plot determined the slope to be

-155 ± 4 mV per decade of chloride concentration. Previous results (CERT40 and CERT49) for SKB OFP welded copper specimens (Ikeda and Litke 2000) also fit this trend.

In this series of experiments, the steady-state potential values moved from positive to increasingly more negative values with an increase in chloride concentration (Figure 7 (B)). The cracking characteristics of the associated specimens moved from brittle-like crack growth to ductile tearing. Both visual evidence and calculated data support this trend. The oxidation on the specimens (Figure 6 (A)) changed from a bluish/brown precipitate to a reddish-purple film which became thicker and more adherent, until chloride saturation was reached and the film became a thin, multicoloured translucent layer. The amount of etching on the underlying surface also appeared to increase with increasing chloride concentration.

The region above the crack became rounder, and the cracks progressed from sharp SCC cracks to ductile tears. The crack surfaces (Figure 6 (B)) were shredded in appearance at the positive potential values, and smooth with a blunted tip at more negative potential values. The amount of necking in and bulging out of the specimen in the crack images (Figure 6 (B)) also increased throughout the series. The increasing chloride concentration increased the ductility and dissolution of the copper specimens.

The decay in the load curves after the maximum load (Figure 7 (A)) progressed from rapid (SCC) to slow, with the load curves becoming flatter (more ductile) after the maximum load, as the chloride concentration increased and the steady-state potentials decreased. The potential transient plots differed somewhat in initial shape (Figure 7 (B)), but were relatively flat after reaching steady-state values. A negative steady-state potential suggests active corrosion, and an increased corrosion rate may be assisted by the formation of copper complex ions in solution (Ikeda and Litke 2008). The negative potential value suggests that the anodic dissolution reaction is dominated by dissolution as soluble Cu(I)-chloro complexes such as $CuCl_2^-$; rather than by oxide formation (King et al. 1999a). In this series, only the saturated chloride condition showed a significant amount of copper in solution (Table 7), although a blue/green precipitate, generally thought to be basic cupric chloride, was present on some of the test specimens (i.e., Figure 6iii & iv (B)). The SCCF1 and SCER values (Table 7) moved from the SCC range to the purely ductile range.

The specimens suffered more uniform corrosion when tested in solutions with a chloride concentration equal to or greater than the nitrite concentration. The rate of copper dissolution was sufficiently rapid that crack tip blunting appeared to prevent stress intensification and crack growth. Although the presence of an oxide film on copper is a necessary condition before SCC can occur, the visible appearance of a film is not sufficient to indicate SCC (Ikeda and Litke 2008). Our previous results indicated that SCC did not occur when a precipitated film was present, as supported by the characteristics of CERT35 and CERT126, which had the thickest films in the overall chloride series, but did not crack.

Additional data was also available from a sub-set of tests that did not initially have pre-added chloride, but where small concentrations of chloride were present at the end of the test. These data were added to the data of Figure 8 to produce Figure 9. The measured chloride concentrations in all these cases fell below 100 $mg \cdot L^{-1}$, and the potential values were less predictable. Although these potential values were generally positive, they fell below the linear dependence shown by the experiments with intentionally added chloride. The presence of these smaller concentrations of chloride was generally due to leakage from the reference electrode into the solution.

The SCCF1 values for nitrite solutions with a concentration of at least 0.1 mol·L^{-1} and an applied current density of 1 μA·cm^{-2} were also plotted against the log of the measured chloride concentration (Figure 10(A)). A regression analysis for this plot gave a linear dependence of ~1 SCCF1 unit per decade of chloride concentration. The point where the trend line crosses the predicted threshold value for SCC (SCCF1 = 4) may correspond to a possible threshold concentration for chloride to suppress SCC. The data implies that 0.04 mol·L^{-1} chloride would be enough to suppress SCC at these nitrite concentrations. This chloride concentration fits into the range predicted for the interfacial chloride concentration (0.01 – 0.05 mol·L^{-1}) for the first several thousand years in the DGR (King et al. 1999a).

In an attempt to substantiate this prediction, a further test (CERT130) was performed in 2010 to assess the effect of adding 0.05 mol·L^{-1} chloride to a 1.0 mol·L^{-1} nitrite solution under an applied current density of 1 μA·cm^{-2} (Table 1). The specimen surface and crack overviews are shown in Figure 11A and 11B, respectively, while the corresponding load curve and potential transient plot are illustrated in Figure 12A and 12B, respectively.

A tightly adherent purple/brown film, with variegated red and green areas, was evident on the specimen surface, along with a more loosely adherent brown/blue-green precipitate in the ductile zone (Figure 11ii (A)). A coarse blue-green oxide was deposited on some crack edges, and also on the inside surfaces of the crack itself (Figure 11ii (B)). The adherent film was similar to the purple film noted in the nitrite-alone test (CERT129, Figure 11i (A)). The values for SCCF1 (1.72 and 1.18, respectively) and SCER (7.10 and 10.4 nm·s^{-1}, respectively) from both of these tests indicated brittle-like crack behaviour. In contrast, a comparable test containing saturated chloride (CERT128, Figure 11iii (A)) showed only a thin, translucent film on the surface. The SCCF1 (4.84) and SCER (2.43 nm·s-1) values from this test were indicative of ductile tearing.

The shape of the load curves (Figure 12(A)) for both CERT129 and CERT130, which declined dramatically after the maximum load, was consistent with the visual evidence for SCC behaviour. The potential transient plots (Figure 12 (B)) were relatively flat after reaching steady-state values of approximately 0.05 V, also indicative of SCC. In contrast, as shown in CERT128, the shape of the load curve and steady-state potential values more negative than -0.2 V were as expected for suppression of SCC. These results showed that the addition of 0.05 mol·L^{-1} chloride had little effect on the suppression of SCC behaviour in 1.0 mol·L^{-1} nitrite. However, that chloride concentration could still be important for the suppression of SCC in less concentrated nitrite solutions. Further testing would be required to support that hypothesis.

In Figure 10(B), the data from the lower nitrite concentrations, the lower applied current densities, and the freely corroding conditions (OCP) were added to Figure 10(A). These data points are scattered above the trend line with all of the lower nitrite concentrations (≤ 0.01 mol·L^{-1}) falling in the SCC suppression (ductile failure) region. The majority of data from the tests using lower applied current densities or freely corroding conditions fell into the brittle-like crack growth region (SCCF1 < 4). These results imply that the amount of nitrite present at the lower nitrite concentrations was not sufficient to induce SCC, consistent with Benjamin et al. (1988).

In Figure 10(B), it was also possible to group the test results according to their SCCF1 values. Values greater than 4 indicated ductile behaviour while values less than 4 indicated brittle-like crack growth behaviour. Generally, specimens tested in low nitrite concentrations; in nitrite

solutions containing high chloride concentrations; or in nitrite solutions having a chloride to nitrite concentration ratio of at least 1:1, had SCCF1 values above 4 or exhibited ductile failure. As noted in Ikeda and Litke (2008), these conditions appeared to increase the uniform corrosion of OFP copper, which coincided with a blunting of the crack tip. When tested either in nitrite solutions having a chloride to nitrite concentration ratio less than one or in higher nitrite concentrations, the specimens generally had SCCF1 values below 4 or exhibited brittle-like crack growth behaviour.

Data from the copper corrosion model used to predict the time dependence of the corrosion potential (E_{CORR}) of a copper container in a DGR (Figure 6-15 in King et al. 2001) suggested that Cu will always undergo active dissolution at a potential sufficiently negative to preclude the possibility of SCC. Those E_{CORR} values were calculated on the basis of a Cl^--dominated dissolution process (King et al. 1999a) and did not include the effect of nitrite as a passivating agent. Our results suggest that in nitrite-containing solutions the E_{CORR} values started at more positive values, indicative of passive corrosion, but were more dependent upon the added-chloride concentration than the amount of nitrite present.

The analysis of the effect of chloride on SCC susceptibility does depend on the amount of nitrite present. In a 0.1 mol·L^{-1} nitrite solution the susceptibility of OFP copper to SCC appeared to decrease with increasing chloride concentration. However, small amounts of chloride were not sufficient to move the steady-state potential into the negative potential range required to suppress SCC. Lower concentrations of nitrite (≤0.01 mol·L^{-1}) did not appear to be sufficient to induce SCC, and the addition of chloride did not change this outcome.

3.1.3 Effect of Applied Current in 0.1 mol·L^{-1} Nitrite

The predicted rate of supply of O_2 to the container surface (expressed as current density) varies from ~0.1 μA·cm^{-2} initially to <10^{-10} μA·cm^{-2} as the O_2 in the DGR is consumed (King and Litke 1997). Although our experimental range does not correspond exactly with that expected in the DGR, there is considerable overlap and reasonable extrapolations should be possible based on the experimentally available fluxes (King and Litke 1997).

Data was consolidated from our body of experiments in deaerated 0.1 mol·L^{-1} pH 9 nitrite to illustrate the effect of applied current on the SCC of SKB OFP copper (Table 8). Although the applied current tests were performed in duplicate, a single experiment from each of the conditions has been chosen to illustrate the trend. As the results from the two freely corroding condition tests were less reproducible, a repeat experiment (CERT127) was completed in 2009. All three experiments will be discussed. The specimen surface and crack images are shown in Figure 13A and 13B, respectively, while the load curve and potential transient plot are shown in Figure 14A and 14B, respectively.

The test specimens in the applied current tests all showed visible evidence of SCC, with the severity of the cracks and the thickness of the surface film increasing with increasing current (Figure 13i to iii (A)). The shape of the region above the crack also illustrated this trend. The roundness of this region was most predominant at the lowest current density where a mixture of ductility and brittle-like failure is more likely. All crack surfaces were shredded in appearance and covered with a combination of purple-blue to reddish-purple film (Figure 13i to iii (B)). As the current density increased, the film colour transitioned from predominantly reddish-purple to a purple-blue. Prevalence of the purple-blue film in the crack corresponded to that seen in other specimens undergoing SCC (see
Figure 2iv & v (B)).

The load curves, as shown in Figure 14 (A), had a rapid decrease after the maximum load, with the lowest current density (0.01 $\mu A \cdot cm^{-2}$) having the lowest slope. The SCCF1 and SCER values showed stronger indications of brittle-like SCC (Table 8) with increasing applied current. Generally the steady-state potential values (Figure 14(B)) became more positive with increasing applied current, although all measured values were between 0 and 0.12 V.

The tests carried out under freely corroding conditions (CERT32, CERT88 and CERT127) exhibited a variety of surface and crack conditions (Figure 13iv to vi). CERT32 (Figure 13iv) was the most similar in physical appearance and experimental result to the lower applied current tests (CERT58 and CERT28, Figure 13ii and iii, respectively). It had a translucent surface film and the crack region in the zone above the crack had a rounded appearance, although brittle-like cracking was evident. The crack surface was shredded in appearance and covered with the reddish-purple to purple-blue colouration, despite the fact that some ductility was evident by the necking in and bulging of the specimen. The load curve decreased fairly rapidly after the maximum load, while the steady-state potential, the SCCF1, and the SCER values fell between the values observed for the 0.01 and 0.1 $\mu A \cdot cm^{-2}$ applied current tests. The unusual shape of the early portion of the potential transient plot could be explained by an initially high surface oxygen concentration (Ikeda and Litke 2000). The sum of these observations would imply that the corrosion current density for this test falls between 0.01 and 0.1 $\mu A \cdot cm^{-2}$.

CERT127 (Figure 13v) also had characteristics that were similar to the lower applied current tests. The zone above the crack still had a rounded look, although some brittle-like cracking was evident (Figure 13v (A)). The crack surface was shredded, although the necking in and bulging of the specimen (Figure 13v (B)) showed evidence of increased ductility. The specimen and crack surfaces were covered with a more pinkish-purple colouration (Figure 13v) than seen previously. The shape of the load curve was similar to load curves from the applied current tests, but it flattened-out over the last 100 h of the test. The steady-state potential value still fell between the values observed for the 0.01 and 0.1 $\mu A \cdot cm^{-2}$ tests. The SCCF1 (3.46) and SCER values (3.53 $nm \cdot s^{-1}$) fell within the mixed brittle-like/ductile tearing range, which matched the overall characteristics of this test. The corrosion current density for this test appears to fall around or slightly below the 0.01 $\mu A \cdot cm^{-2}$ condition.

The behaviour of CERT88 (Figure 13vi) was in direct contrast to most of what had been observed for the other tests in the series. The zone above the crack was extremely rounded, there was no evidence of shredding of the crack surface, and there was significant necking in and bulging out, of the specimen, indicating ductility. The specimen and crack surfaces were mottled with the pinkish-purple colouration while the crack surface tended towards a darker purple colouration. The load curve was fairly flat and the potential transient plot was negative with a steady-state potential around -0.02 V (Figure 14). The SCCF1 (5.75) and SCER (3.30 $nm \cdot s^{-1}$) values are clear indications of ductile failure.

The experimental set-up of test CERT88 allowed for the measurement of the redox potential between the internal platinum electrode and the reference electrode, as well as the measurement of the steady-state potential of the specimen. This measurement set-up may have led to ground loops in the system and may have induced a small anodic potential on the specimen. This would account for the appearance and characteristics of this test.

The evidence from these three tests showed the difficulty in obtaining reproducible results for tests under freely corroding conditions. This issue suggests that all the independent variables are not known and controlled. Reproducibility is improved by forcing the corrosion reaction to occur at a known rate by using galvanostatic conditions. Under applied current conditions, as the current increased from 0.01 $\mu A \cdot cm^{-2}$ to 1 $\mu A \cdot cm^{-2}$, the susceptibility to SCC increased. The potentials produced under the applied current conditions did not push the system into active dissolution (potentials more negative than -0.2 V), but allowed it to remain in the passive zone (Figure 15) and thus susceptible to SCC (Ikeda and Litke 2001).

3.1.4 Effect of Added Copper

The concentration of copper in solution appears to be a factor in the SCC behaviour of copper in ammonia solutions. The measured copper concentration in those ammonia solutions was far higher than those seen in nitrite tests exhibiting SCC. To examine the effect of a higher solution copper concentration on SCC behaviour in nitrite, a copper concentration of 8 $mmol \cdot L^{-1}$ was added to a 0.1 $mol \cdot L^{-1}$ nitrite solution under freely corroding conditions (CERT89). The results from that test will be compared to the same test conditions without added copper. The specimen surface and crack images are shown in Figure 16A and 16B, respectively, while the load curve and potential transient plot are shown in Figure 17A and 17B, respectively.

The test specimen from CERT89 was completely covered in a turquoise blue coating (Figure 16iii). The measured concentration of copper in solution was lower at the end of the test as compared to what was added initially (Table 9). This difference may account for the heavy deposit on the specimen surface. There were fewer small cracks along the crack front, but the interior of the crack still had a roughened appearance (Figure 16iii (B)). The specimen showed minimal evidence of ductility. The load curve was indicative of SCC, showing a steady decrease in the measured load after having reached the maximum load (Figure 17 (A)). The potential values remained relatively stable at 0.05 V after approx 50 h (Figure 17 (B)), which coincided with the time to reach maximum load. An SCCF1 value of 0.95 and a SCER value of 4.84 $nm \cdot s^{-1}$ were both strongly indicative of SCC behaviour.

In previous tests containing 0.1 $mol \cdot L^{-1}$ nitrite without added copper under freely corroding conditions (CERT32 and CERT127), there was evidence for both ductile and brittle-like cracking behaviour. The crack view images showed both necking in and bulging out of the specimens, along with shredded crack surfaces, i.e., numerous small cracks along the crack front (Figure 16i & ii (B)). There were large SCC cracks on the specimens (Figure 16i &ii (A)). The shape of the load curves, showing a steady decrease in the measured load after having reached the maximum load (Figure 17(A)), and the final measured potential values (Figure 17(B)) were both indicative of SCC. The SCCF1 and SCER values were in the mixed brittle-like cracking/ductile tearing range.

Although a higher concentration of copper in solution is not necessary for the occurrence of SCC in nitrite-containing solutions, it appeared to enhance the brittle-like cracking behaviour. The SCC crack was more well-defined, the specimen exhibited less ductility, the load curve had a large decrease in slope after the maximum load, and the SCCF1 and SCER values were in the brittle-like crack region.

3.2 AMMONIA

The intention behind this year's work was twofold – to optimize the threshold ammonia concentration which allowed for SCC, and to show that once SCC conditions were established, the addition of a sufficient amount of chloride could suppress the SCC. The data for Tables 10 through 13 were compiled from our current and previous studies and represents several completed series of experiments in the ammonia environment. The effect of ammonia concentration in solutions containing 4 mmol·L^{-1} added copper under 1 $\mu A/cm^2$ applied current conditions, the effect of 1:1 chloride to ammonia concentration ratio, the effect of chloride concentration in solutions containing 1.0 mol·L^{-1} ammonia and 4 mmol·L^{-1} copper under 1 $\mu A/cm^2$ applied current, and the effect of chloride concentration in solutions containing 0.5 mol·L^{-1} ammonia and 4 mmol·L^{-1} copper under 1 $\mu A/cm^2$ applied current.

3.2.1 Effect of Ammonia Concentration in Solutions Containing 4 mmol·L^{-1} Added Copper under 1 $\mu A/cm^2$ Applied Current Conditions

In an effort to narrow down the threshold ammonia concentration required for SCC, a range of ammonia concentrations between 0.1 and 0.5 mol·L^{-1} were chosen for testing in 2010 (Table 3): 0.1 mol·L^{-1} (CERT131), 0.3 mol·L^{-1} (CERT137), and 0.5 mol·L^{-1} (CERT132). Earlier work in 2003 showed that SCC would occur under 1 $\mu A/cm^2$ applied current conditions in a 1.0 mol·L^{-1} ammonia solution containing 4 mmol·L^{-1} added copper (CERT70, CERT74, and CERT76). For illustrative and comparative purposes, CERT74 has been chosen to be representative of this group. The specimen surface and crack overview images are shown in Figure 18A and 18B, respectively, while the load curve and potential transient plot are shown in Figure 19A and 19B, respectively.

The degree of ductility decreased, and the tendency towards SCC increased as the ammonia concentration increased throughout the full range of ammonia concentrations (Figure 18). The copper specimen exposed to 0.1 mol·L^{-1} ammonia concentration (CERT131) exhibited ductile tearing and no evidence for SCC. Physical indications of the ductility in the specimen included a drawn-out, but rounded crack region (Figure 18i (A)), a narrowing of the centre of the specimen and bulging out of the specimen end, as seen in Figure 18i (B). The ductility in the specimen exposed to the 0.3 mol·L^{-1} ammonia concentration (CERT137, Figure 18ii (B)) was similar to that seen in CERT131. The crack surface was quite smooth with minimal evidence of SCC cracks. In the 0.5 mol·L^{-1} ammonia concentration (CERT132) the crack surface started out smooth, but became coarser near to the crack tip, i.e., in the lower region of Figure 18iii (B) where the SCC cracks were quite evident. For the specimen exposed to the 1.0 mol·L^{-1} ammonia concentration (CERT74), the initial crack surfaces were smooth with a large SCC crack at the base (Figure 18iv (B)).

SCCF1 and SCER values mirrored these observations (Table 10). For CERT131, the SCCF1 value of 5.17 and the SCER value of 2.4 nm·s^{-1} were consistent with ductile behaviour. A combination of ductile and brittle-like cracking behaviours were observed in both the 0.3 mol·L^{-1} (CERT137) and 0.5 mol·L^{-1} (CERT132) ammonia concentrations (Table 10). SCCF1 values of 3.66 and 3.34, respectively, and SCER value of 2.96 and 3.63 nm·s^{-1}, respectively, fit into the range for mixed ductile/brittle-like cracking behaviour. For CERT74, the SCCF1 value of 2.54 and the SCER value of 4.81 nm·s^{-1} were stronger indicators for mainly brittle-like crack growth.

In this series of experiments, the potential transient plots for the three higher concentrations showed a potential transition that is indicative of SCC, but the associated load curves did not all exhibit the expected behaviour (Figure 19 (B)). In CERT131, which exhibited only ductile

behaviour, the potential values started around -0.15 V, moved more negative to -0.3 V and then oscillated around that value for the remainder of the experiment with no evidence for the upward potential transition normally seen with SCC behaviour. The associated load curve began to flatten-out after the maximum load. Although there was a potential transition in CERT137, the load curve did not show a decrease in slope at the point of the transition and instead followed the trend of the curve from CERT131, which was to flatten-out. The load curve for CERT132 did not show a decrease in load at the point of the potential transition, but there was a change in slope approximately 75 h later. In CERT74, the occurrence of a potential transition was followed closely by a decrease in the measured load values, with a more dramatic decrease occurring approximately 50 h later. In this series of experiments, the load curves were not strong indicators of the SCC tendency.

Although a light blue grey oxide layer with a pink underlying layer and some etching were visible in CERT131 (Figure 18i (A)), the crack was extended by ductile tearing with no evidence for SCC. The crack surface was fairly smooth and shiny in appearance with a pink colouration. The concentration of copper in solution at the end of the test dropped from the initial added concentration (Table 10) suggesting that some copper precipitated on the specimen. In CERT137, a light, golden brown coloured tarnish, some areas of crack coalescence, and brittle-like cracks on the specimen surface were seen (Figure 18ii (A)) and were indicative of SCC. There was also some surface etching. Although the interior crack surface was relatively smooth, indicative of ductile tearing, there were small brittle-like cracks in several places near the crack tip, and there was a purple blue oxide on the fatigue crack surfaces (Figure 18ii (B)).

There was a light tarnish on the surface of CERT132, with a pink underlying layer similar to CERT131. However, the dominating feature was the etching and grain boundary attack on all surfaces of the specimen (Figure 18iii). A dark brown precipitate appeared at the base of these grain boundaries. The cracks on the surface of the specimen (Figure 18iii (A)) appeared to follow the grain boundaries and these cracks were evident throughout the ductile zone. Some purple blue oxide was also evident on the fatigue crack. In contrast, CERT74 had an overall covering of dark brown and purple, and although it was difficult to see the underlying surface, it appeared to be finely etched. A large SCC crack had penetrated to the far end of the specimen and there were large secondary cracks, some of which appeared to have coalesced (Figure 18iv (A)).

The specimen exposed to the 0.1 $mol \cdot L^{-1}$ ammonia concentration (CERT131) exhibited purely ductile behaviour. Although the load curves from tests CERT131 and CERT137 were similar, several other test results for the 0.3 $mol \cdot L^{-1}$ ammonia concentration (CERT137) indicated SCC (Table 10). These results suggest that under the chosen test conditions, the 0.3 $mol \cdot L^{-1}$ ammonia concentration is close to the threshold concentration required for SCC.

3.2.2 Effect of Chloride Concentration

3.2.2.1 Effect of 1:1 Chloride to Ammonia Concentration Ratio

In 2010, a test involving the addition of 1.0 $mol \cdot L^{-1}$ chloride to a 1.0 $mol \cdot L^{-1}$ ammonia solution containing 4 $mmol \cdot L^{-1}$ added copper, under an applied current density of 1 $\mu A \cdot cm^{-2}$ (CERT136), was completed. A previous test with similar characteristics, only with 8 $mmol \cdot L^{-1}$ added copper and under freely corroding conditions (OCP) (CERT81), had been completed in 2003. In both these tests there were similarities in the results regardless of the added copper concentration or the applied current conditions (Table 11). The specimen surface and crack overview images

are shown in Figure 20A and 20B, respectively, while the load curve and potential transient plot are shown in Figure 21A and 21B, respectively.

The parallel results between the two tests included the obvious signs of ductility in the specimens; the roundedness of the crack region, the necking in and the bulging out of the specimen, the smoothness of the crack surface, and the blunting of the crack tip (Figure 20i and ii). The specimens were both covered in a shiny iridescent coating. There were gradual declines in the load values some time after the maximum load was achieved, but the values stabilized over time (Figure 21 (A)). The SCER values (2.01 and 2.04 $nm \cdot s^{-1}$) and the SCCF1 values (5.58 and 5.99) also fit the visual observations.

The measured potential values (Figure 21 (B)) remained quite negative (between -0.4 V and -0.5 V), indicative of active dissolution. The redox potentials measured after the completion of the experiment were approx -0.35 V and -0.34 V, respectively (Table 11). A thermodynamic analysis of the Cu/NH_3 system suggests that for potentials more negative than -0.3 V, a stable oxide phase cannot form at any pH <~12 until the copper concentration exceeds 9.8 $mmol \cdot L^{-1}$ at pH 12.0 (or 24 $mmol \cdot L^{-1}$ at pH 11.6) (Ikeda and Litke 2004). As the concentration of copper in solution increases further, the potential for the mixed oxide film moves to more positive values (i.e., at approx 40 $mmol \cdot L^{-1}$ the calculated potential is approx. -0.22 V). In CERT81 and CERT136, the measured concentrations of copper in solution were 47.2 $mmol \cdot L^{-1}$ and 36.2 $mmol \cdot L^{-1}$, respectively (Table 11). In these cases, the combination of very negative potential values and higher copper concentrations could result in the formation of a thin Cu_2O film.

For comparison, similar tests had been carried out in 1.0 $mol \cdot L^{-1}$ ammonia solutions using the same test conditions as for CERT81 and CERT136, but without chloride (CERT78 and CERT74, respectively) (Table 11). The specimens exposed to those environments exhibited SCC (Ikeda and Litke 2004).

In 2010, a test involving the addition of 0.5 $mol \cdot L^{-1}$ chloride to a 0.5 $mol \cdot L^{-1}$ ammonia solution containing 4 $mmol \cdot L^{-1}$ added copper, under an applied current density of 1 $\mu A \cdot cm^{-2}$ (CERT133), was also completed. It was expected that the experimental results from CERT133 would follow an SCC behaviour similar to CERT136. Instead, the potential transient plot from CERT133 showed the start of a shift in potential after approximately 250 h (Figure 21 (B)), with a rapid transition at about 300 h. Shortly after that transition, the load values began to decrease (Figure 21 (A)).

The relatively long (300 h) and gradual decay of the load curve after the maximum load in CERT136 (Figure 21 (A)) is consistent with the visual evidence of some initial ductility in the specimen; the crack region is rounded (Figure 20iii (A)), there is a degree of necking-in and bulging out of the specimen, and there are smooth portions of the interior crack surfaces (Figure 20iii (B)).

The sponge-like, etched appearance of the specimen surface, the presence of a heavy oxide covering, and the large brittle-like crack were more obvious signs of SCC (Figure 20iii (A)). The specimen surface characteristics fit with the behaviour of the load and potential values after the transition. The SCCF1 value of 2.51 and the SCER value of 5.02 $nm \cdot s^{-1}$ indicated a mix of ductile and brittle-like cracking behaviour.

The sponge-like appearance of the surface suggests that appropriate conditions for pitting may exist in the crack. If pitting occurs at the crack tip and the pit grows parallel to the crack propagation direction, then crack advance could be assisted by a tunnel growth mechanism (Jones and Ricker 1992). However, evidence of this crack growth mechanism may be obscured by corrosion of the fracture surface following the crack advance. The influence of stress on the direction of pit propagation has been demonstrated for etch-pit growth (Sieradzki and Kim 1992). The etched surfaces may be similar to the etch pitting reported by Sieradzki and Kim where specific micropitting conditions were correlated to SCC. Their experiments were performed on small, tensile specimens where the crack initiation process was an important step in the generation of SCC. This contrasts to the experiments reported here where the specimens contain a sharp fatigue crack to start an SCC crack. Also, Sieradzki and Kim completed their experiments in less than 1 h, minimizing the post-cracking corrosion of the fracture surface and allowing a more definite interpretation of the fracture process. Even with this short corrosion exposure following crack advance, the authors conceded that some features may have been compromised by corrosion following the crack advance.

The speciation of copper appears to influence the establishment of a stable oxide film suitable for SCC. The addition of chloride initially increases the solution copper concentration. The critical chloride concentration may depend upon the ammonia concentration if the SCC process is dependent upon the copper speciation. Detailed calculations to predict the stability of various complex copper species may prove useful for experimentally determining the critical ammonia/chloride concentration values (Ikeda and Litke 2004).

For comparison, a parallel experiment containing 0.5 mol·L^{-1} ammonia solution, but no chloride (CERT132, Figure 18iii) showed even more evidence of ductility along with the SCC. Multiple cracks were distributed throughout the ductile zone (Figure 18iii (A)) rather than a single central crack, as observed in CERT133 (Figure 20iii (A)). A potential transition occurred for CERT132, but the corresponding dramatic decrease in the load curve was not present (Figure 19). The SCCF1 value of 3.34 and the SCER value of 3.63 nm·s^{-1} (Table 11) lie in the middle of the mixed ductile and brittle-like crack growth range. Perhaps this is the result of selective dissolution (de-alloying) of the grain boundaries (Figure 18iii (A)) rather than the pitting seen in CERT133 (Figure 20iii (A)).

Thus, in the case of 1.0 mol·L^{-1} ammonia solutions with added copper, a 1:1 concentration ratio of chloride to ammonia is sufficient to suppress SCC. However, in a 0.5 mol·L^{-1} ammonia solutions with added copper, under an applied current density of 1 $\mu A/cm^2$, the results suggest that the addition of chloride contributes to film growth and enhances brittle-like failure.

3.2.2.2 Effect of Chloride Concentration in Solutions Containing 1.0 mol·L^{-1} Ammonia and 4 mmol·L^{-1} Copper under 1 $\mu A/cm^2$ Applied Current

In 2010, a test involving the addition of 0.1 mol·L^{-1} chloride to a 1.0 mol·L^{-1} ammonia solution (CERT134) was performed to complete the chloride addition series in 1.0 mol·L^{-1}ammonia containing 4 mmol·L^{-1} added copper, under an applied current density of 1 $\mu A \cdot cm^{-2}$ (Table 3). A trio of experiments had been performed in 1.0 mol·L^{-1} ammonia with 4 mmol·L^{-1} added copper without added chloride under an applied current density of 1 $\mu A/cm^2$, and all showed similar results (Table 12). CERT74 was chosen to represent this group, and its characteristics (Figure 18iv) have been described previously (Section 3.2.1). The specimen surface and crack overview images for this series are shown in Figure 22A and 22B, respectively, while the load curve and potential transient plot are shown in Figure 23A and 23B, respectively.

The addition of 0.1 mol·L^{-1} chloride (CERT134) to the 1.0 mol·L^{-1} ammonia environment caused very little change to the specimen appearance. The brown oxide film was present although it did not appear as thick, and a bright blue film was more predominant in the ductile zone (Figure 22ii (A)) and on the fatigue crack surfaces (Figure 22ii (B)). Some ductile characteristics were evident; the rounded crack region (Figure 22ii (A)), the narrowing of the specimen centre, and the bulging out of the specimen end (Figure 22ii (B)). The interior crack region was quite smooth in both cases. Brittle-like cracks were evident on the specimen surface (Figure 22ii (A)) and were just breaking through near to the crack tip (Figure 22ii (B)). The subtle differences between the specimens in CERT134 and CERT74 may simply be due to the shorter experiment time (342 h vs. 477 h, respectively). If, in fact, the brown oxide film continued to be deposited throughout the experiment, then that would account for the appearance of the underlying layer of blue film and its apparent darker colouration on CERT74 (Figure 22i (A)). The load curves were similar in shape, although the decrease in load was slightly steeper for CERT134 (Figure 23 (A)). The potential transition, which is indicative of brittle-like failure in ammonia solutions, occurred in both tests (Figure 23 (B)) but the transition for CERT134 coincided more directly with its change in load. The SCER values (5.13 nm s^{-1} vs. 4.81 nm·s^{-1} for CERT74) and the SCCF1 values (2.33 vs. 2.54 for CERT74) were in the same range and were indicative of a mixed ductile and brittle-like cracking mode of failure.

The addition of 0.5 mol·L^{-1} chloride (CERT109) to the same environment resulted in the creation of a darker brown/blue film over a considerable portion of both the specimen and crack surfaces (Figure 22iii (A & B)). A significant SCC crack travelled down the centre of the specimen. Although the shape of the load curve was quite different from CERT134, there was a steep decline in the load that corresponded to the transition in the potential transient plot (Figure 23). There was very little difference between the SCER (5.34 nm·s^{-1}) and SCCF1 (2.39) values of CERT109 when compared to the values for CERT134 noted above.

Upon adding 1.0 mol·L^{-1} chloride (CERT136) to the environment, changes to the sample characteristics and the cracking process took place. The heavier brown oxide coating and the various deposits of blue precipitate disappeared and were replaced by a thin, iridescent multicoloured coating (Figure 22iv (A)). Ductile tearing characteristics now dominated the physical appearance of the specimen (Figure 22iv (B)). Similarly, when the solution was saturated with chloride (CERT108), the specimen appearance was comparable to CERT136, but more visibly etched (Figure 22v (A)). The load curves from both experiments flattened-out after the maximum load, and the potential values remained more negative than -0.45 V, with no sign of the potential transition (Figure 23). The SCCF1 values (5.99 and 6.04, respectively), and the SCER values (2.04 and 1.98 nm·s^{-1}, respectively) were indicative of purely ductile tearing.

The presence of chloride in concentrations ≤ 0.5 mol·L^{-1} has little effect on the SCC behaviour of OFP copper in a 1.0 mol·L^{-1} ammonia solution containing 4 mmol·L^{-1} added copper under an applied current density of 1 $\mu A/cm^2$. A significant amount of chloride (≥ 1 mol·L^{-1}) must be added to the environment before there is suppression of SCC.

3.2.2.3 Effect of Chloride Concentration in Solutions Containing 0.5 mol·L^{-1} Ammonia and 4 mmol·L^{-1} Copper under 1 $\mu A/cm^2$ Applied Current

Two additional tests involving 0.5 mol·L^{-1} ammonia, one with no added chloride (CERT132) and one with the addition of 0.7 mol·L^{-1} chloride (CERT138), were also completed in 2010 (Table 3). All the test solutions in this series contained 4 mmol·L^{-1} added copper and were carried out

under an applied current density of 1 $\mu A/cm^2$. The specimen surface and crack overview images are shown in Figure 24A and 24B, respectively, while the load curve and potential transient plot are shown in Figure 25A and 25B, respectively.

As the conditions moved through the range of added chloride concentrations, the specimen appearance changed. The specimen surfaces went from marked etching of the grain boundaries (Figure 24i (A)) to a sponge-like covering of mainly large-sized pits (Figure 24ii (A)) and then to a finely pitted surface (Figure 24iii (A)). All specimens showed indications of ductility along with the presence of SCC cracks, but the severity of the cracking appeared higher in the chloride-containing solutions.

Increasing the chloride concentration from no added chloride to 0.7 $mol \cdot L^{-1}$ chloride increased the length of time to the potential transition in the potential transient plots (Figure 25 (B)). In the chloride containing tests, the beginning of the dramatic decrease in the load values corresponded to the time of the potential transition. All SCCF1 and SCER values for this series of tests were in the mixed ductile/brittle-like cracking region (Table 13).

There was no evidence of a blue film on the specimen exposed to the chloride-free environment, but as the amount of chloride increased the presence of the blue film also increased. The film characteristics in CERT133 (Figure 24ii (A & B)) were similar to those in CERT74 (Figure 22i (A & B)) where the blue film appeared darker and was covered by the brown oxide deposit. In the former however, the bright blue film also covered the ductile regions of the interior crack surface (Figure 24ii (B)) even though the experimental time was shorter (380 h vs. 477 h for CERT74). At the highest chloride concentration tested (0.7 mol L^{-1}, CERT138) the blue-grey film dominated the specimen surface (Figure 24iii). This effect may have been in part due to the longer test duration of 622 h.

In ammonia solution both cuprous and cupric-ammonia complexes can be formed. The thermodynamic analysis shows that the equilibria will be dominated by the $Cu(NH_3)_2^+$ complex for alkaline pH (Hoar and Rothwell 1970). As the concentration of copper increases in solution, the Cu_2O and CuO films become stable at lower pH and the boundary between the two films shifts to more positive potential. At a cupric ion concentration of ~ 8 $mmol \cdot L^{-1}$ the oxide films are stable at a pH near 12 and the boundary between the Cu_2O and CuO oxides is near -0.25 V. The more negative potentials initially observed are consistent with a bare copper surface, or a dominating Cu_2O layer on the surface. A shift to more positive potentials would indicate a thermodynamic shift to CuO films covering the surface. At potentials more positive than observed in this work, a stable, dominant CuO film would be expected to cover the specimen surface. However, in the intermediate potential range it is possible that the measured value is a mixed potential caused by a thermodynamic competition between regions of Cu_2O and CuO stability. Alternately, the potential may represent a thermodynamic state that has not been studied – a mixed Cu(I)/Cu(II) oxide layer. The presence of a mixed oxide layer, or a bi-layer, has been considered an important condition for SCC of copper (Maak and King 2006).

In this case, the chloride concentration may have been sufficiently high to cause localized depassivation of the surface oxide, but not high enough to cause wide-spread destruction of the film (Ikeda and Litke 2004). A localized depassivation of the passive layer would be a pit or crack initiation site and this chloride to ammonia ratio may be conducive to rapid pitting, similar to the crystallographic etch-pit growth reported by Sieradzki and Kim (1992). The stress corrosion cracking seen in their results was correlated with the development of uniform microscopic porosity driven by the effect of dynamic straining on the etch-pitting process. The

porous surface morphology and the cracking are obtained when a balance is achieved between the rate of corrosive attack, which is manifested as etch pitting, and the strain rate.

We had expected that adding a significant amount of chloride to the 0.5 mol·L^{-1} ammonia environment would decrease the susceptibility to SCC, as observed for the 1.0 mol·L^{-1} ammonia environment. However, the equivalent amount of chloride failed in this regard and even larger additions of chloride (0.7 mol·L^{-1}) still did not bring about the expected effect, SCC suppression. The body of results in chloride-containing ammonia environments suggest that a 1.0 mol·L^{-1} chloride concentration may be the critical concentration required for SCC suppression. These results also suggest that modelling chloride effects would be different for nitrite and ammonia.

4. CONCLUSION

SCC in nitrite appears to be a distinct and simple process. For the most part, there was very little attack on the specimen surface. A tightly adherent purple film was present, along with dramatic SCC cracks and very little ductile tearing. There were fewer examples of mixed ductile and brittle-like cracking failure in our nitrite test environments. The findings are as follows:

- SCC was evident in a range of deaerated nitrite concentrations between 0.1 mol·L^{-1} and 1.0 mol·L^{-1} at an applied current density of 1 $\mu A \cdot cm^{-2}$. Lower concentrations of nitrite ($\leq$ 0.01 mol·L^{-1}) appeared to be insufficient to induce SCC.
- Under the same conditions, ($\geq$ 0.1 mol·L^{-1} nitrite), a 1:1 chloride to nitrite concentration ratio suppressed SCC, as did an overabundance of chloride. High chloride concentrations appeared to increase uniform corrosion, which coincided with a blunting of the crack tip.
- In a deaerated 0.1 mol·L^{-1} nitrite solution, the susceptibility to SCC appeared to decrease with increasing chloride concentration, and increase with increasing applied current density (0.01 $\mu A \cdot cm^{-2}$ to 1 $\mu A \cdot cm^{-2}$).
- Steady-state potential values became more negative with increasing chloride concentration regardless of the nitrite concentration.

SCC in ammonia was always accompanied by some degree of ductile tearing prior to failure. Specimen surfaces were attacked or etched. A minimum concentration of copper appeared to be a prerequisite for SCC. The addition of copper to the test solution increased the reproducibility of the tests. The findings are as follows:

- SCC was evident in a range of ammonia concentrations between 0.3 mol·L^{-1} and 1.0 mol·L^{-1}, while a concentration of 0.1 mol·L^{-1} ammonia did not induce SCC. A concentration of 0.3 mol·L^{-1} ammonia appears to approach the threshold concentration required for SCC.
- In a 1.0 mol·L^{-1} ammonia solution, a 1:1 chloride to ammonia concentration ratio suppressed SCC, as did an overabundance of chloride. The addition of chloride in concentrations $\leq$ 0.5 mol·L^{-1} has little effect on SCC.
- In a 0.5 mol·L^{-1} ammonia solution, a 1:1 chloride to ammonia concentration ratio appeared to enhance SCC . The addition of 0.7 mol·L^{-1} chloride did not bring about SCC suppression.

A minimum concentration of copper in solution is needed for SCC in ammonia but not necessary for SCC in nitrite. Saturated chloride appears to suppress SCC in both environments. In nitrite solutions a 1:1 chloride to nitrite concentration ratio brings about SCC suppression. However in 0.5 $mol \cdot L^{-1}$ ammonia, SCC was not suppressed at that same 1:1 concentration ratio. The body of results from the ammonia work suggest that there may be a threshold concentration of 1.0 $mol \cdot L^{-1}$ chloride required for SCC suppression rather than a concentration ratio. These results also suggest that modelling chloride effects would be different for nitrite and ammonia.

ACKNOWLEDGEMENTS

This work was funded by the Nuclear Waste Management Organization. The authors wish to acknowledge the support and assistance of G. Kwong throughout this project. We also wish to acknowledge R. Herman, C. Kryschuk and N. LaRue for performing the chemical analysis, K.D. Jackson for instrumentation support, D.P. Godin for fatiguing the CT specimens, J.P.L. David for the preparation of specimens, and K. Lodge for SSR rig maintenance.

REFERENCES

ASTM. 1994. Standard test method for plane-strain fracture toughness of metallic materials, 1994 Annual Book of ASTM Standards, Section 3, Volume 03.01. American Society for Testing and Materials, Philadelphia, PA, E 399-90.

Benjamin, L.A., D. Hardie and R.N. Parkins. 1988. Stress corrosion resistance of pure coppers in ground waters and sodium nitrite. British Corrosion Journal, 23(2). 89-95.

Bertocci, U., E.N. Pugh, and R.E. Ricker. 1990. Environment-induced cracking of copper alloys. In Environment-Induced Cracking of Metals, NACE-10, (Editors R.P. Gangloff and M.B. Ives). National Association of Corrosion Engineers, Houston Tx. pp. 273-285.

Cassagne, T.B., J. Kruger, and E.N. Pugh. 1990. Role of the oxide film in the transgranular stress corrosion cracking of copper. In Environmentally Assisted Cracking: Science and Engineering, ASTM STP 1049. (Editors, W.B. Lisagor, T.W. Crooker, and B.N. Leis). American Society for Testing and Materials, Philadelphia, PA. pp. 59-75.

Hoar, T.P. and G.P. Rothwell. 1970. The potential/pH diagram for a copper-water-ammonia system: Its significance in the stress-corrosion cracking of brass in ammoniacal solution. Electrochimica Acta 15, 1037-1045.

Ikeda, B.M. and C.D. Litke. 2000. The effect of oxidant flux, nitrite concentration and chloride concentration on the stress corrosion cracking behaviour of non-welded and electron-beam welded copper. Prepared by Atomic Energy of Canada Limited for Ontario Power Generation. Ontario Power Generation, Nuclear Waste Management Division Report 06819-REP-01200-10049-R00. Toronto, Ontario.

Ikeda, B.M. and C.D. Litke. 2001. The measurement of corrosion parameters on oxygen-free phosphorous-doped copper in nitrite solutions. Prepared by Atomic Energy of Canada Limited for Ontario Power Generation, Nuclear Waste Management Division Report 06819-REP-01300-10033-R00. Toronto, Ontario.

Ikeda, B.M. and C.D. Litke. 2004. Status report for 2003 on Stress corrosion cracking of OFP copper in ammonia. Prepared by Atomic Energy of Canada Limited for Ontario Power Generation. Ontario Power Generation, Nuclear Waste Management Division Report 06819-REP-01300-10078-R00. Toronto, Ontario.

Ikeda, B.M. and C.D. Litke. 2008. The effect of high chloride concentration on stress corrosion cracking behaviour of copper. Nuclear Waste Management Organization Report NWMO TR-2008-12. Toronto, Ontario.

Jones, R.J., and R.E. Ricker. 1992. "Mechanisms of stress-corrosion cracking". In Stress Corrosion Cracking. Ed. R.H. Jones. ASM International, Materials Park, OH. pp. 1-40.

King, F., L. Ahonen, C. Taxén, U. Vuorinen, and L. Werme. 2001. Copper corrosion under expected conditions in a deep geologic repository. Swedish Nuclear Fuel and Waste Management Company Report, SKB TR-01-23 (also published by Posiva 2002-01).

King, F. and M. Kolar. 2005. Preliminary assessment of the stress corrosion cracking of used fuel disposal containers using the CCM-SCC.0 model. Ontario Power Generation, Nuclear Waste Management Division Report 06819-REP-01300-10103-R00. Toronto, Ontario.

King, F. and C.D. Litke. 1997. Stress corrosion cracking of copper – Report on experimental methodologies and preliminary results. Prepared by Atomic Energy of Canada Limited for Ontario Hydro. Ontario Hydro, Nuclear Waste Management Division Report 06819-REP-01200-0010-R00. Toronto, Ontario.

King, F., C.D. Litke and B.M. Ikeda. 1999a. The effects of oxidant supply and chloride ions on the stress corrosion cracking of copper. Ontario Power Generation, Nuclear Waste Management Division Report 06819-REP-01200-10013-R00. Toronto, Ontario.

King, F., G. Greidanus and D.J. Jobe. 1999b. Dissolution of copper in chloride/ammonia mixtures and the implications for the stress corrosion cracking of copper containers. Atomic Energy of Canada Report, AECL-11865, COG-97-412-I.

Litke, C.D., and B.M. Ikeda. 2006. The effect of acetate concentration, chloride concentration, and applied current on stress corrosion cracking of OFP copper. Ontario Power Generation, Nuclear Waste Management Division Report 06819-REP-01300-10005-R00. Toronto, Ontario.

Litke, C.D., and B.M. Ikeda. 2008. The stress corrosion cracking behaviour of copper in acetate solutions. Nuclear Waste Management Organization Report NWMO TR-2008-21. Toronto, Ontario.

Maak, P. 1999. The selection of a corrosion-barrier primary material for used-fuel disposal containers. Ontario Power Generation, Nuclear Waste Management Division Report 06819-REP-01200-10020 R00. Toronto, Ontario.

Maak, P and F. King 2006. A model for predicting stress corrosion cracking of copper containers in a deep geologic repository. In Materials Research Society Symposium Proceedings Volume 932, Materials Research Society, Warrendale, PA pp. 837-843.

Sieradzki, K. and J.S. Kim. 1992. Etch pitting and stress-corrosion cracking of copper. Acta Metallurgia et Materiallia, 40(4), 625-635.

Table 1: Summary of Nitrite Experiments Performed in 2009/2010*

Test Number	[Nitrite] $mol \cdot L^{-1}$	[Chloride] $mol \cdot L^{-1}$	pH Initial	pH Final	Conditions	Sol'n [Cu]† (in Solution) $mmol \cdot L^{-1}$	E_{corr} Final mV	E_{red} Final mV	Total Time h	K_Q $MPa \cdot m^{½}$	SCCF1	Crack Velocity $mm \cdot a^{-1}$	Crack Velocity $nm \cdot s^{-1}$
CERT122	0.5	0	9.0	8.7	1 $\mu A/cm^2$	<0.010	56	48	163.2	19.2	1.01	371	11.8
CERT123	0.5	0.5	9.0	9.5	1 $\mu A/cm^2$	0.292	-210	49	593.6	23.2	5.60	64.7	2.05
CERT124	1.0	0	9.0	8.7	1 $\mu A/cm^2$	<0.010	51	63	99.3	18.7	0.70	581	18.5
CERT125	1.0	1.0	9.0	9.2	1 $\mu A/cm^2$	1.22	-249	60	335.9	23.3	6.20	58.5	1.85
CERT126	0.1	1.0	9.0	8.8	1 $\mu A/cm^2$	<0.010	-240	80	431.1	24.2	5.52	67.5	2.14
CERT127	0.1	0	9.1	8.4	OCP	<0.010	21	86	339.6	25.9	3.46	111	3.53
CERT128	1.0	Sat'd	9.0	9.7	1 $\mu A/cm^2$	0.012	-366	-11	407.3	25.6	4.84	76.6	2.43
CERT129	1.0	0	9.1	9.0	1 $\mu A/cm^2$	0.013	50	59	192.4	16.7	1.18	328	10.4
CERT130	1.0	0.05	9.1	7.5	1 $\mu A/cm^2$	0.008	38	65	230.9	23.5	1.72	224	7.10

* All experiments performed in deaerated solutions at 22 ± 2°C, at a cross-head speed of 8.5×10^{-6} $mm \cdot s^{-1}$ with SKB4 compact tension specimens cut from plate, Section B2, in a T-S orientation

† 2σ error interval ± 10% for CERT125; ± 11% for CERT123; ± 17% for CERT129; ± 27% for CERT130; ± 27% for CERT128.

Table 2: Summary of Observations for 2009/2010 Nitrite Experiments

Test number	[Nitrite] $mol \cdot L^{-1}$	[Chloride] $mol \cdot L^{-1}$	pH	Current $\mu A \cdot cm^{-2}$	SCER $nm \cdot s^{-1}$	SCCF1	SCC	Observed Crack*	Observed Surface*
CERT122	0.5	0	9	1	11.8	1.01	yes	2 large SCC cracks, multiple secondary cracks	Surface mottled with some bright exposed portions and mainly adherent blue/brown film. Some blue/green crystals present. Crack surface granular with red/brown film.
CERT123	0.5	0.5	9	1	2.05	5.60	no	ductile, blunt tip	Surface covered in red/brown film, some portions loosely adherent. Blue/green crystals on ductile portion of specimen surface and on interior crack surfaces.
CERT124	1.0	0	9	1	18.5	0.70	yes	multiple large SCC cracks and small secondary cracks	Surface and interior of crack covered in adherent purple/brown film.
CERT125	1.0	1.0	9	1	1.85	6.20	no	ductile, blunt tip	Surface covered in red/brown film, some portions loosely adherent. Blue/green crystals on ductile portion of specimen surface.
CERT126	0.1	1.0	9	1	2.14	5.52	no	ductile, some surface dislocations	Surface covered in brown to purple/brown adherent film. Dark purple on crack surfaces. Blue/green crystals on some portions of specimen.
CERT127	0.1	0	9	OCP	3.53	3.46	yes	large SCC crack, multiple secondary cracks in ductile zone	Surface mottled with some tarnished exposed portions and mainly adherent blue/brown film. Crack surface coarse with purple/brown film.
CERT128	1.0	Sat'd	9	1	2.43	4.84	no	ductile, blunt tip	Specimen tarnished with orange, yellow and blue portions and remainder covered in blue/grey film. Crack surfaces covered with orange and blue tarnish.
CERT129	1.0	0	9	1	10.4	1.18	yes	large SCC cracks, multiple secondary cracks in ductile zone	Specimen covered in purple /brown adherent film with some loosely adherent green star-like crystals. Some blue/green crystals on interior crack surfaces.
CERT130	1.0	0.05	9	1	7.10	1.72	yes	multiple large SCC cracks and numerous secondary cracks	Surface covered in adherent brown film with additional variegated purple, red and green areas. Blue/green crystals on interior of crack and surface crack edges.

*See Figures 2, 4, 6, 11, and 13

Table 3: Summary of Ammonia Experiments Performed in 2010*

Test Number	[Ammonia] $mol \cdot L^{-1}$	[Chloride] $mol \cdot L^{-1}$	pH Initial	pH Final	Conditions	[Cu]† (in Solution) $mmol \cdot L^{-1}$	E_{corr} Final mV	E_{red} Final mV	Total Time h	K_Q $MPa \cdot m^{½}$	SCCF1	Crack Velocity $mm \cdot a^{-1}$	Crack Velocity $nm \cdot s^{-1}$
CERT131	0.1	0	10.8	10.9	1 $\mu A/cm^2$	2.92	-272	76	600.1	25.9	5.17	75.4	2.39
CERT132	0.5	0	11.7	12.2	1 $\mu A/cm^2$	23.1	-164	-90	524.6	23.3	3.34	114	3.63
CERT133	0.5	0.5	11.8	12.1	1 $\mu A/cm^2$	25.0	-144	-52	379.5	23.9	2.51	158	5.02
CERT134	1.0	0.1	12.1	12.6	1 $\mu A/cm^2$	29.1	-256	-111	341.8	25.6	2.33	162	5.13
CERT136	1.0	1.0	12.0	12.5	1 $\mu A/cm^2$	36.2	-458	-341	503.6	21.4	5.99	64.3	2.04
CERT137	0.3	0	11.4	11.6	1 $\mu A/cm^2$	11.8	-202	-152	456.1	23.4	3.66	93.2	2.96
CERT138	0.5	0.7	11.8	12.3	1 $\mu A/cm^2$	34.6	-244	-225	622.2	23.4	2.88	106.9	3.39

* All experiments performed in deaerated solutions containing 4 $mmol \cdot L^{-1}$ added copper at 22 ± 2°C, at a cross-head speed of 8.5×10^{-6} $mm \cdot s^{-1}$ with SKB4 compact tension specimens cut from plate, Section B2, in a T-S orientation

† 2σ error interval ± 9% for CERT138; ± 10% for CERT131, CERT132, CERT133, CERT134; ± 11% for CERT137; ± 13% for CERT136

Table 4: Summary of Observations for 2010 Ammonia Experiments

Test number	[Ammonia][1] $mol \cdot L^{-1}$	[Chloride] $mol \cdot L^{-1}$	pH	Current $\mu A \cdot cm^{-2}$	SCER $nm \cdot s^{-1}$	SCCF1	SCC	Observed Crack*	Observed Surface*
CERT131	0.1	0	10.8	1	2.39	5.17	no	Ductile tearing, blunt tip	Heavy etching on exposed surfaces of specimen. Surface golden brown. Fresh pink/brown colouration on inner crack surface with evidence of black precipitate on fatigue crack.
CERT132	0.5	0	11.7	1	3.63	3.34	yes	Multiple SCC cracks, initial ductile tearing prior to cracking	Grain boundaries heavily etched as well as etching of grains on surface of specimen. Brown/black precipitate in etched grain boundaries.
CERT133	0.5	0.5	11.8	1	5.02	2.51	yes	Several major SCC cracks and smaller secondary cracks.	Heavy attack on exposed portions of specimen. Evidence of grain fallout. Specimen covered in brown precipitate with patches of blue/grey. Some areas of golden brown iridescence on ductile surfaces.
CERT134	1.0	0.1	12.1	1	5.13	2.33	yes	Two main SCC cracks and small secondary cracks	Fine etching of specimen surface with overall brown precipitate. Patches of blue precipitate on specimen and crack surfaces. Crack surface golden brown.
CERT136	1.0	1.0	12.0	1	2.04	5.99	no	Ductile tearing, blunt crack tip.	Specimen surface is etched, but edges are smoothed out. Iridescent surface film, mainly brown in colour.
CERT137	0.3	0	11.4	1	2.96	3.66	yes	Multiple SCC cracks, multiple secondary cracks in ductile zone	Attack on exposed portions of specimen with surface brown to golden brown. Evidence of grain fallout. Crack surface relatively smooth.
CERT138	0.5	0.7	11.8	1	3.39	2.88	yes	One main SCC crack with secondary cracks.	Specimen etched and coated with dark blue/green covering which has bright turquoise blue precipitate on top of it. Cracks on surface away from ductile zone – may be in surface precipitate or on raised grain boundaries.

[1] All solutions contain 4 $mmol \cdot L^{-1}$ added copper.
*See Figures 18, 20, 22, and 24

Table 5: Summary of Comparative Experimental Results as a Function of Nitrite Concentrations*

Test Number	Section	[Nitrite] $mol \cdot L^{-1}$	[Cl] ‡ (in Solution) $mol \cdot L^{-1}$	Log [Cl] (in Solution) $mol \cdot L^{-1}$	[Cu]† (in Solution) $mmol \cdot L^{-1}$	E_{corr} Final mV	E_{red} Final mV	Total Time h	K_Q $MPa \cdot m^{½}$	SCCF1	Crack Velocity $mm \cdot a^{-1}$	Crack Velocity $nm \cdot s^{-1}$
CERT50	B2	0.001	0.001	-2.87	<0.002	80	n/a	381.7	23.6	5.49	66.5	2.11
CERT51	B2	0.01	0.001	-2.96	<0.002	-157	n/a	312.5	22.9	8.05	44.5	1.41
CERT43	C2	0.1	n/a	n/a	0.002	122	n/a	168.0	16.2	1.34	280	8.86
CERT38 (W)	C2	0.1	0.0003	-3.60	0.003	137	n/a	281.9	7.75	1.73	226	7.19
CERT46 (W)	C2	0.1	n/a	n/a	0.006	119	n/a	167.0	9.17	1.23	291	9.24
CERT122	B2	0.5	<0.0001	-4.07	<0.002	56	48	163.2	19.2	1.01	371	11.8
CERT124	B2	1.0	<0.0001	-4.07	<0.002	51	63	99.3	18.7	0.70	581	18.5

* All experiments performed in deaerated solutions under an applied current density of 1 $\mu A/cm^2$ at 22 ± 2°C, at a cross-head speed of 8.5×10^{-6} $mm \cdot s^{-1}$ with SKB4 compact tension specimens cut from plate, Sections B2 and C2, in a T-S orientation except for CERT43, CERT46, and CERT38 in L-T orientation.
(W) refers to a welded specimen.

‡ 2σ error interval CERT50 ± 29%; CERT51 ± 36%

† 2σ error interval ± 10%

n/a not available

Table 6: Summary of Comparative Experimental Results for the Effect of 1:1 Chloride to Nitrite Concentration Ratio*

Test Number	[Nitrite] $mol \cdot L^{-1}$	[Cl] $mol \cdot L^{-1}$	[Cu]† (in Solution) $mmol \cdot L^{-1}$	E_{corr} Final mV	E_{red} Final mV	Total Time h	K_Q $MPa \cdot m^{½}$	SCCF1	Crack Velocity $mm \cdot a^{-1}$	Crack Velocity $nm \cdot s^{-1}$
CERT33	0.01	0.01	0.002	50	n/a	334.4	22.4	5.23	70.3	2.23
CERT35	0.1	0.1	0.008	-135	n/a	331.9	21.0	5.62	65.6	2.08
CERT123	0.5	0.5	0.070	-210	49	593.6	23.2	5.60	64.7	2.05
CERT125	1.0	1.0	0.293	-249	60	335.9	23.3	6.20	58.5	1.85

* All experiments performed in deaerated solutions under an applied current density of 1 $\mu A/cm^2$ at 22 ± 2°C, at a cross-head speed of 8.5×10^{-6} $mm \cdot s^{-1}$ with SKB4 compact tension specimens cut from plate, Section B2 in a T-S orientation.

† 2σ error interval ± 11% for CERT123; ± 10% for CERT33, CERT35 and CERT125

n/a not available

Table 7: Summary of Comparative Experimental Results for the Effect of Chloride Concentration in Nitrite Solutions*

Test Number	Section	[Nitrite] $mol \cdot L^{-1}$	Added [Cl] $mol \cdot L^{-1}$	[Cl] ‡ (in Solution) $mol \cdot L^{-1}$	Log [Cl] (in Solution) $mol \cdot L^{-1}$	[Cu]† (in Solution) $mmol \cdot L^{-1}$	E_{corr} Final mV	E_{red} Final mV	Total Time h	K_Q $MPa \cdot m^{½}$	SCCF1	Crack Velocity $mm \cdot a^{-1}$	Crack Velocity $nm \cdot s^{-1}$
CERT43	C2	0.1	0	n/a	n/a	0.002	122	n/a	168.0	16.2	1.34	280	8.86
CERT124	B2	1.0	0	<0.0006	-4.07	<0.003	51	63	99.3	18.7	0.70	581	18.5
CERT129	B2	1.0	0	0.013	-1.89	0.013	50	59	192.4	16.7	1.18	328	10.4
CERT30	B2	0.1	0.001	0.001	-3.00	0.009	n/a	n/a	69.3	21.5	1.37	241	7.66
CERT29	B2	0.1	0.01	0.008	-2.10	0.013	70	n/a	333.2	26.3	2.70	139	4.40
CERT40 (W)	C2	0.1	0.01	0.008	-2.05	0.004	64	n/a	334.7	7.64	2.88	130	4.11
CERT49 (W)	C2	0.1	0.01	0.01	-2.00	0.005	49	n/a	382.6	10.1	3.03	114	3.60
CERT34	B2	0.001	0.01	0.009	-2.05	<0.001	n/a	n/a	335.9	23.5	5.46	65.8	2.09
CERT33	B2	0.01	0.01	0.01	-2.00	0.002	50	n/a	334.4	22.4	5.23	70.3	2.23
CERT35	B2	0.1	0.1	0.13	-0.89	0.008	-135	n/a	331.9	21.0	5.62	65.6	2.08
CERT130	B2	1.0	0.05	0.053	-1.28	0.007	38	65	230.9	23.5	1.72	224	7.10
CERT123	B2	0.5	0.5	0.42	-0.38	0.072	-210	49	593.6	23.2	5.60	64.7	2.05
CERT126	B2	0.1	1.0	1.02	0.01	<0.003	-240	80	431.1	24.2	5.52	67.5	2.14
CERT125	B2	1.0	1.0	0.76	-0.11	0.302	-249	60	335.9	23.3	6.20	58.5	1.85
CERT107	B2	0.1	Sat'd	5.78	0.76	0.27	-374	8	428.2	20.0	6.54	55.7	1.77
CERT128	B2	1.0	Sat'd	4.63	0.67	0.003	-366	-11	407.3	25.6	4.84	76.6	2.43

* All experiments performed in deaerated solutions under an applied current density of 1 $\mu A/cm^2$ at 22 ± 2°C, at a cross-head speed of 8.5 x 10^{-6} $mm \cdot s^{-1}$ with SKB4 compact tension specimens cut from plate, Sections B2 and C2, in a T-S orientation except for CERT40, CERT43, and CERT49, L-T orientation. (W) - welded specimen.

‡ 2σ error interval ± 10% for CERT29, CERT34, CERT40, CERT107, CERT123, CERT128, CERT129, CERT130; ± 11% for CERT33, CERT35, CERT125, CERT126; ± 40% for CERT30

† 2σ error interval ± 10% except CERT123 ± 11%; CERT128 ± 32%; CERT129 ± 17%; CERT130 ± 27%

Table 8: Summary of Comparative Experimental Results for the Effect of Applied Current Density and OCP in 0.1 mol·L^{-1} Nitrite*

Test Number	Section	[Nitrite] mol·L^{-1}	Current μA·cm^{-2}	[Cl]‡ (in Solution) mol·L^{-1}	Log [Cl] (in Solution) mol·L^{-1}	[Cu]† (in Solution) mmol·L^{-1}	E_{corr} Final mV	E_{red} Final mV	Total Time h	K_Q MPa·m^{½}	SCCF1	Crack Velocity mm·a^{-1}	Crack Velocity nm·s^{-1}
CERT43	C2	0.1	1	n/a	n/a	0.002	122	n/a	168.0	16.2	1.34	280	8.86
CERT27	B2	0.1	1	n/a	n/a	0.009	40	n/a	257.7	23.4	1.66	229	7.27
CERT38 (W)	C2	0.1	1	<0.001	n/a	0.003	137	n/a	281.9	7.75	1.73	226	7.19
CERT46 (W)	C2	0.1	1	n/a	n/a	0.006	119	n/a	167.0	9.17	1.23	291	9.24
CERT28	B2	0.1	0.1	n/a	n/a	0.002	110	n/a	238.1	22.3	2.23	172	5.46
CERT26	B2	0.1	0.1	<0.001	n/a	0.002	93	n/a	211.7	24.3	2.36	161	5.10
CERT39 (W)	C2	0.1	0.1	n/a	n/a	0.003	91	n/a	216.6	8.01	2.04	184	5.84
CERT47 (W)	C2	0.1	0.1	n/a	n/a	0.001	102	n/a	262.3	8.98	2.43	151	4.78
CERT58	B2	0.1	0.01	0.0003	-3.44	0.003	7	n/a	189.7	21.1	3.10	121	3.83
CERT31	B2	0.1	0.01	0.001	-3.17	0.001	55	n/a	431.4	24.5	3.36	92	2.91
CERT41 (W)	C2	0.1	0.01	<0.001	n/a	0.002	85	n/a	287.4	8.03	2.73	140	4.44
CERT48 (W)	C2	0.1	0.01	<0.001	-3.77	0.003	74	n/a	335.7	8.78	2.98	124	3.92
CERT32	B2	0.1	OCP	<0.001	-3.32	0.004	85	n/a	430.0	20.8	2.97	109	3.47
CERT127	B2	0.1	OCP	0.001	-3.03	<0.003	21	86	339.6	25.9	3.46	111	3.53
CERT88	B2	0.1	OCP	0.002	-2.74	<0.001	-17	64	480.2	19.6	5.75	104	3.30

* All experiments performed in deaerated solutions at 22 ± 2°C, at a cross-head speed of 8.5 x 10^{-6} mm·s^{-1} with SKB4 compact tension specimens cut from plate, Sections B2 and C2, in a T-S orientation except for CERT38, CERT39, CERT41, CERT43, CERT46, CERT47 and CERT48, L-T orientation. (W) refers to a welded specimen.

‡ 2σ error interval ± 10% for CERT58; CERT31, CERT88; ± 42% for CERT127

† 2σ error interval ± 10%

n/a not available

Table 9: Summary of Comparative Experimental Results for the Effect of Added Copper in Nitrite Solutions*

Test Number	[Nitrite] $mol \cdot L^{-1}$	[Cu] $mmol \cdot L^{-1}$	[Cu]† (in Solution) $mmol \cdot L^{-1}$	E_{corr} Final mV	E_{red} Final mV	Total Time h	K_Q $MPa \cdot m^{1/2}$	SCCF1	Crack Velocity $mm \cdot a^{-1}$	Crack Velocity $nm \cdot s^{-1}$
CERT89	0.1	8	6.6	50	289	306.8	23.7	0.95	153	4.84
CERT32	0.1	0	0.004	85	n/a	430.0	20.7	2.97	109	3.47
CERT127	0.1	0	<0.002	21	86	339.6	25.6	3.46	111	3.53

* All experiments performed in deaerated solutions under freely corroding conditions at 22 ± 2°C, at a cross-head speed of 8.5×10^{-6} $mm \cdot s^{-1}$ with SKB4 compact tension specimens cut from plate, Section B2 in a T-S orientation.

† 2σ error interval ± 10%

n/a not available

Table 10: Summary of Comparative Experimental Results for Effect of Ammonia Concentration*

Test Number	[Ammonia] $mol \cdot L^{-1}$	[Cl] ‡ (in Solution) $mol \cdot L^{-1}$	[Cu]† (Added) $mmol \cdot L^{-1}$	[Cu]† (in Solution) $mmol \cdot L^{-1}$	E_{corr} Final mV	E_{red} Final mV	Total Time h	K_Q $MPa \cdot m^{½}$	SCCF1	Crack Velocity $mm \cdot a^{-1}$	Crack Velocity $nm \cdot s^{-1}$
CERT131	0.1	0.001	4	2.93	-272	76	600.1	25.88	5.17	75.4	2.39
CERT137	0.3	n/a	4	11.8	-202	-152	456.1	23.40	3.66	93.2	2.96
CERT132	0.5	0.001	4	23.1	-164	-90	524.6	23.31	3.34	114.4	3.63
CERT74	1.0	0.003	4	26.8	-268	-242	476.6	23.28	2.54	151.8	4.81
CERT70	1.0	0.012	4	27.1	-267	-250	501.4	23.67	3.24	122.5	3.88
CERT76	1.0	0.001	4	31.5	-265	-259	575.4	24.21	2.55	108.6	3.44

* All experiments performed in naturally aerated solutions under an applied current density of 1 $\mu A/cm^2$ at 22 ± 2°C, at a cross-head speed of 8.5×10^{-6} $mm \cdot s^{-1}$ with SKB4 compact tension specimens cut from plate, Sections B2, in a T-S orientation.

‡ 2σ error interval ± 6% for CERT76; ± 7% for CERT70, CERT74; ± 10% for CERT131, CERT132

† 2σ error interval ± 9% for CERT70; ± 10% for CERT131, CERT132; ± 11% for CERT137; ± 12% for CERT74; ± 15% for CERT76

n/a not available

Table 11: Summary of Comparative Experimental Results for Effect of 1:1 Chloride to Ammonia Concentration Ratio*

Test Number	[Ammonia] $mol \cdot L^{-1}$	Current $\mu A \cdot cm^{-2}$	[Cl] ‡ (in Solution) $mol \cdot L^{-1}$	[Cu]† (Added) $mmol \cdot L^{-1}$	[Cu]† (in Solution) $mmol \cdot L^{-1}$	E_{corr} Final mV	E_{red} Final mV	Total Time h	K_Q $MPa \cdot m^{½}$	SCCF1	Crack Velocity $mm \cdot a^{-1}$	Crack Velocity $nm \cdot s^{-1}$
CERT81	1.0	OCP	1.07	8	47.2	-438	-347	623.1	24.27	5.58	63.4	2.01
CERT136	1.0	1	1	4	36.2	-458	-341	503.6	21.42	5.99	64.3	2.04
CERT78	1.0	OCP	0.002	8	29.9	-239	-224	262.7	25.58	1.89	211.9	6.71
CERT74	1.0	1	0.003	4	26.8	-268	-242	476.6	23.28	2.54	151.8	4.81
CERT133	0.5	1	0.54	4	25.0	-144	-52	379.5	23.93	2.51	158.4	5.02
CERT132	0.5	1	0.001	4	23.1	-164	-90	524.6	23.31	3.34	114.4	3.63

* All experiments performed in naturally aerated solutions at 22 ± 2°C, at a cross-head speed of 8.5×10^{-6} mm•s^{-1} with SKB4 compact tension specimens cut from plate, Sections B2, in a T-S orientation.

‡ 2σ error interval ± 7% for CERT74, CERT78; ± 8% for CERT81; ± 10%for CERT132, CERT133

† 2σ error interval ± 10% for CERT132, CERT133;± 12% for CERT74; ± 13% for CERT81, CERT136; ± 16% for CERT78

Table 12: Summary of Comparative Experimental Results for Effect of Chloride Concentration in 1.0 mol·L^{-1} Ammonia*

Test Number	[Ammonia] mol·L^{-1}	[Cl] ‡ (in Solution) mol·L^{-1}	[Cu]† (in Solution) mmol·L^{-1}	E_{corr} Final mV	E_{red} Final mV	Total Time h	K_Q MPa·m^{½}	SCCF1	Crack Velocity mm·a^{-1}	Crack Velocity nm·s^{-1}
CERT74	1.0	0.003	26.8	-268	-242	476.6	23.28	2.54	151.8	4.81
CERT134	1.0	0.11	29.1	-256	-111	341.8	25.58	2.33	161.7	5.13
CERT109	1.0	0.68	45.6	-285	43	432.0	21.21	2.39	168.6	5.34
CERT136	1.0	1.0$^{\#}$	36.2	-458	-341	503.6	21.42	5.99	64.3	2.04
CERT108	1.0	4.8	42.5	-462	-277	502.7	21.95	6.04	62.6	1.98

* All experiments performed in naturally aerated solutions with 4 mmol·L^{-1} added copper, under an applied current density of 1 μA/cm^2 at 22 ± 2°C, at a cross-head speed of 8.5 x 10^{-6} mm·s^{-1} with SKB4 compact tension specimens cut from plate, Sections B2, in a T-S orientation.

‡ 2σ error interval ± 10%; except for CERT109 ± 8%,

† 2σ error interval ± 10%; except for CERT108 ± 11%; CERT136 ± 13%

\# Added chloride concentration

Table 13: Summary of Comparative Experimental Results for Effect of Chloride Concentration in 0.5 mol·L^{-1} Ammonia*

Test Number	[Ammonia] mol·L^{-1}	[Cl] ‡ (in Solution) mol·L^{-1}	[Cu]† (in Solution) mmol·L^{-1}	E_{corr} Final mV	E_{red} Final mV	Total Time h	K_Q MPa·m^{½}	SCCF1	Crack Velocity mm·a^{-1}	Crack Velocity nm·s^{-1}
CERT132	0.5	0.001	23.1	-164	-90	524.6	23.31	3.34	114.4	3.63
CERT133	0.5	0.54	25.0	-144	-52	379.5	23.93	2.51	158.4	5.02
CERT138	0.5	0.7$^{\#}$	34.6	-244	-225	622.2	23.43	2.88	106.9	3.39

* All experiments performed in naturally aerated solutions with 4 mmol·L^{-1} added copper, under an applied current density of 1 μA/cm^2 at 22 ± 2°C, at a cross-head speed of 8.5 x 10^{-6} mm·s^{-1} with SKB4 compact tension specimens cut from plate in a T-S orientation.

‡ 2σ error interval ± 10%

† 2σ error interval ± 10% except for CERT138 ± 9%

\# Added chloride concentration

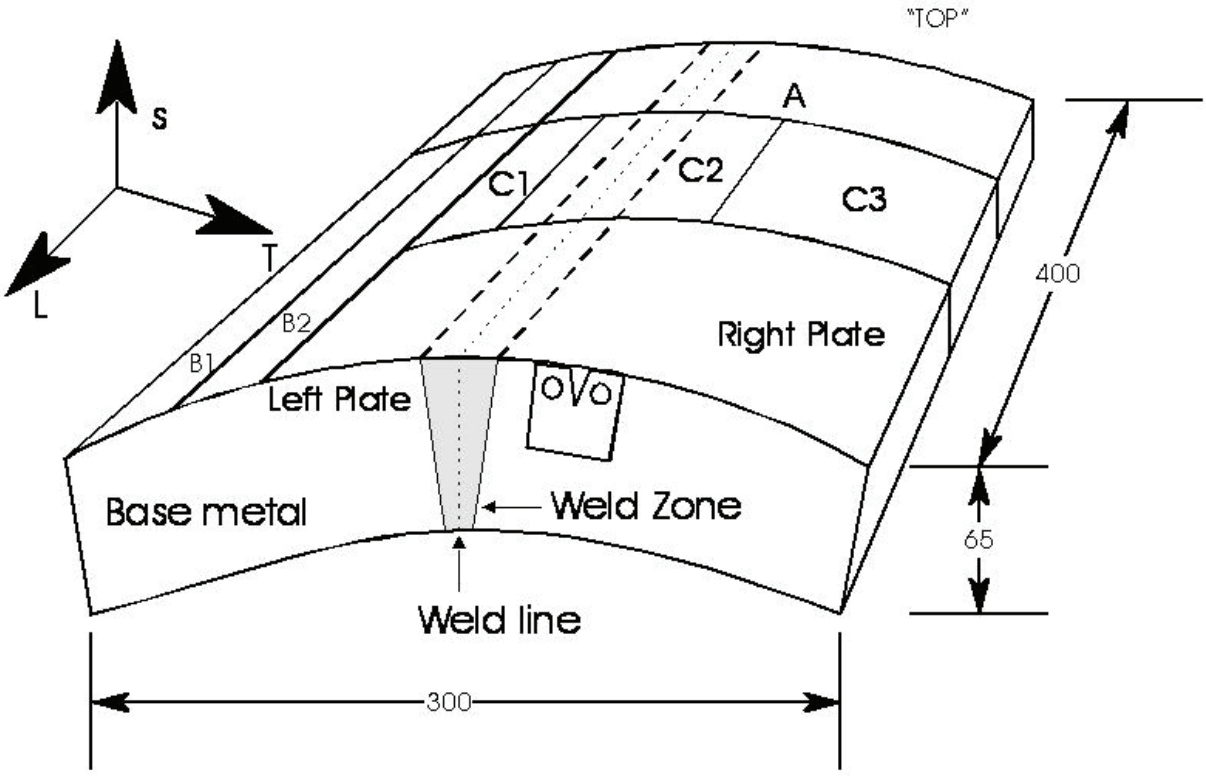

Figure 1: Schematic of SKB4 Plate Material Showing the Location of Specimen Cuts
Example of CT specimen is shown in T-S orientation.

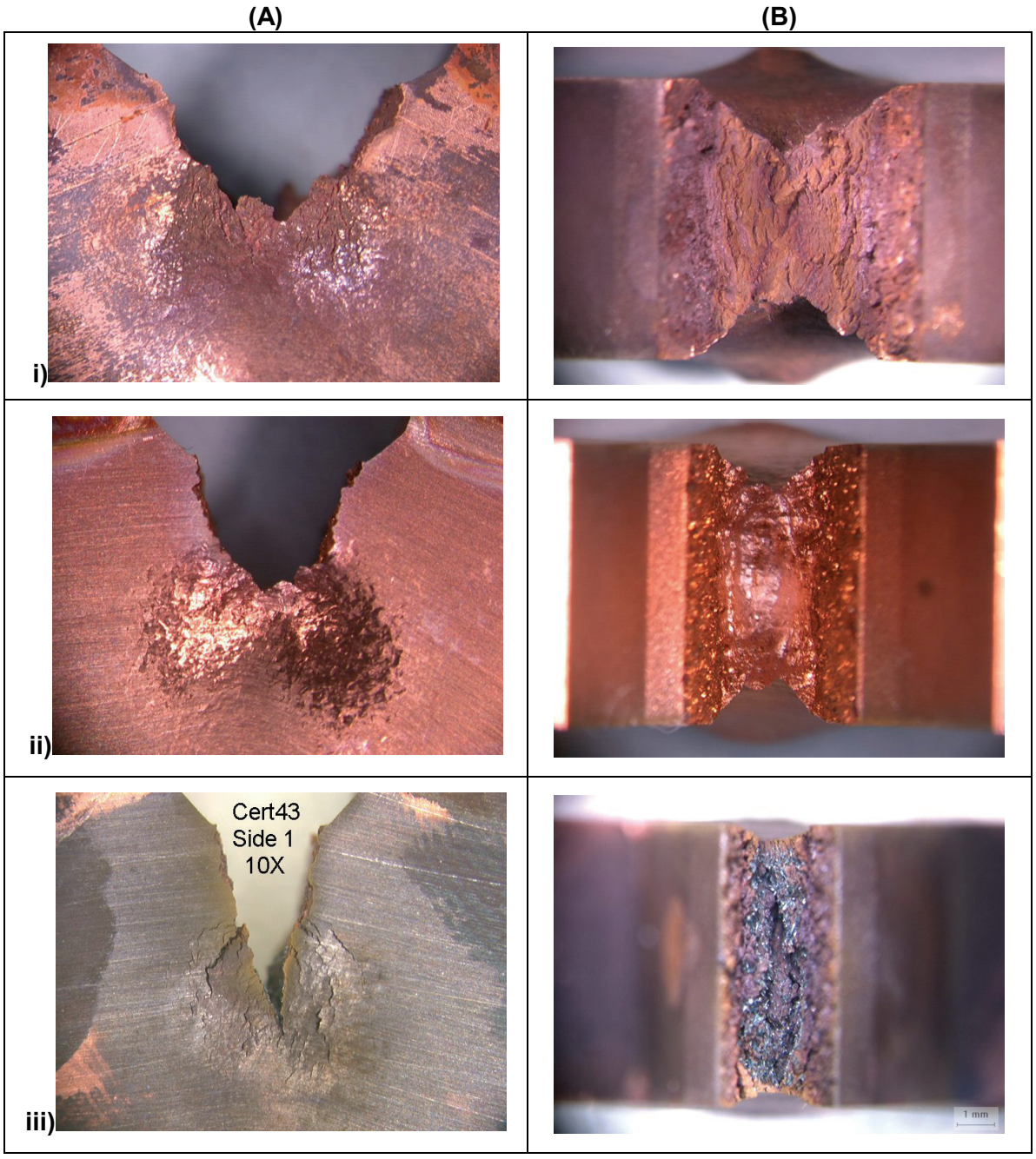

Figure 2: Macrographs of SKB4 Copper Plate CT Specimen Surface and Crack Overviews Showing the Effect of Varying Nitrite Concentrations (continued next page)

Macrographs of CT specimen surface (A) and crack overview (B) images (10X) following CERTs at 1 $\mu A \cdot cm^{-2}$ applied current in varying nitrite concentrations: i) 0.001 $mol \cdot L^{-1}$ nitrite (CERT50, 382 h), ii) 0.01 $mol \cdot L^{-1}$ nitrite (CERT51, 313 h), iii) 0.1 $mol \cdot L^{-1}$ nitrite (CERT43, 168 h), iv) 0.5 $mol \cdot L^{-1}$ nitrite (CERT122, 163 h), and v) 1.0 $mol \cdot L^{-1}$ nitrite (CERT124, 99 h). The scale marker represents 1 mm on the specimen.

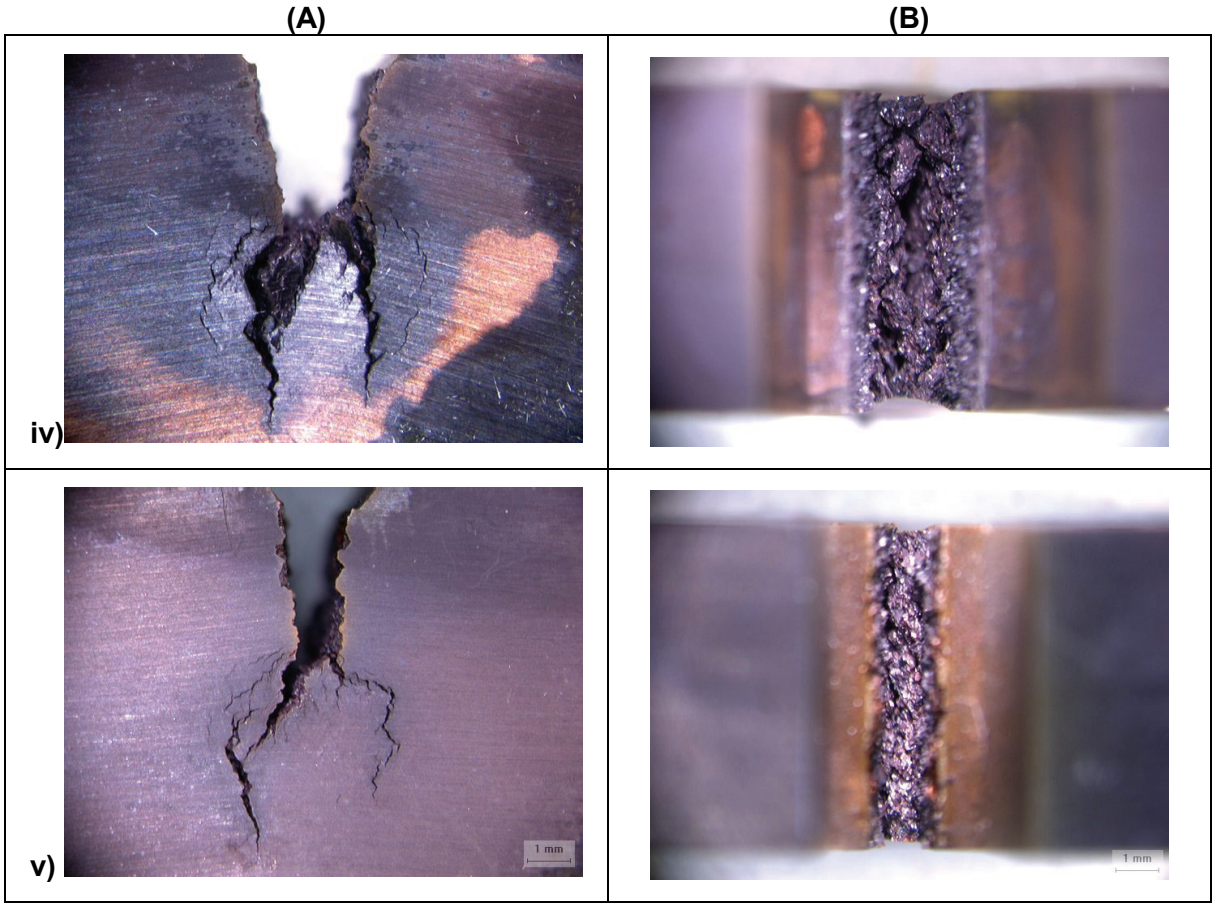

Continuing Figure 2: Macrographs of SKB4 Copper Plate CT Specimen Surface and Crack Overviews Showing the Effect of Varying Nitrite Concentrations

Macrographs of CT specimen surface (A) and crack overview (B) images (10X) following CERTs at 1 $\mu A \cdot cm^{-2}$ applied current in varying nitrite concentrations: i) 0.001 $mol \cdot L^{-1}$ nitrite (CERT50, 382 h), ii) 0.01 $mol \cdot L^{-1}$ nitrite (CERT51, 313 h), iii) 0.1 $mol \cdot L^{-1}$ nitrite (CERT43, 168 h), iv) 0.5 $mol \cdot L^{-1}$ nitrite (CERT122, 163 h), and v) 1.0 $mol \cdot L^{-1}$ nitrite (CERT124, 99 h). The scale marker represents 1 mm on the specimen.

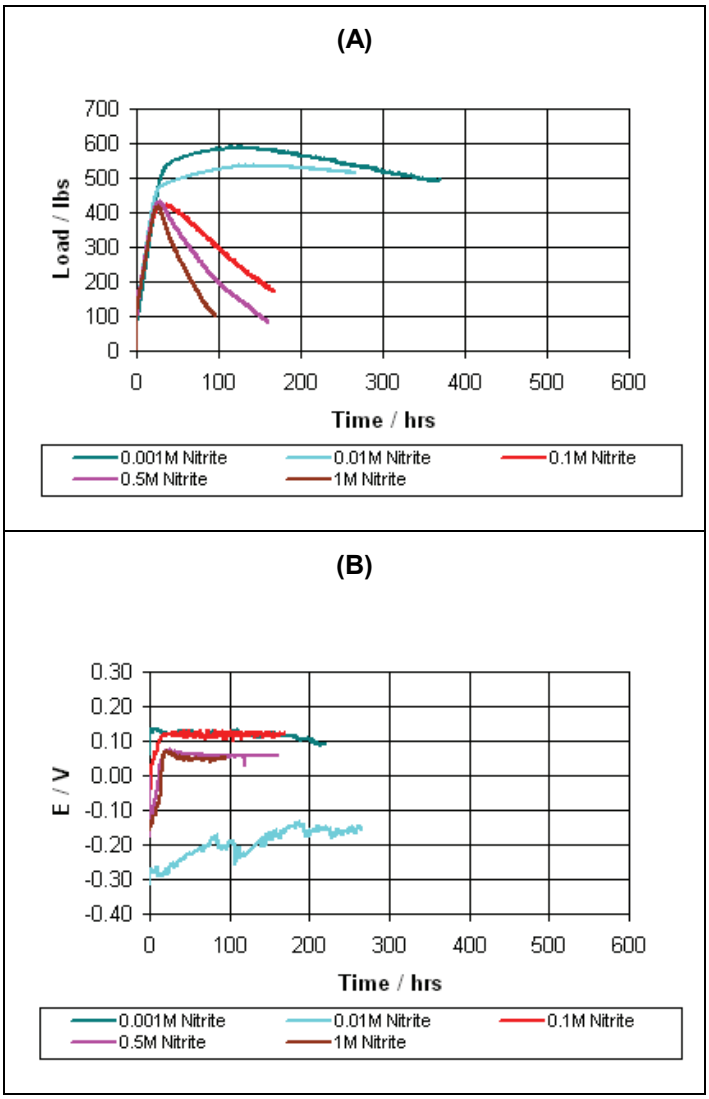

Figure 3: Graphs Showing the Effect of Varying Nitrite Concentrations on Load and Potential in Deaerated Solutions Under a Galvanically Applied Current of 1 μA·cm^{-2}

Graph (A) depicts the load curves and graph (B) follows the potential transient behaviour of OFP Cu CT specimens immersed in 0.001 mol·L^{-1} nitrite (CERT50), 0.01 mol·L^{-1} nitrite (CERT51), 0.1 mol·L^{-1} nitrite (CERT43), 0.5 mol·L^{-1} nitrite (CERT122), and 1.0 mol·L^{-1} nitrite (CERT124).

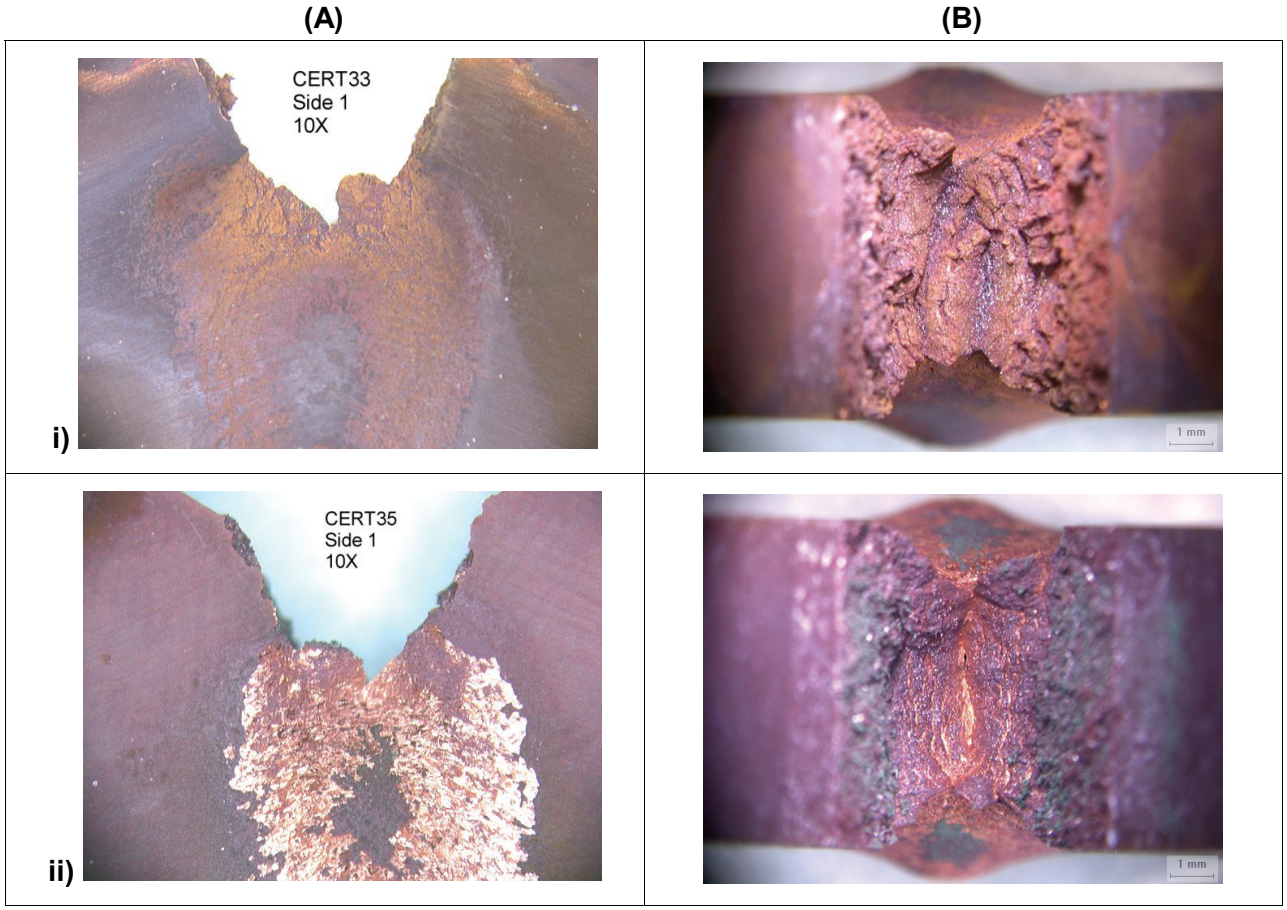

Figure 4: Macrographs of SKB4 Copper Plate CT Specimen Surface and Crack Overviews Showing the Effect of a 1:1 Ratio of Chloride to Nitrite at Various Nitrite Concentrations (continued next page)

Macrographs of CT specimen surface (A) and crack overview (B) images (10X) following CERTs at 1 $\mu A \cdot cm^{-2}$ applied current in 1:1 concentration ratio of chloride to nitrite: i) 0.01 $mol \cdot L^{-1}$/0.01 $mol \cdot L^{-1}$ (CERT33, 334 h), ii) 0.1 $mol \cdot L^{-1}$/0.1 $mol \cdot L^{-1}$ (CERT35, 332 h), iii) 0.5 $mol \cdot L^{-1}$/0.5 $mol \cdot L^{-1}$ (CERT123, 594 h), and iv) 1.0 $mol \cdot L^{-1}$/1.0 $mol \cdot L^{-1}$ (CERT125, 336 h). The scale marker represents 1 mm on the specimen.

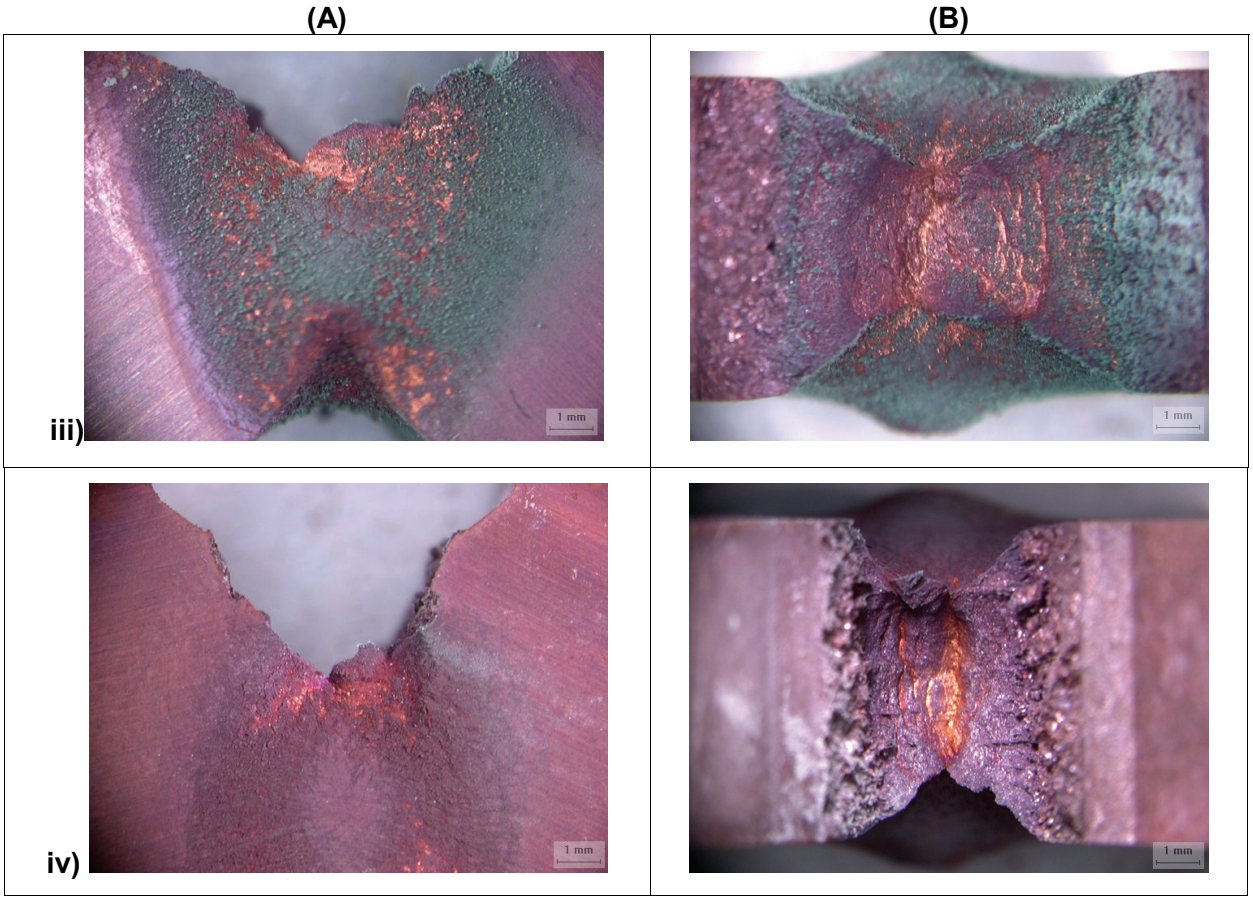

Continuing Figure 4: Macrographs of SKB4 Copper Plate CT Specimen Surface and Crack Overviews Showing the Effect of a 1:1 Ratio of Chloride to Nitrite at Various Nitrite Concentrations

Macrographs of CT specimen surface (A) and crack overview (B) images (10X) following CERTs at 1 $\mu A \cdot cm^{-2}$ applied current in 1:1 concentration ratio of chloride to nitrite: i) 0.01 $mol \cdot L^{-1}$/0.01 $mol \cdot L^{-1}$ (CERT33, 334 h), ii) 0.1 $mol \cdot L^{-1}$/0.1 $mol \cdot L^{-1}$ (CERT35, 332 h), iii) 0.5 $mol \cdot L^{-1}$/0.5 $mol \cdot L^{-1}$ (CERT123, 594 h), and iv) 1.0 $mol \cdot L^{-1}$/1.0 $mol \cdot L^{-1}$ (CERT125, 336 h). The scale marker represents 1 mm on the specimen.

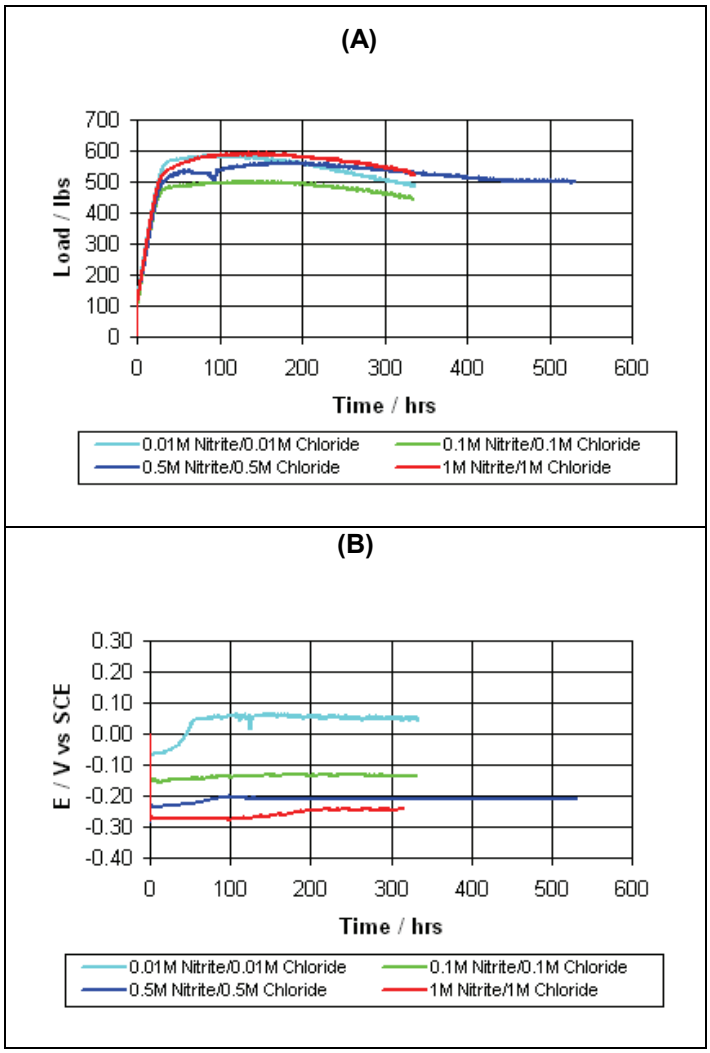

Figure 5: Graphs Showing the Effect of a 1:1 Ratio of Chloride to Nitrite at Various Nitrite Concentrations on Load and Potential in Deaerated Solutions Under a Galvanically Applied Current of 1 μA·cm^{-2}

Graph (A) depicts the load curves and graph (B) follows the potential transient behaviour of OFP Cu CT specimens immersed in 0.01 mol·L^{-1} nitrite/0.01 mol·L^{-1} chloride (CERT33), 0.1 mol·L^{-1} nitrite/0.1 mol·L^{-1} chloride (CERT35), 0.5 mol·L^{-1} nitrite/0.5 mol·L^{-1} chloride (CERT123), and 1.0 mol·L^{-1} nitrite/1.0 mol·L^{-1} chloride (CERT125).

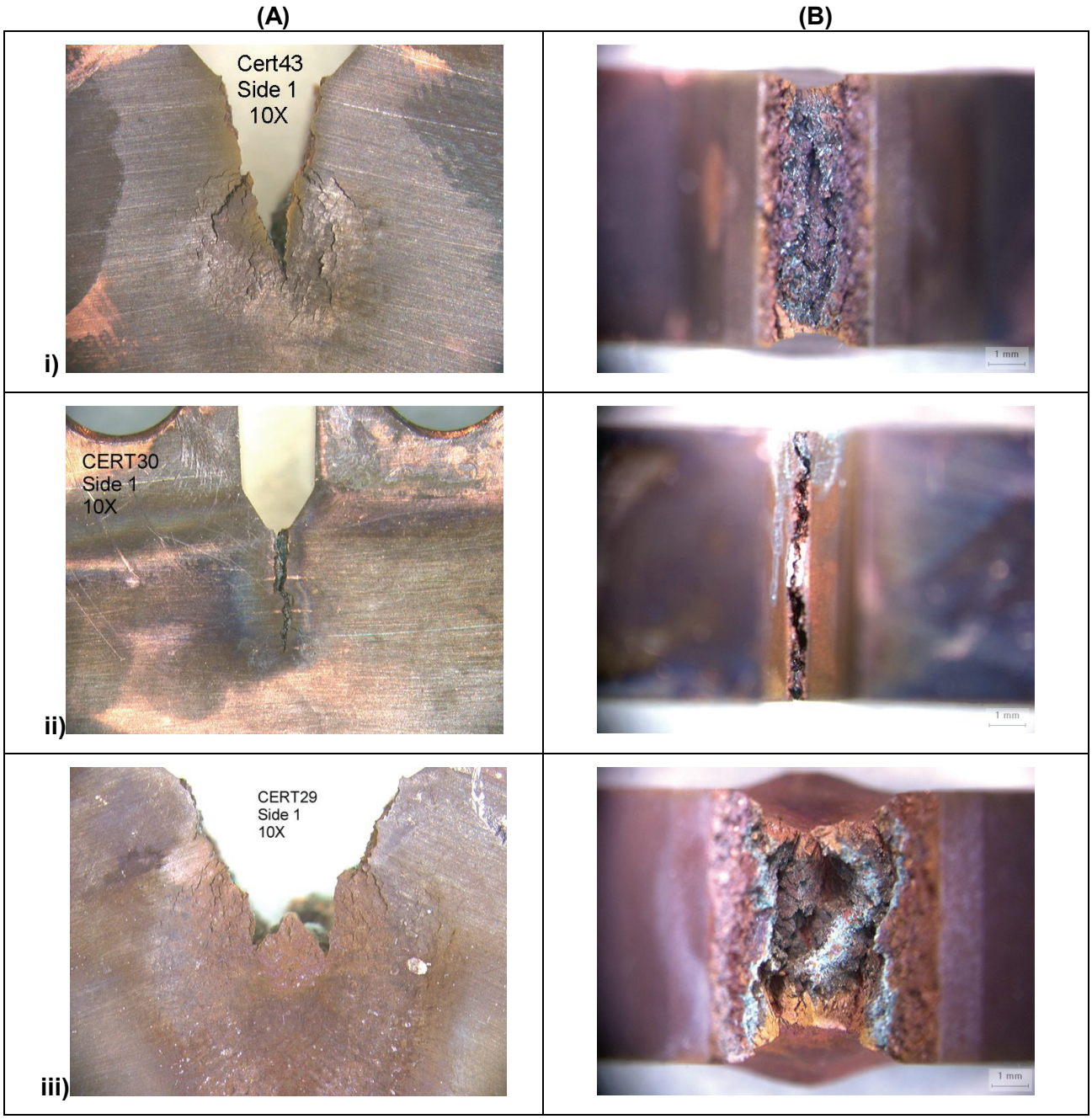

Figure 6: Macrographs of SKB4 Copper Plate CT Specimen Surface and Crack Overviews Showing the Effect of Chloride Concentration in 0.1 mol·L^{-1} Nitrite Under a Galvanically Applied Current of 1 μA·cm^{-2} (continued next page).

Macrographs of CT specimen surface (A) and crack overview (B) images (10X) following CERTs in 0.1 mol·L^{-1} nitrite with chloride: i) 0 mol·L^{-1} (CERT43, 168 h), ii) 0.001 mol·L^{-1} (CERT30, 51 h), iii) 0.01 mol·L^{-1} (CERT29, 333 h), iv) 0.1 mol·L^{-1} (CERT35, 332 h), v) 1.0 mol·L^{-1} (CERT126, 431 h), and vi) saturated (~5 mol·L^{-1}) (CERT107, 428 h).

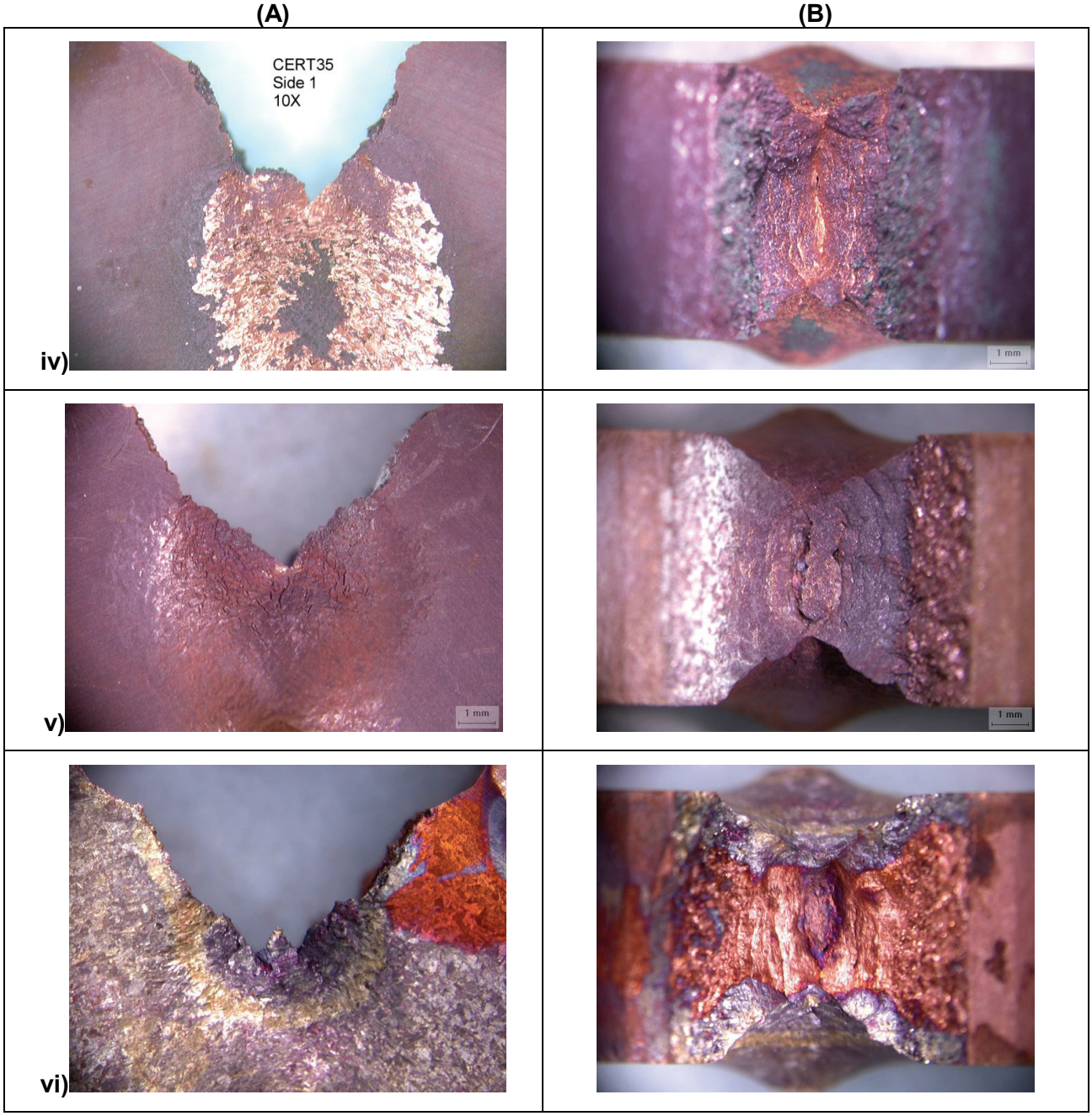

Continuing Figure 6: Macrographs of SKB4 Copper Plate CT Specimen Surface and Crack Overviews Showing the Effect of Chloride Concentration in 0.1 mol·L^{-1} Nitrite under a Galvanically Applied Current of 1 μA·cm^{-2}.

Macrographs of CT specimen surface (A) and crack overview (B) images (10X) following CERTs in 0.1 mol·L^{-1} nitrite with chloride: i) 0 mol·L^{-1} (CERT43, 168 h), ii) 0.001 mol·L^{-1} (CERT30, 51 h), iii) 0.01 mol·L^{-1} (CERT29, 333 h), iv) 0.1 mol·L^{-1} (CERT35, 332 h), v) 1.0 mol·L^{-1} (CERT126, 431 h), and vi) saturated (~5 mol·L^{-1}) (CERT107, 428 h).

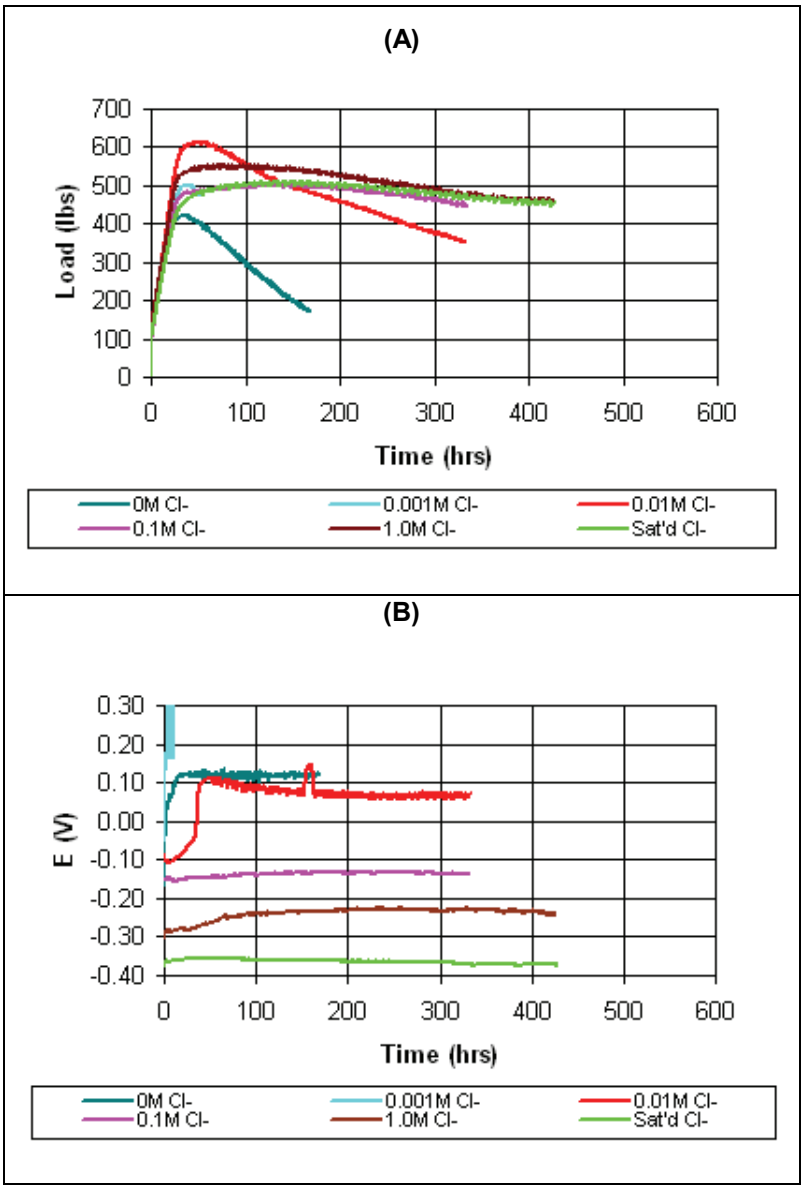

Figure 7: Graphs Showing the Effect of Chloride Concentration on Load and Potential in 0.1 mol·L^{-1} Nitrite Solutions Under a Galvanically Applied Current of 1 μA·cm^{-2}

Graph (A) depicts the load curves and graph (B) follows the potential transient behaviour of OFP Cu CT specimens immersed in 0.1 mol·L^{-1} nitrite solutions containing: 0 mol·L^{-1} chloride (CERT43), 0.001 mol·L^{-1} chloride (CERT30), 0.01 mol·L^{-1} nitrite (CERT29), 0.1 mol·L^{-1} chloride (CERT35), 1.0 mol·L^{-1} chloride (CERT126), and ~5 mol·L^{-1} (saturated) chloride (CERT107).

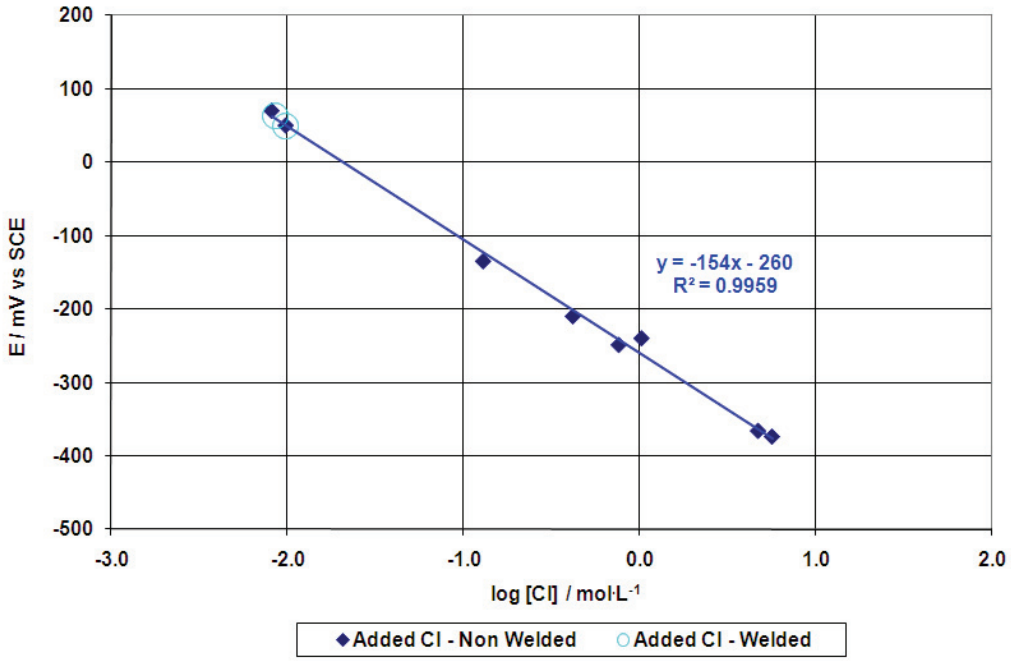

Figure 8: Graph Showing the Dependence of Potential on the Added Chloride Concentration in Deaerated Nitrite/Chloride Solutions under a Galvanically Applied Current of 1 μA·cm^{-2}

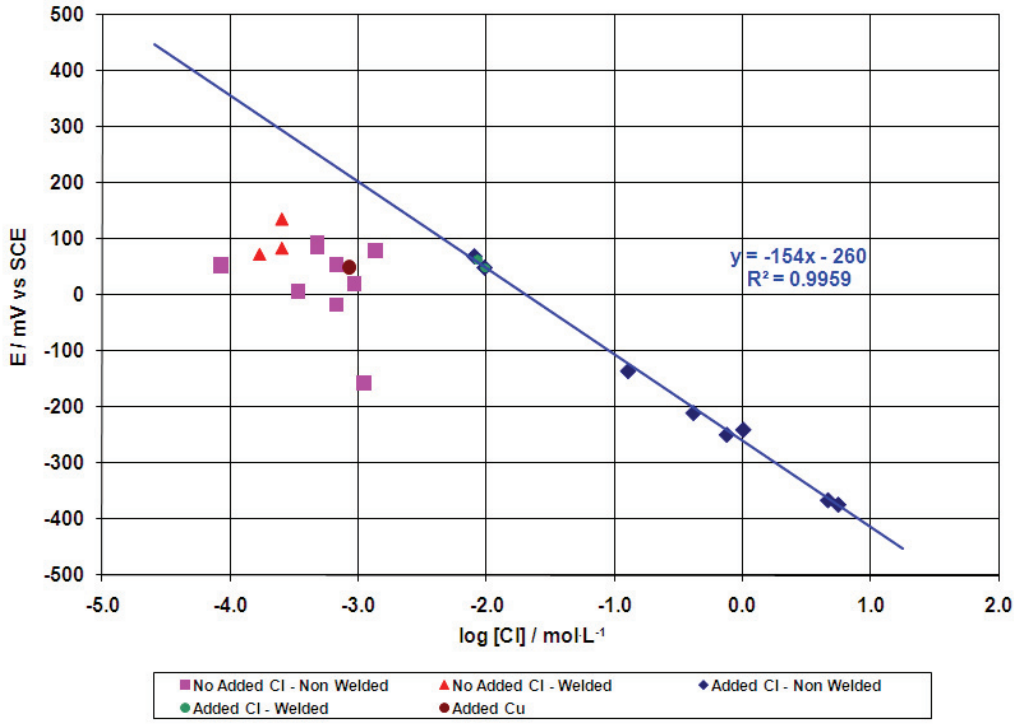

Figure 9: Relationship between the Steady-State Potential and the Measured Final Chloride Concentration

Plots of the steady-state potential values (vs SCE) against the log of the measured final chloride concentration for all nitrite tests. Note: The trend line was fit using only the added chloride data and indicates a dependence of the steady-state potential on the added chloride concentration. In nitrite alone solutions, the presence of chloride is due to reference electrode leakage and the steady-state potential of these experiments does not appear to have a dependence on the final chloride concentration.

(A)

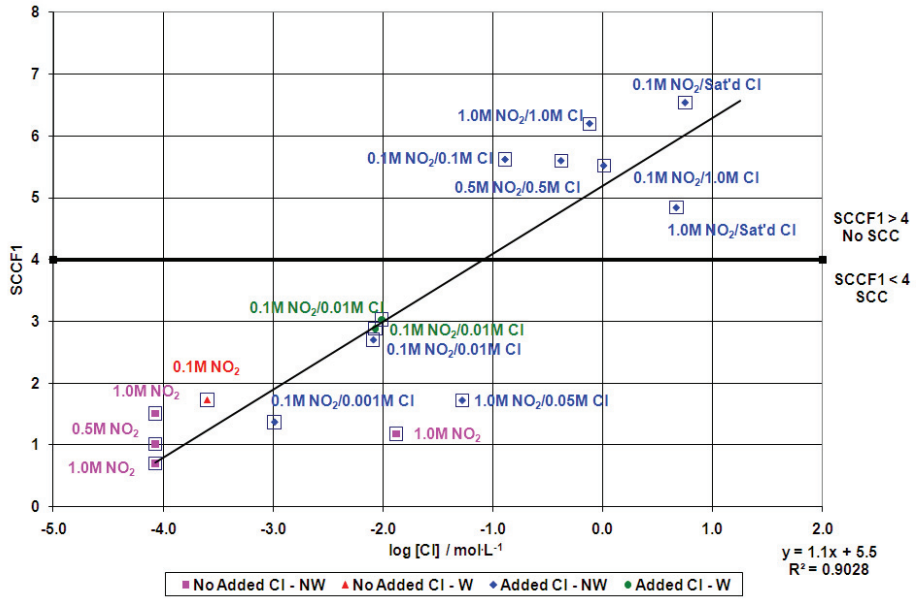

(B)

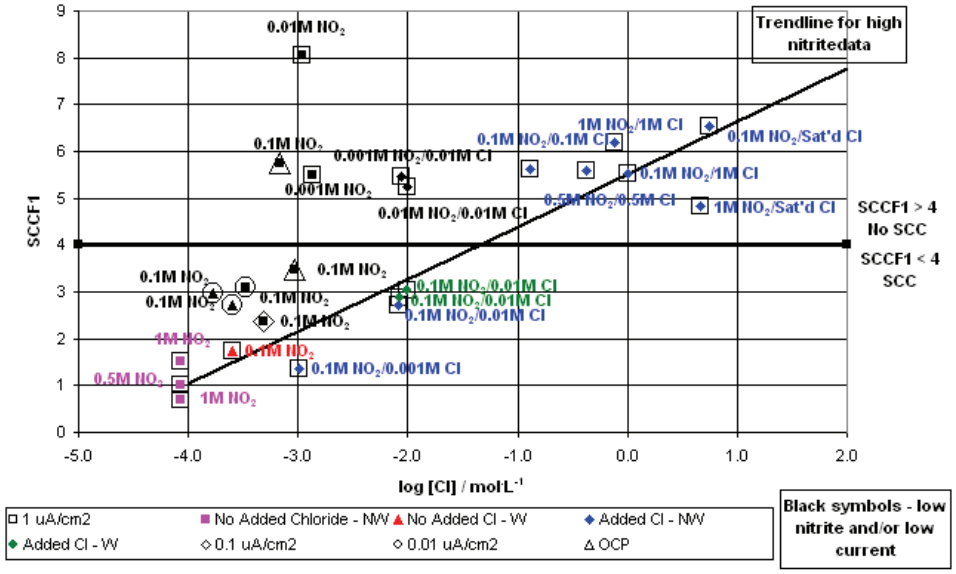

Figure 10: Relationship between the SCCF1 Values and the Measured Final Chloride Concentration

Plots of the SCCF1 values against the log of the measured final chloride concentration for: (A) tests with a nitrite concentration of 0.1 mol·L^{-1} or greater under an applied current density of 1 μA·cm^2 and (B) all nitrite tests. Note: The trend lines for both plots indicate the fit for the higher concentration nitrite data (Figure 10(A)).

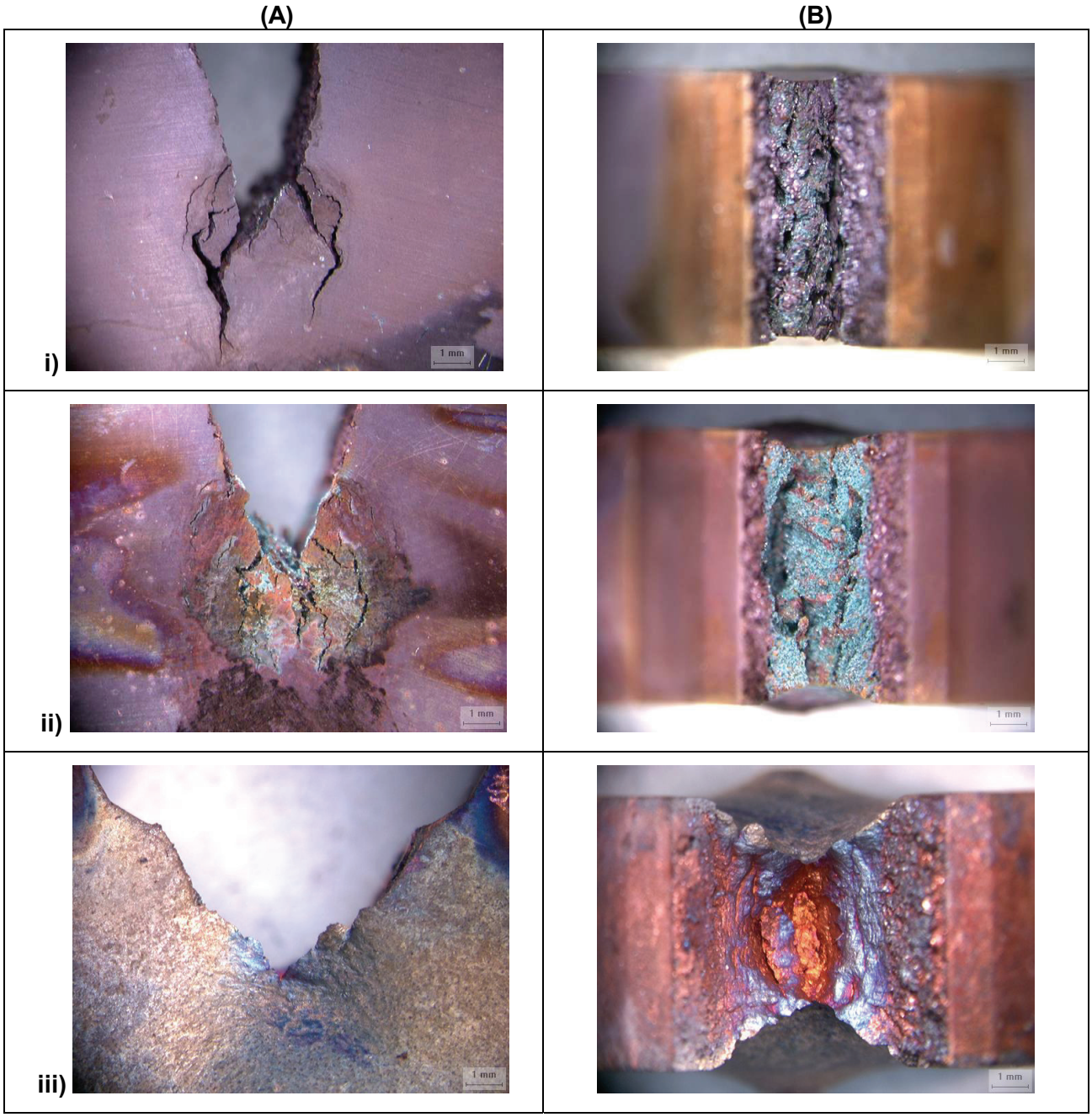

Figure 11: Macrographs of SKB4 Copper Plate CT Specimen Surface and Crack Overviews Showing the Effect of High Nitrite/Low Chloride Concentration

Macrographs of CT specimen surface (A) and crack overview (B) images (10X) following CERTs at 1 $\mu A \cdot cm^{-2}$ applied current in nitrite/chloride mixtures: i) 1.0 $mol \cdot L^{-1}$/0 $mol \cdot L^{-1}$ (CERT129, 328 h), ii) 1.0 $mol \cdot L^{-1}$/0.05 $mol \cdot L^{-1}$ (CERT130, 231 h), and iii) 1.0 $mol \cdot L^{-1}$/~5 $mol \cdot L^{-1}$(saturated) (CERT128, 407 h). The scale marker represents 1 mm on the specimen.

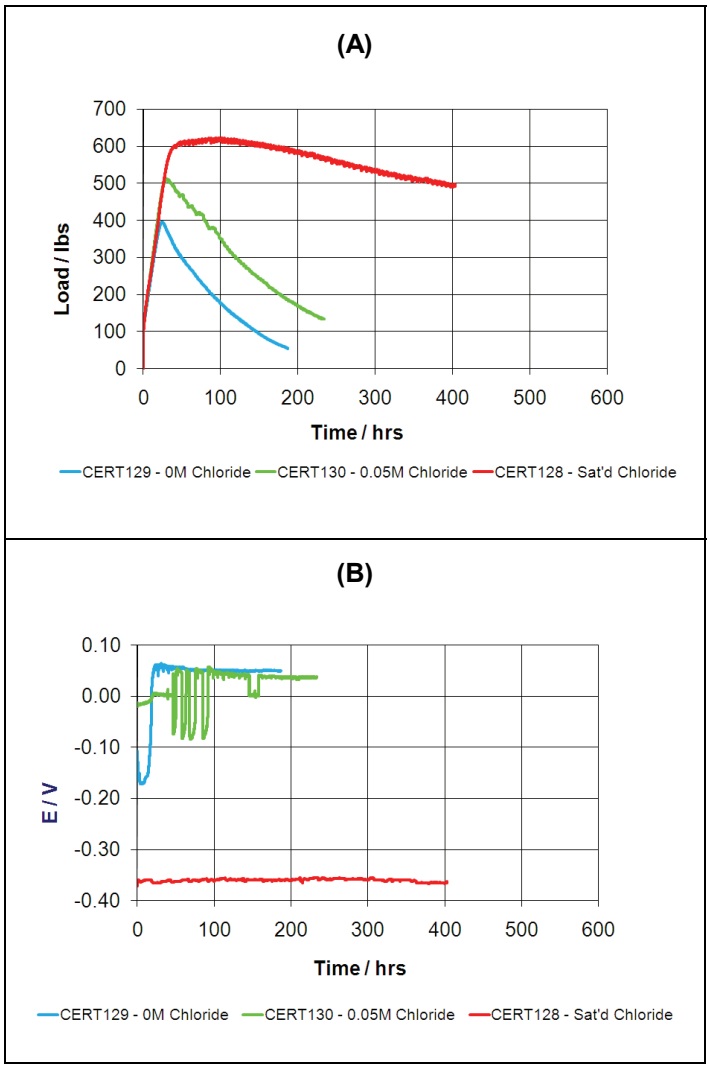

Figure 12: Graphs Showing the Effect of High Nitrite/Low Chloride Concentration on Load and Potential in Deaerated Solutions Under a Galvanically Applied Current of 1 μA·cm^{-2}

Graph (A) depicts the load curves and graph (B) follows the potential transient behaviour of OFP Cu CT specimens immersed in: 1.0 mol·L^{-1} nitrite/0 mol·L^{-1} chloride (CERT129), 1.0 mol·L^{-1} nitrite/0.05 mol·L^{-1} chloride (CERT130), and 1.0 mol·L^{-1} nitrite/~5 mol·L^{-1} (saturated) chloride (CERT128).

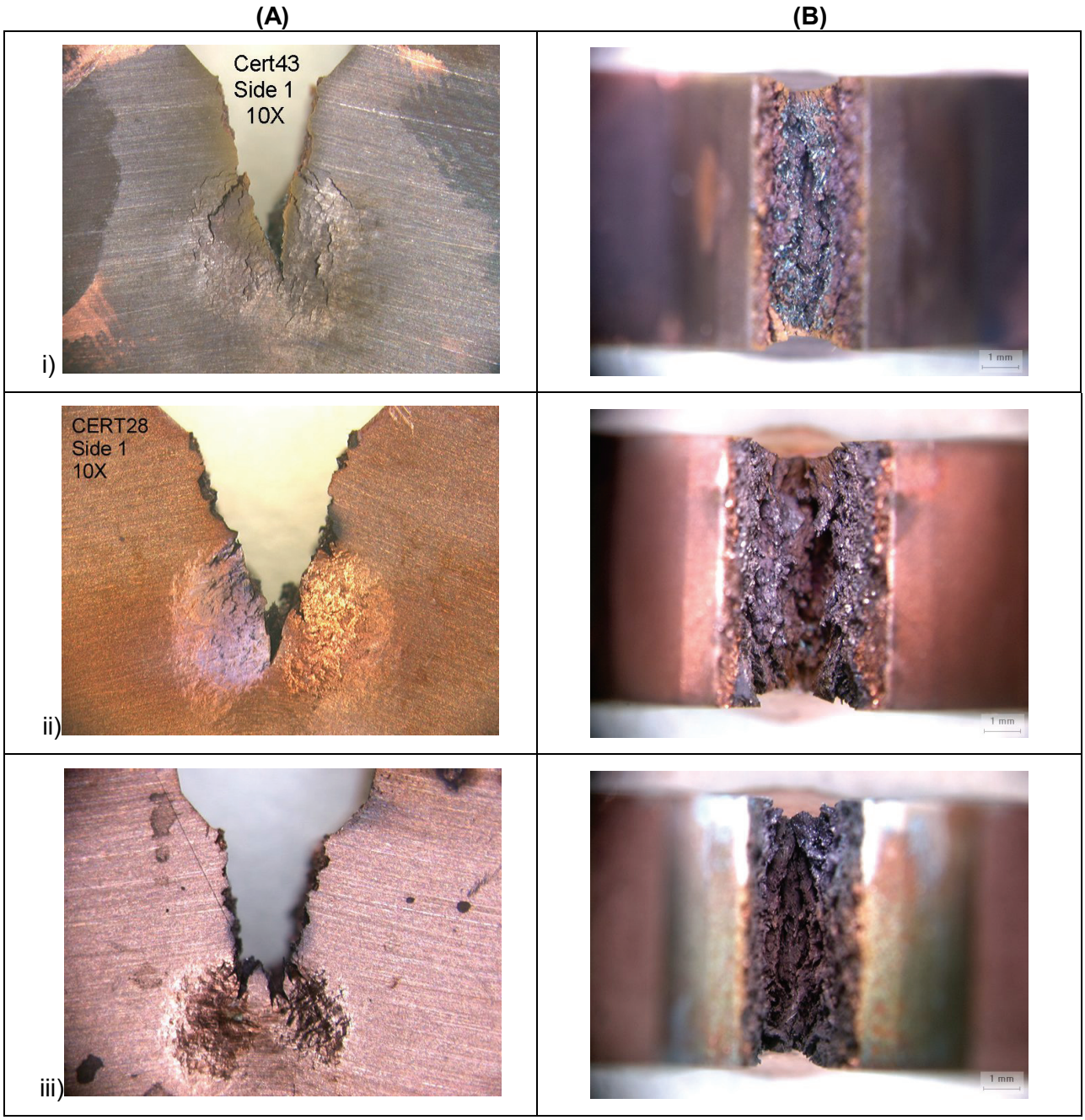

Figure 13: Macrographs of SKB4 Copper Plate CT Specimen Surface and Crack Overviews Showing the Effect of Applied Current Density and Freely Corroding Conditions (OCP) in 0.1 mol·L^{-1} Nitrite (continued next page)

Macrographs of CT specimen surface (A) and crack overview (B) images (10X) following CERTs in 0.1 mol·L^{-1} nitrite at: i) 1 μA·cm^{-2} (CERT43, 168 h), ii) 0.1 μA·cm^{-2} (CERT28, 238 h), iii) 0.01 μA·cm^{-2} (CERT58, 189 h), iv) OCP (CERT32, 430 h), v) OCP (CERT127, 340 h), and vi) OCP (CERT88, 480 h). The scale marker represents 1 mm on the specimen.

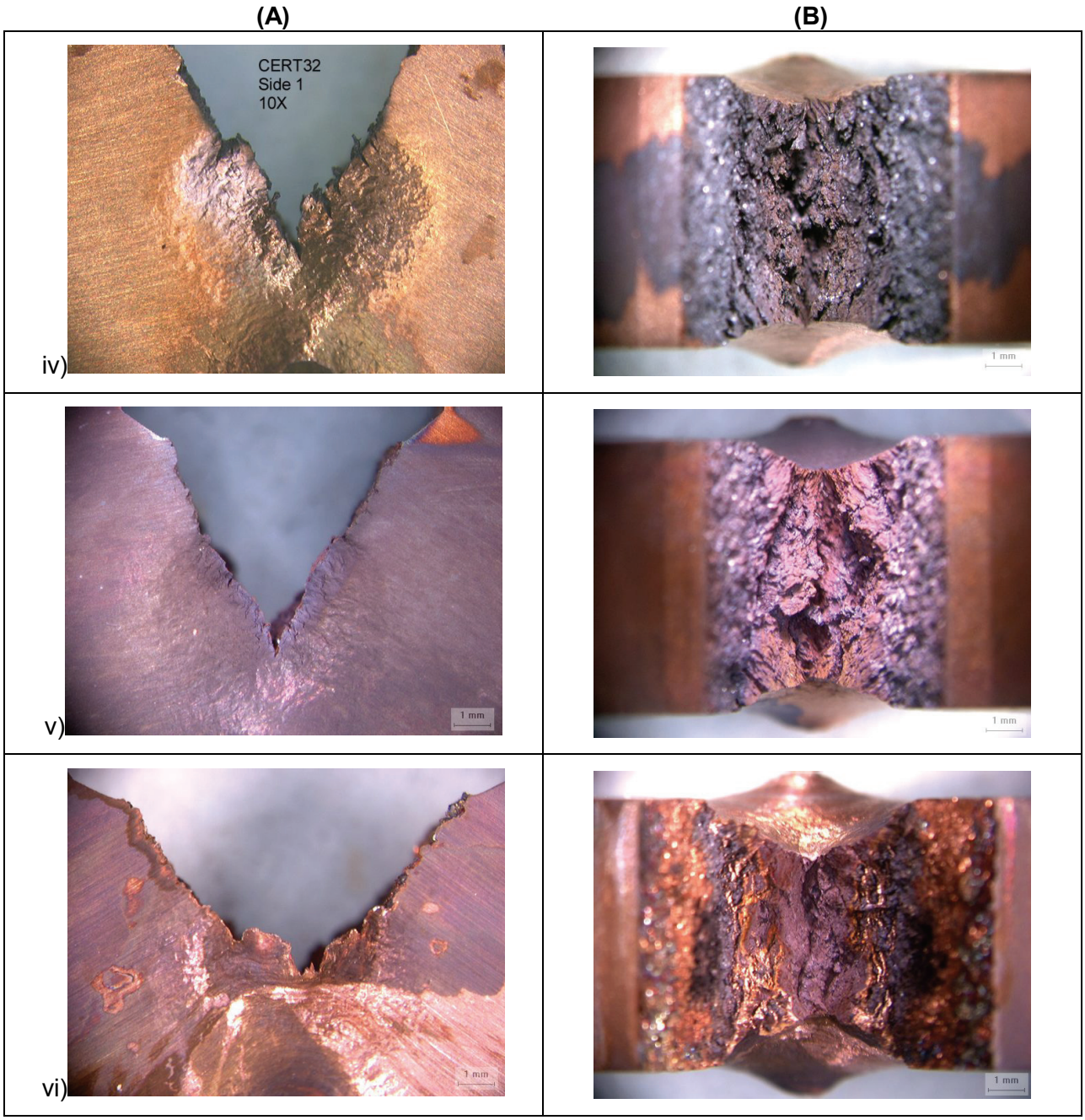

Continuing Figure 13: Macrographs of SKB4 Copper Plate CT Specimen Surface and Crack Overviews Showing the Effect of Applied Current Density and Freely Corroding Conditions (OCP) in 0.1 mol·L^{-1} Nitrite

Macrographs of CT specimen surface (A) and crack overview (B) images (10X) following CERTs in 0.1 mol·L^{-1} nitrite at: i) 1 μA·cm^{-2} (CERT43, 168 h), ii) 0.1 μA·cm^{-2} (CERT28, 238 h), iii) 0.01 μA·cm^{-2} (CERT58, 189 h), iv) OCP (CERT32, 430 h), v) OCP (CERT127, 340 h), and vi) OCP (CERT88, 480 h). The scale marker represents 1 mm on the specimen.

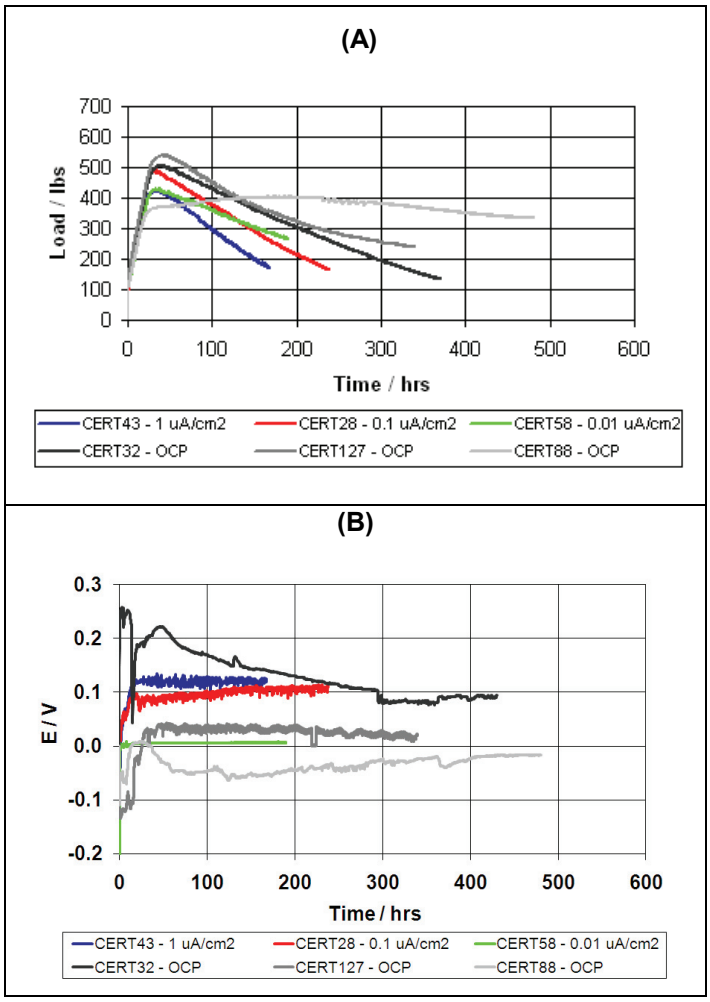

Figure 14: Graphs Showing the Effect of Applied Current Density and Freely Corroding Conditions (OCP) in 0.1 mol·L^{-1} Nitrite on Load and Potential

Graph (A) depicts the load curves and graph (B) follows the potential transient behaviour of applied current density tests: CERT43 (1 μA·cm^{-2}), CERT28 (0.1 μA·cm^{-2}), and CERT58 (0.01 μA·cm^{-2}), and freely corroding conditions (OCP) tests: CERT32, CERT127, and CERT88 in deaerated 0.1 mol·L^{-1} nitrite.

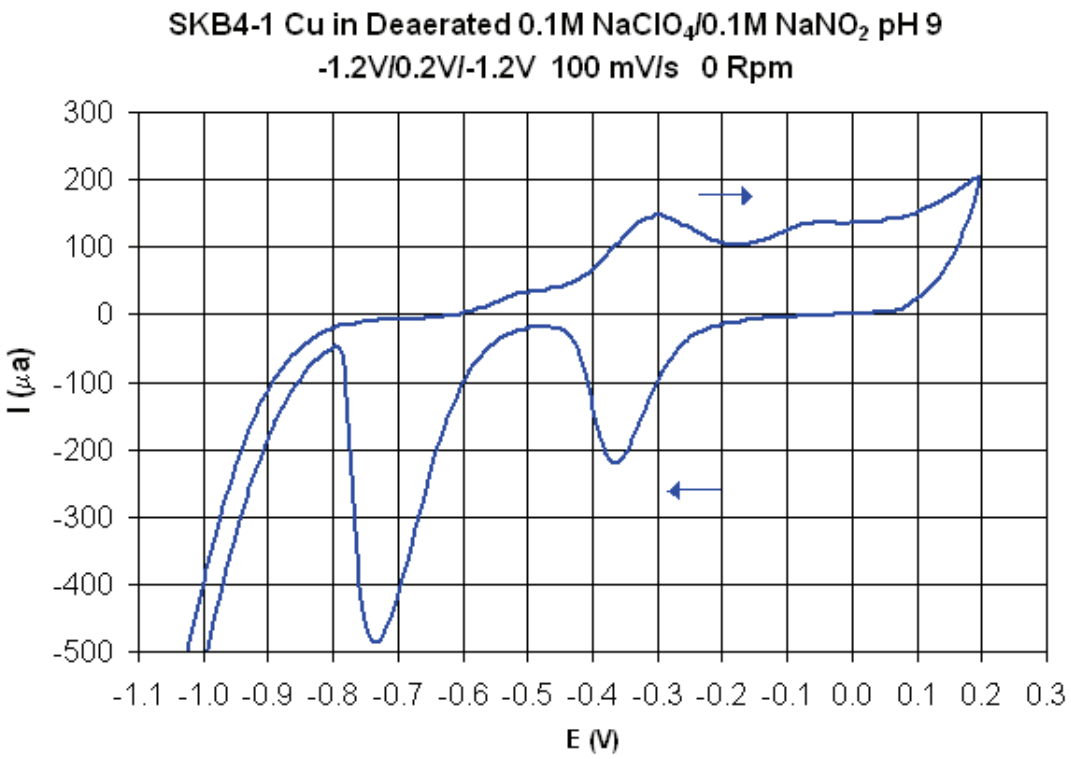

Figure 15: Cyclic Voltammogram of SKB4 Copper in 0.1 mol·L^{-1} $NaClO_4$ pH 9 Solution Containing 0.1 mol·L^{-1} $NaNO_2$.

Graph depicts the voltammetric behaviour of SKB4 copper rotated at 0 RPM in 0.1 mol·L^{-1} $NaClO_4$ pH 9 solution containing 0.1 mol·L^{-1} $NaNO_2$. Arrows indicate direction of sweep beginning.

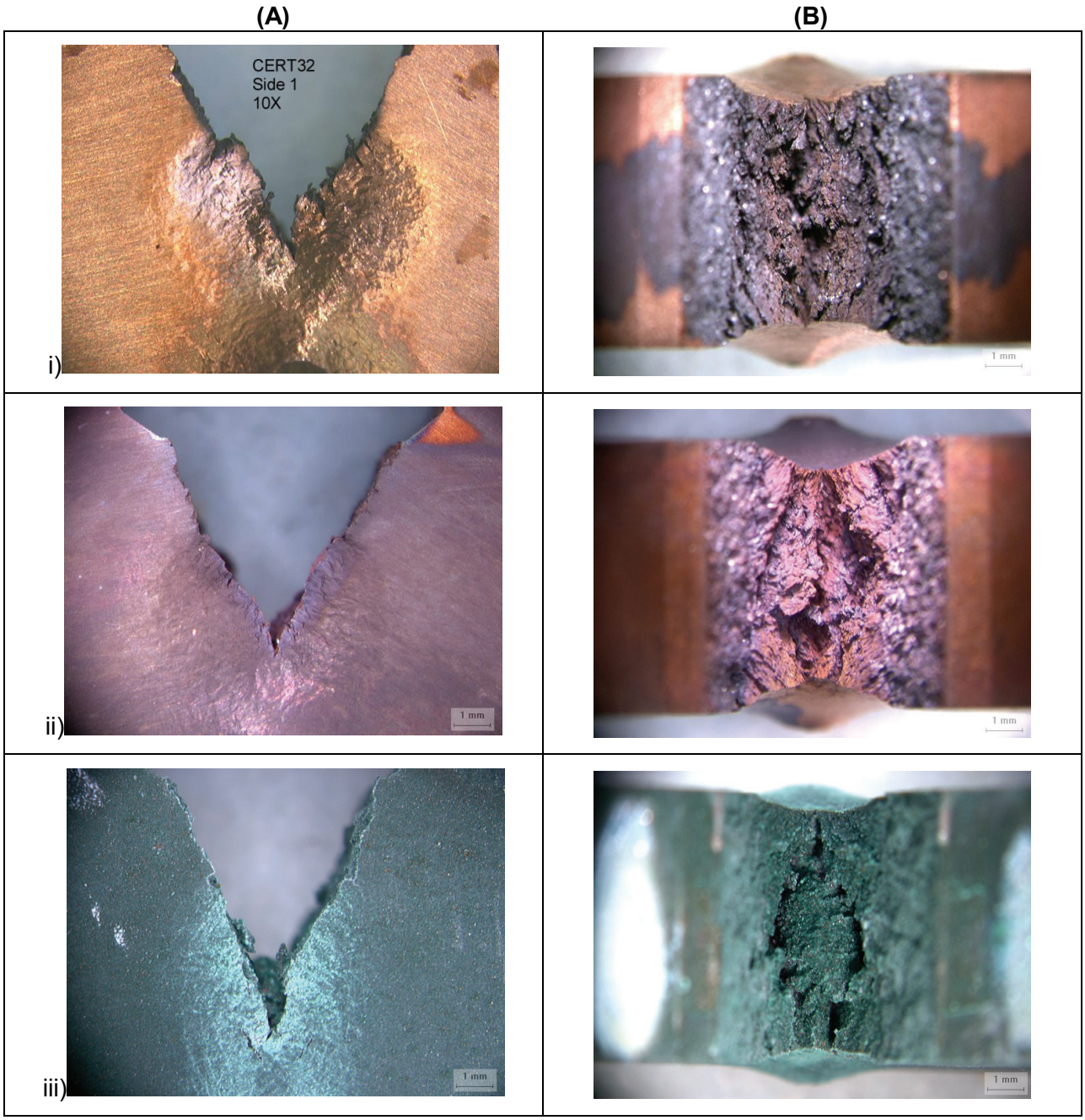

Figure 16: Macrographs of SKB4 Copper Plate CT Specimen Surface and Crack Overviews Showing the Effect of Added Copper under Freely Corroding Conditions (OCP) in 0.1 mol·L^{-1} Nitrite

Macrographs of CT specimen surface (A) and crack overview (B) images (10X) following CERTs in 0.1 mol·L^{-1} nitrite at OCP with i) no added copper (CERT32, 430 h) and ii) (CERT127 340 h), and iii) 8 mmol·L^{-1} added copper (CERT89, 307 h). The scale marker represents 1 mm on the specimen.

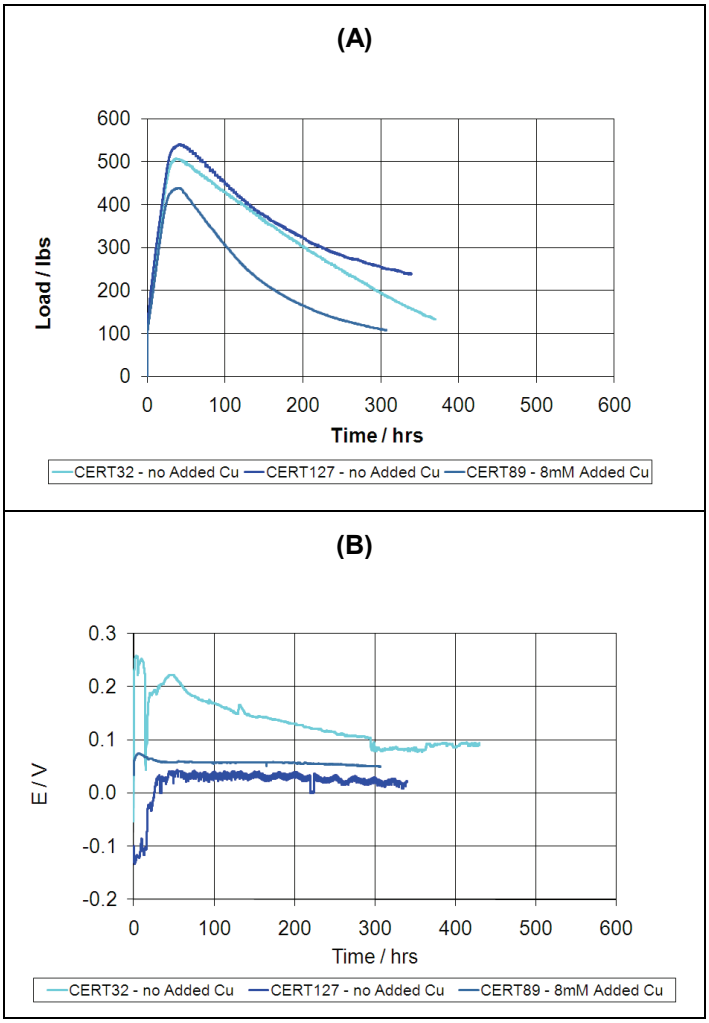

Figure 17: Graphs Showing the Effect of Added Copper under Freely Corroding Conditions (OCP) in 0.1 mol·L^{-1} Nitrite on Load and Potential

Graph (A) depicts the load curves and graph (B) follows the potential transient behaviour of OFP Cu CT specimens immersed in 0.1 mol·L^{-1} nitrite at OCP: CERT32 (no added copper), CERT127 (no added copper), and CERT89 (8 mmol·L^{-1} added copper).

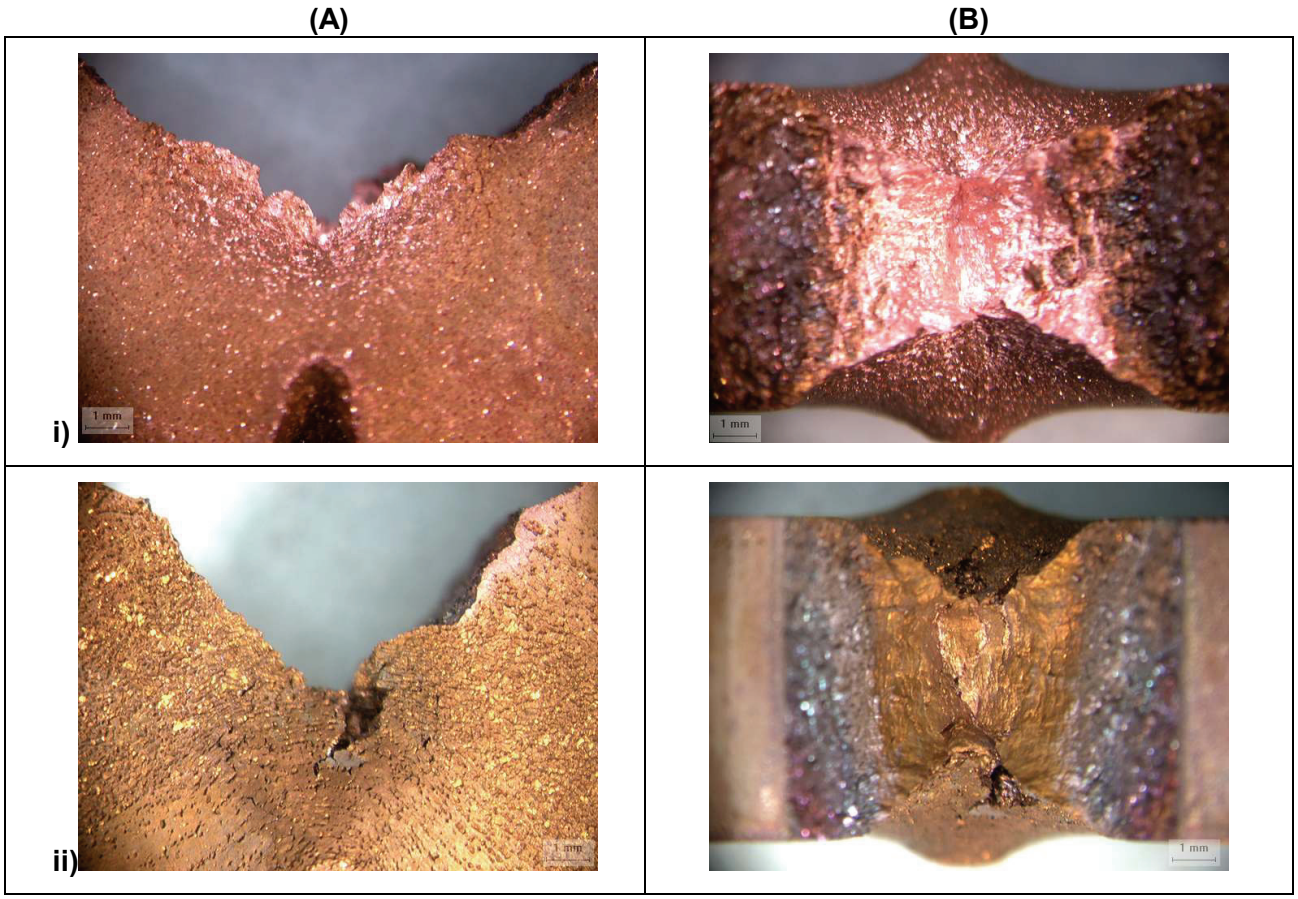

Figure 18: Macrographs of SKB4 Copper Plate CT Specimen Surface and Crack Overviews Showing the Effect of Ammonia Concentration (continued next page)

Macrographs of CT specimen surface (A) and crack overview (B) images (10X) following CERTs at 1 $\mu A \cdot cm^{-2}$ applied current in ammonia solutions: i) 0.1 $mol \cdot L^{-1}$ (CERT131, 600 h), ii) 0.3 $mol \cdot L^{-1}$ (CERT137, 456 h), iii) 0.5 $mol \cdot L^{-1}$ (CERT132, 525 h), and iv) 1.0 $mol \cdot L^{-1}$ (CERT74, 477 h). The scale marker represents 1 mm on the specimen.

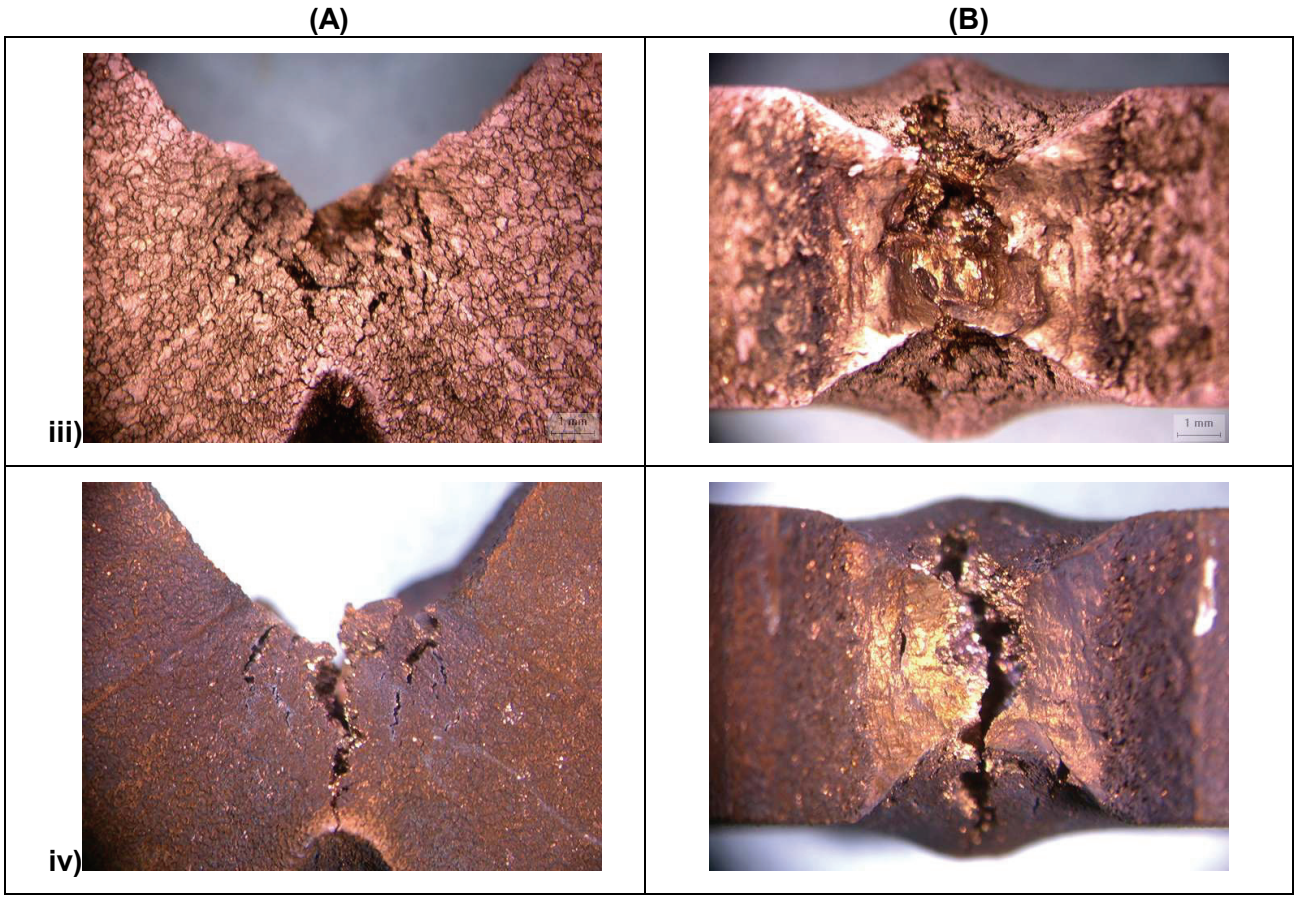

Continuing Figure 18: Macrographs of SKB4 Copper Plate CT Specimen Surface and Crack Overviews Showing the Effect of Ammonia Concentration

Macrographs of CT specimen surface (A) and crack overview (B) images (10X) following CERTs at 1 $\mu A \cdot cm^{-2}$ applied current in ammonia solutions: i) 0.1 $mol \cdot L^{-1}$ (CERT131, 600 h), ii) 0.3 $mol \cdot L^{-1}$ (CERT137, 456 h), iii) 0.5 $mol \cdot L^{-1}$ (CERT132, 525 h), and iv) 1.0 $mol \cdot L^{-1}$ (CERT74, 477 h). The scale marker represents 1 mm on the specimen.

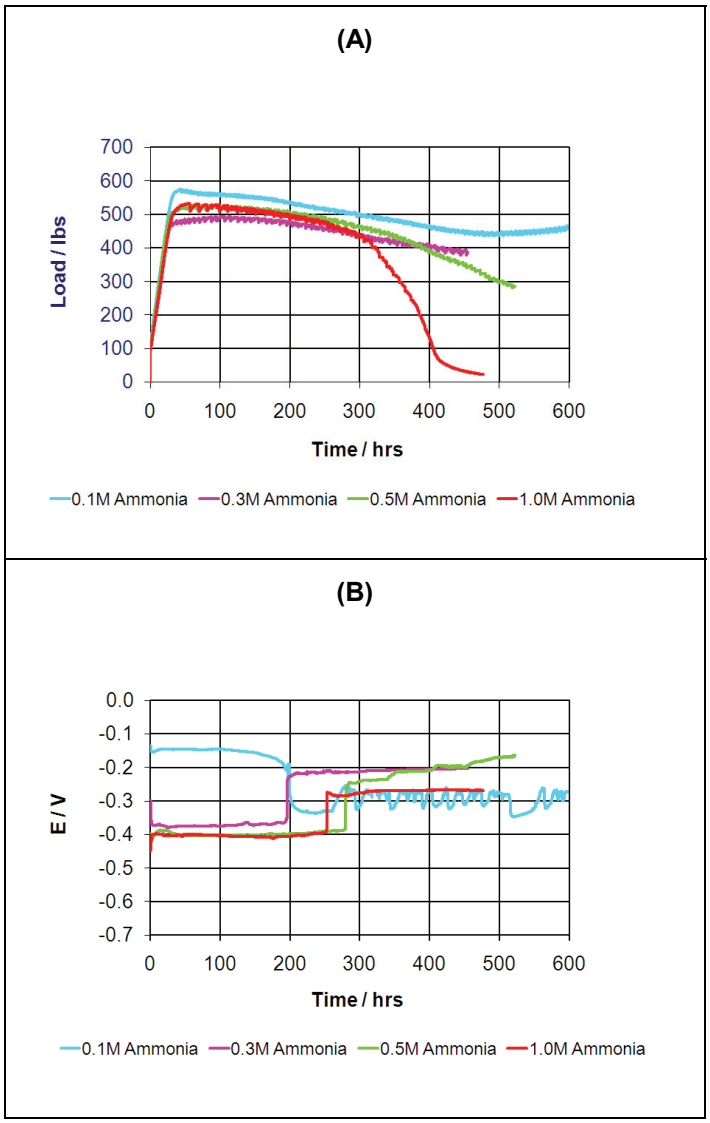

Figure 19: Graphs Showing the Effect of Ammonia Concentration on Load and Potential in Naturally Aerated Solutions Containing 4 mmol·L^{-1} Added Copper Under a Galvanically Applied Current of 1 μA·cm^{-2}

Graph (A) depicts the load curves and graph (B) follows the potential transient behaviour of OFP Cu CT specimens immersed in: 0.1 mol·L^{-1} ammonia (CERT131), 0.3 mol·L^{-1} ammonia (CERT137), 0.5 mol·L^{-1} ammonia (CERT132), and 1.0 mol·L^{-1} ammonia (CERT74).

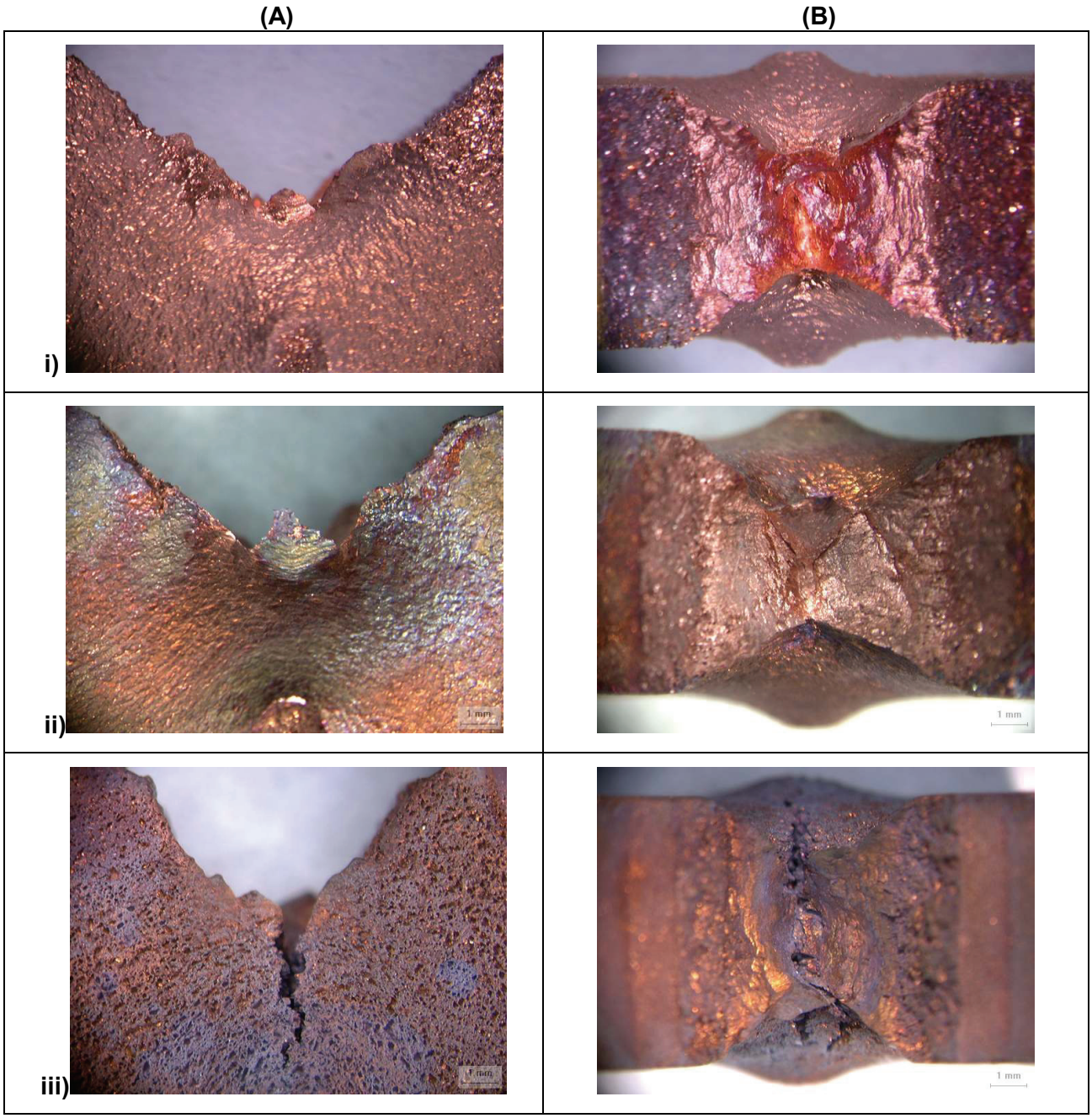

Figure 20: Macrographs of SKB4 Copper Plate CT Specimen Surface and Crack Overviews Showing the Effect of a 1:1 Chloride to Ammonia Concentration Ratio

Macrographs of CT specimen surface (A) and crack overview (B) images (10X) following CERTs in i)1.0 mol·L^{-1} ammonia/1.0 mol·L^{-1} chloride/8 mmol·L^{-1} added copper at OCP (CERT81, 623 h), ii) 1.0 mol·L^{-1} ammonia/1.0 mol·L^{-1} chloride/4 mmol·L^{-1} added copper at 1 μA/cm^2 (CERT136, 504 h), and iii) 0.5 mol·L^{-1} ammonia/0.5 mol·L^{-1} chloride and 4 mmol·L^{-1} added copper at 1 μA/cm^2 (CERT133, 380 h). The scale marker represents 1 mm on the specimen.

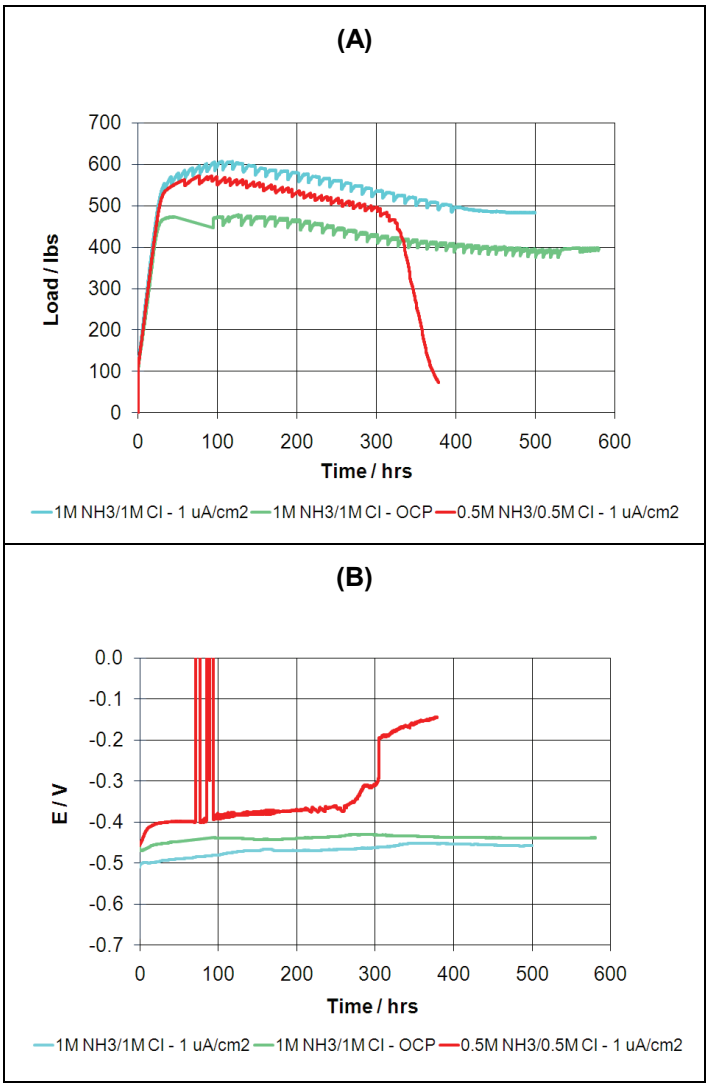

Figure 21: Graphs Showing the Effect of a 1:1 Chloride to Ammonia Concentration

Graph (A) depicts the load curves and graph (B) follows the potential transient behaviour of OFP Cu CT specimens immersed in: i)1.0 mol·L^{-1} ammonia/1.0 mol·L^{-1} chloride/8 mmol·L^{-1} added copper at OCP (CERT81), ii) 1.0 mol·L^{-1} ammonia/1.0 mol·L^{-1} chloride/4 mmol·L^{-1} added copper at 1 μA/cm^2 (CERT136), and iii) 0.5 mol·L^{-1} ammonia/0.5 mol·L^{-1} chloride and 4 mmol·L^{-1} added copper at 1 μA/cm^2 (CERT133).

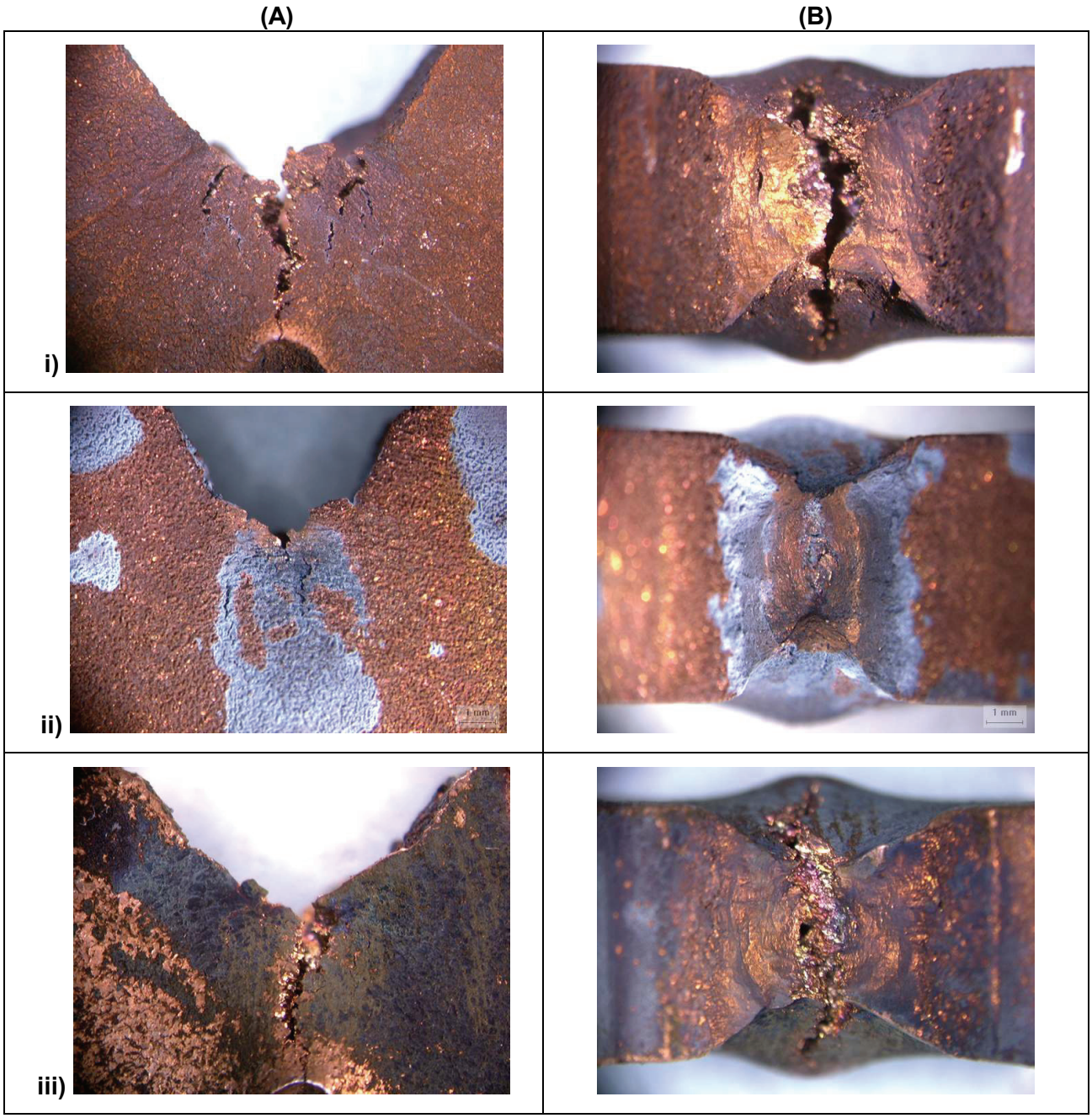

Figure 22: Macrographs of SKB4 Copper Plate CT Specimen Surface and Crack Overviews Showing the Effect of Chloride Concentration in 1.0 mol·L^{-1} Ammonia Containing 4 mmol·L^{-1} Copper under 1 μA/cm^2 Applied Current (continued next page)

Macrographs of CT specimen surface (A) and crack overview (B) images (10X) following CERTs in i) 0 mol·L^{-1} chloride (CERT74, 477 h), ii) 0.1 mol·L^{-1} chloride (CERT134, 342 h), iii) 0.5 mol·L^{-1} chloride (CERT109, 432 h), iv) 1.0 mol·L^{-1} chloride (CERT136, 504 h), and v) Saturated (~5 mol·L^{-1}) chloride (CERT108, 503 h). The scale marker represents 1 mm on the specimen.

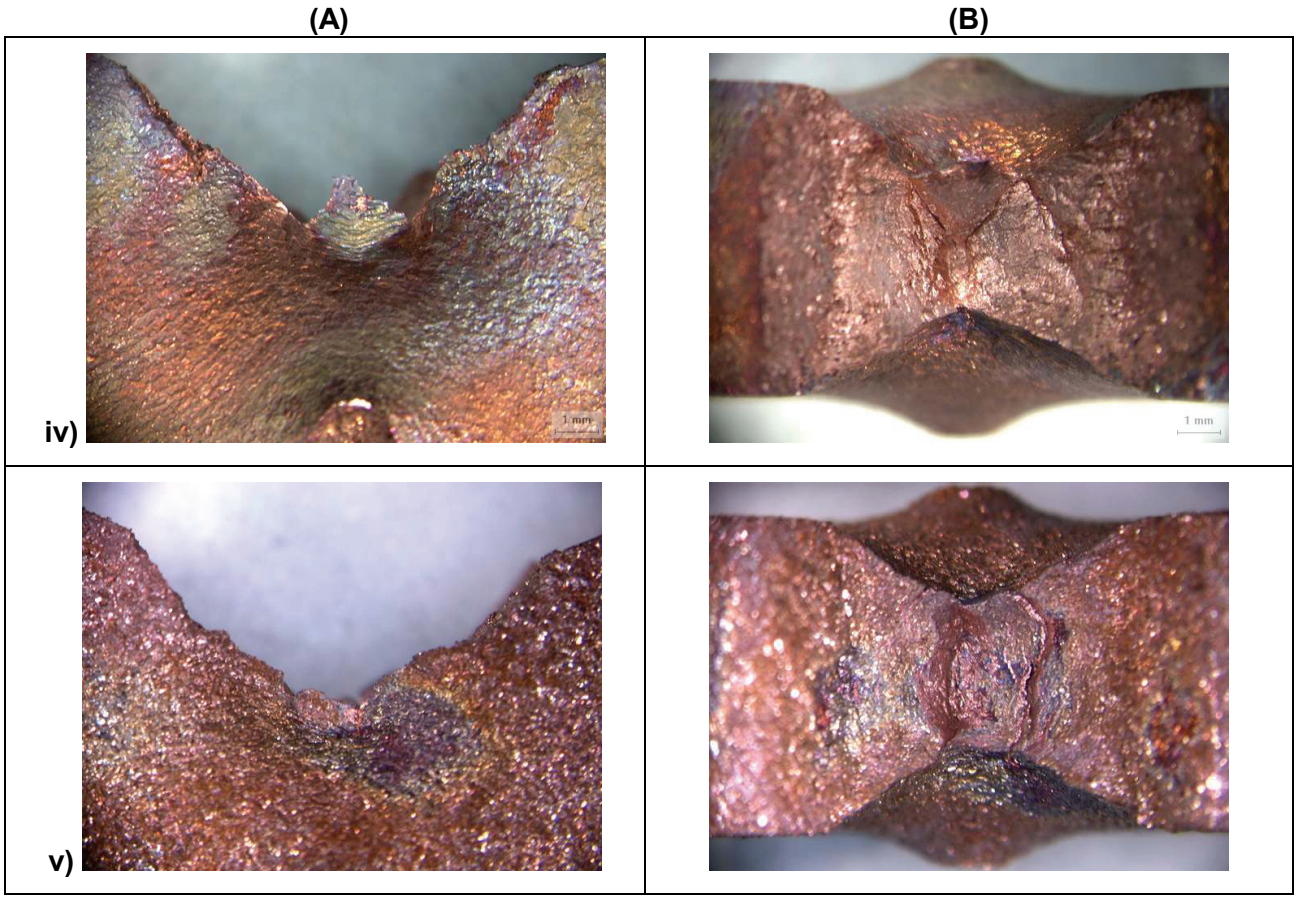

Continuing Figure 22: Macrographs of SKB4 Copper Plate CT Specimen Surface and Crack Overviews Showing the Effect of Chloride Concentration in 1.0 mol·L^{-1} Ammonia Containing 4 mmol·L^{-1} Copper under 1 μA/cm^2 Applied Current

Macrographs of CT specimen surface (A) and crack overview (B) images (10X) following CERTs in i) 0 mol·L^{-1} chloride (CERT74, 477 h), ii) 0.1 mol·L^{-1} chloride (CERT134, 342 h), iii) 0.5 mol·L^{-1} chloride (CERT109, 432 h), iv) 1.0 mol·L^{-1} chloride (CERT136, 504 h), and v) Saturated (~5 mol·L^{-1}) chloride (CERT108, 503 h). The scale marker represents 1 mm on the specimen.

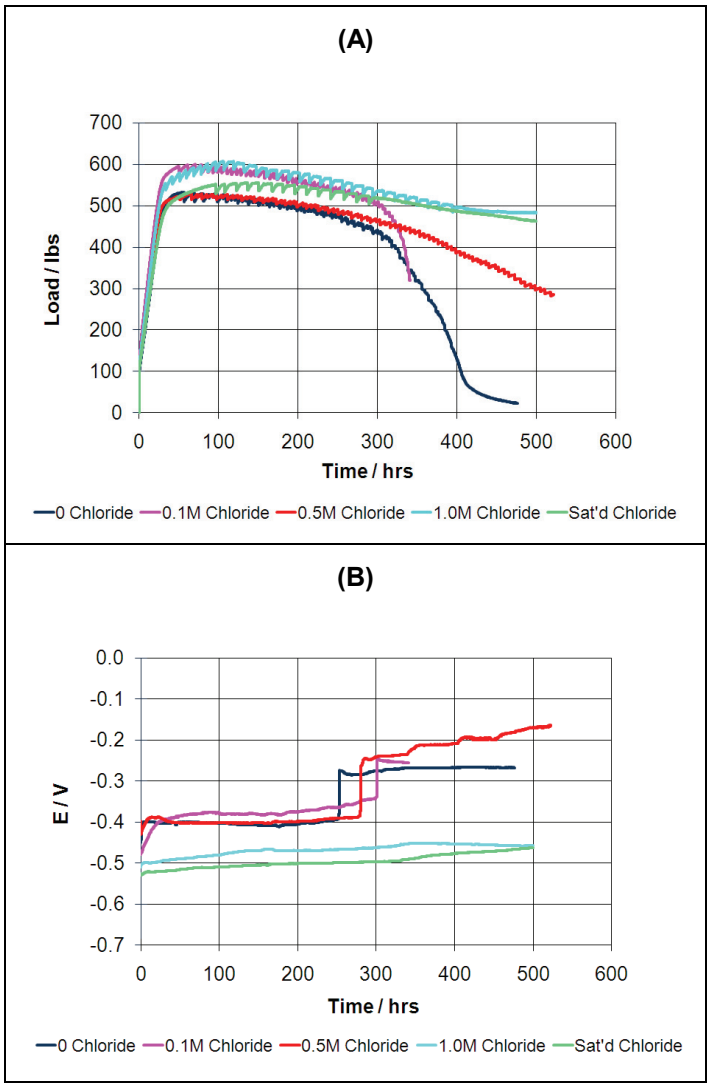

Figure 23: Graphs Showing the Effect of Chloride Concentration in 1.0 mol·L^{-1} Ammonia with 4 mmol·L^{-1} Added Copper under 1 μA/cm^2 Applied Current

Graph (A) depicts the load curves and graph (B) follows the potential transient behaviour of OFP Cu CT specimens immersed in 1.0 mol·L^{-1} ammonia/4 mmol·L^{-1} copper under 1 μA/cm^2 applied current with the addition of i) 0 mol·L^{-1} chloride (CERT74), ii) 0.1 mol·L^{-1} chloride (CERT134), iii) 0.5 mol·L^{-1} chloride (CERT132), iv) 1.0 mol·L^{-1} chloride (CERT136), and v) Saturated (~5 mol·L^{-1}) chloride (CERT108).

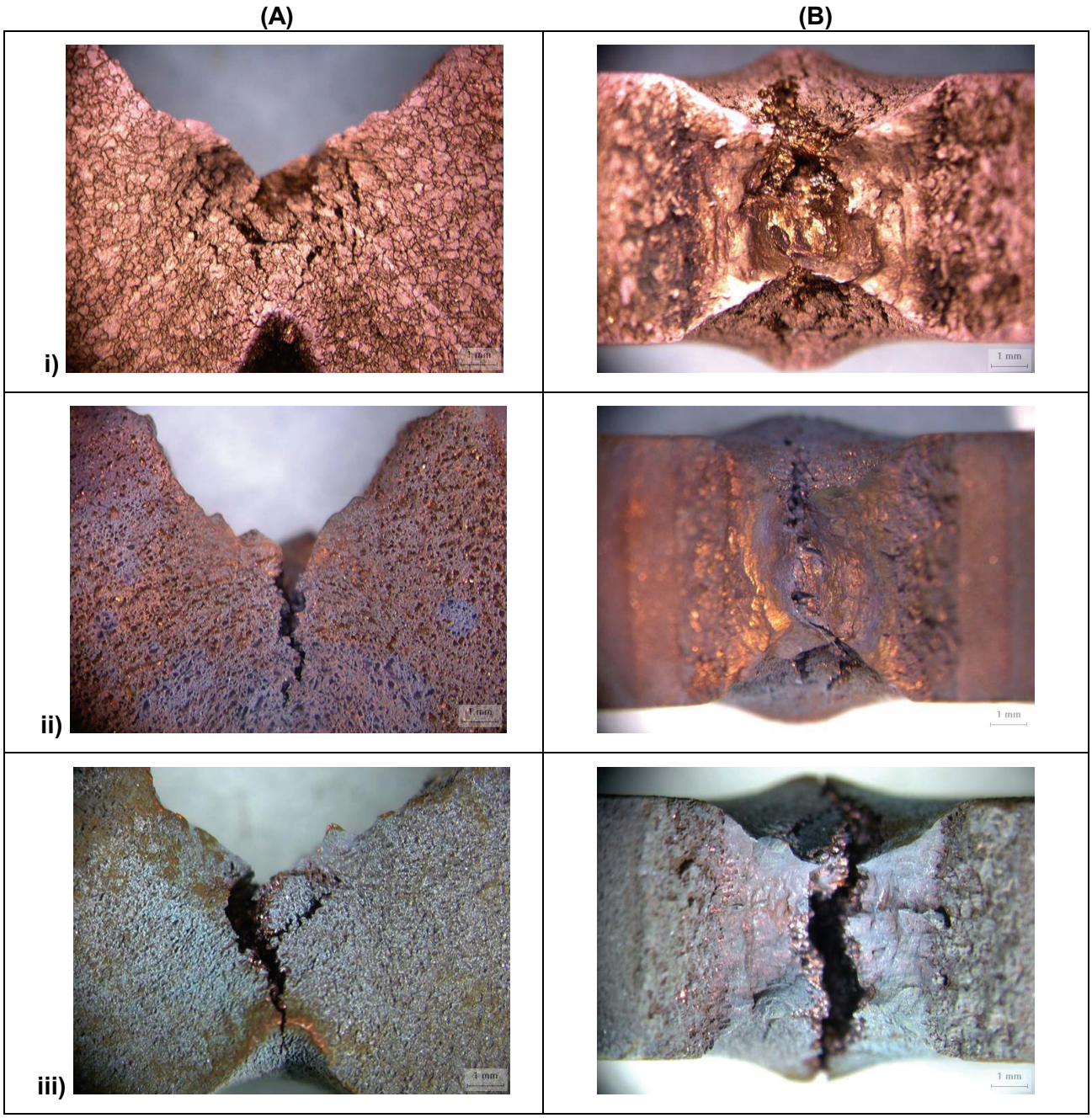

Figure 24: Macrographs of SKB4 Copper Plate CT Specimen Surface and Crack Overviews Showing the Effect of Chloride Concentration in 0.5 mol·L^{-1} Ammonia Containing 4 mmol·L^{-1} Copper under 1 μA/cm^2 Applied Current

Macrographs of CT specimen surface (A) and crack overview (B) images (10X) following CERTs in i) 0 mol·L^{-1} chloride (CERT132, 525 h), ii) 0.5 mol·L^{-1} chloride (CERT133, 380 h), and iii) 0.7 mol·L^{-1} chloride (CERT138, 622 h). The scale marker represents 1 mm on the specimen.

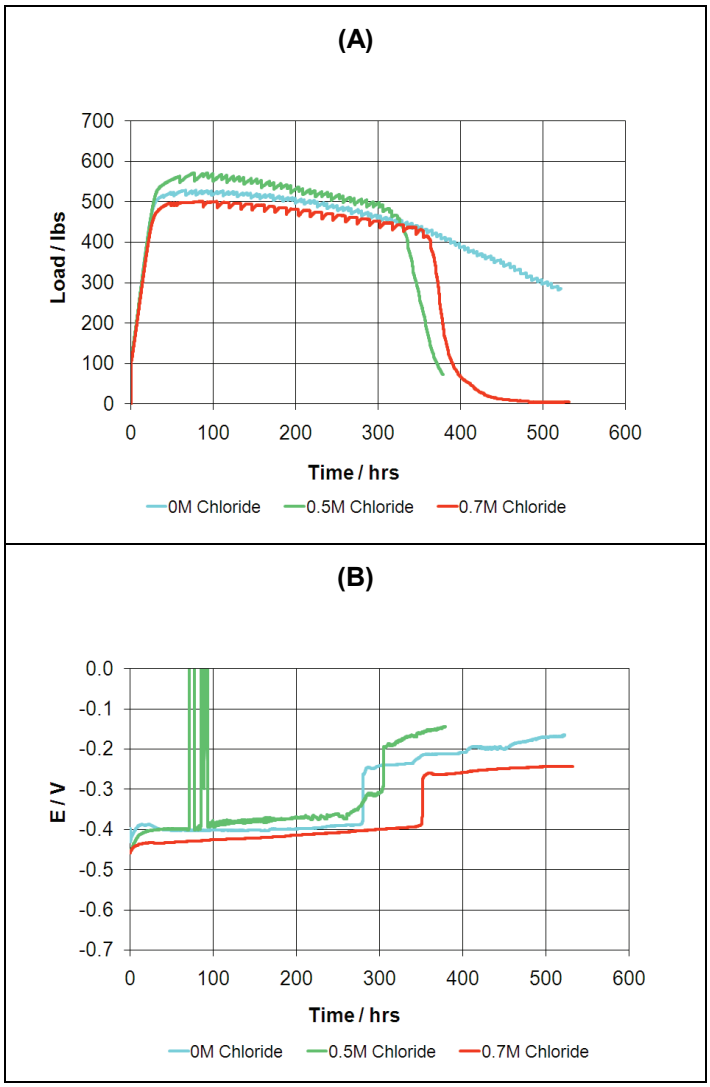

Figure 25: Graphs Showing the Effect of Chloride Concentration in 0.5 mol·L^{-1} Ammonia/4 mmol·L^{-1} Copper under 1 μA/cm^2 Applied Current

Graph (A) depicts the load curves and graph (B) follows the potential transient behaviour of OFP Cu CT specimens immersed in 0.5 mol·L^{-1} ammonia with 4 mmol·L^{-1} added copper under 1 μA/cm^2 applied current with the addition of i) 0 mol·L^{-1} chloride (CERT132), ii) 0.5 mol·L^{-1} chloride (CERT133), and iii) 0.7 mol·L^{-1} chloride (CERT138).